# MODELLING AND CONTROL OF AN ELECTRIC ARC FURNACE OFF-GAS PROCESS

by

**Johannes Gerhardt Bekker**

Submitted in partial fulfillment of the requirements for the degree

Master of Engineering (Electronic-engineering)

in the

Faculty of Engineering

UNIVERSITY OF PRETORIA

November 1998

To my mother who taught me principles.

**Abstract:**

Title: Modelling and Control of an Electric Arc Furnace Off-gas Process
By: Johannes Gerhardt Bekker
Supervisor: Professor Ian K. Craig
Department: Electrical and Electronic Engineering
Degree: Master of Engineering (Electronic Engineering)

This dissertation investigates the automation of manually controlled variables such as fan speed and slip-gap width for the electric arc furnace (EAF) off-gas process. An extensive modelling effort is conducted and results in a comprehensive plant model. The model derived in this dissertation is intended for the testing of control strategies using off-gas variables in the control of an electric arc furnace. Derivation of a multivariable non-linear state-space model for the process is handled. The assumptions that are made and the state space representation provide a comprehensive framework for the development of an electric arc furnace process model. First principles of thermodynamics are used to derive the model, ensuring behaviour consistent with physical observations. Typical operating conditions for a furnace are discussed, and a simulation is conducted with these operating conditions. In order to apply the model representing a specific industrial furnace the adjustable parameters in the model are selected such that the model responses concur with those of the actual furnace. After verification, this plant model is regarded as the process for which a controller must be designed. A linear model approximates the plant model to give a simplified mathematical abstraction of the process. The linear model is accepted as a reasonable approximation of the process for the controller design purpose, and an analysis of the linear system shows that the linear system is stable. The analysis also shows that the linear system is output controllable with respect to particular outputs, although the internal state vector is not completely observable. Qualitative control objectives are translated to quantitative control specifications.

Control design for the linear system is performed in the Matlab environment. Model Predictive Control is the preferred control design method, due to the use of an internal model and the use of optimisation. Experiments with the controller parameters are done to obtain the best nominal controller. These include the cost function multipliers for the controlled and manipulated variables, as well as the manipulation and prediction horizons. The effect of various inputs and disturbances is determined. A trade-off is made between improving electric arc furnace efficiency and ensuring environmental protection, and the nominal controller is obtained. The controller is then applied to the plant model, and tested on the process it was intended for. A final "on-line tuning" session on the plant model concluded the design. The controller was evaluated against the option of no control, and the controller improved process operation. The controller achieved good regulation, setpoint tracking and disturbance rejection.

Keywords: Electric Arc Furnace, Off-gas Process, Process Control, State Space Modelling, Model Predictive Control, Quadratic Programming, Real-time Optimal Control.

**Opsomming:**

Titel: Modelling and Control of an Electric Arc Furnace Off-gas Process
Deur: Johannes Gerhardt Bekker
Leier: Professor Ian K. Craig
Departement: Electriese en Electroniese Ingenieurswese
Graad: Magister in Ingenieurswese (Electroniese Ingenieurswese)

Hierdie verhandeling ondersoek die outomatisasie van handbeheerde veranderlikes soos waaierspoed en sleur gapingwydte vir die elektriese boogoond afgas proses. 'n Deeglike modellering-fase word uitgevoer, en die nie-lineêre model word so verkry. Die model wat in hierdie verhandeling ontwikkel word, is bedoel vir die toets van beheer-strategieë deur van die afgas-veranderlikes gebruik te maak om 'n elektriese boogoond te beheer. Die afleiding vir 'n multi-veranderlike nie-lineêre toestand-ruimte model van die proses word behandel. Die gebruikte aannames en die toestand ruimte voorstelling verskaf 'n deeglike raamwerk vir die ontwikkeling van 'n elektriese boogoond proses model. Eerste beginsels van termodinamika word gebruik om die model af te lei, ten einde ooreenstemming te kry met fisiese waarnemings. Tipiese bedryftoestande vir 'n boogoond word bespreek, en 'n simulasie word met hierdie toestande uitgevoer. Ten einde die model toe te pas om 'n spesifieke industrieële oond voor te stel is die verstelbare parameters in die model gekies sodat die model reaksies ooreenstem met die van die werklike oond. Na model-verifikasie, is die model as 'n plaasvervanger vir die proses gebruik, en beskou as die proses waarvoor 'n beheerder ontwerp moes word. 'n Lineêre model is gebruik om die aanleg model te benader ten einde 'n vereenvoudigde wiskundige voorstelling te kry. Die lineêre model word aanvaar as 'n redelike benadering van die aanleg model vir beheerder ontwerp doeleindes, en 'n lineêre stelsel analise toon aan dat dit 'n stabiele stelsel is. Die lineêre stelsel analise wys ook dat die stelsel uitset-beheerbaar is, alhoewel dit nie volledig waarneembaar is nie. Die kwalitatiewe beheer doelwitte word herlei na kwantitatiewe beheer spesifikasies.

Beheerder-ontwerp vir die lineêre stelsel word in die Matlab omgewing gedoen. Model Voorspellende Beheer is gekies as die beheerder-ontwerp metode by voorkeur, te danke aan die gebruik van 'n interne model en optimisasie. Eksperimente met die beheerder parameters word uitgevoer om die beste nominale beheerder te bepaal. Hierdie parameters sluit die koste-funksie koeffisiënte vir die uitsette en insette, so wel as die manipulasie horison en die voorspellings horison in. Die effek van verskeie insette en steurings word bepaal. 'n Kompromie word verkry tussen die verbetering van die boogoond effektiwiteit en die voorkoming van omgewings-besoedeling. Die nominale beheerder wat gekry is, word op die aanleg-model toegepas en getoets op die proses waarvoor dit aanvanklik bedoel is. 'n Finale fyn-stelling sessie op die aanleg-model se beheerder sluit die ontwerp af. Die beheerder word vergelyk met operateur-beheer, en die outomatiese beheerder verbeter die proses bedryf. Goeie regulasie, stelpunt volging en steuring verwerping word met die beheerder verkry.

Sleutelterme: Elektriese Boogoond, Afgas Proses, Toestand Ruimte Modellering, Model Voorspellende Beheer, Proses Beheer, Kwadratiese Programmering, Intydse Optimale Beheer.

## ACKNOWLEDGEMENTS

I wish to thank Prof. I.K. Craig and Prof. P.C. Pistorius for their meaningful guidance in the course of this dissertation. I also wish to thank Prof. F.W. Leuschner who made it possible for me to undertake this Master's dissertation.

The plant data used in Chapter 5 was obtained from Iscor with the help of Mr. Philip Schutte and Mr. Jaco Lubbe. Many thanks to them, because not only did I get a set of meaningful data, but also the opportunity to visit and witness the operation of an actual EAF tap.

I wish to thank Ms Maryna Bekker for her support, and also to Ms Cornel Freislich for her assistance. Many thanks to Ms Helen Nel for proof reading most of the dissertation. I wish to thank Rhoanè my girlfriend for her patience and support with the dissertation.

Many thanks also to the guys at the laboratory, Ernst, Fernando, Martin and Niel. Their discussions always throw a new light on old problems.

I would like to thank the reader for undertaking the task of reading this dissertation. It is hoped that the contents were meaningful to the reader, and that it provided new insights and information.

## LIST OF ABBREVIATIONS

| | |
|---|---|
| BOF | Basic Oxygen Furnace |
| CV | Controlled Variable |
| C# | Controller number # |
| DRI | Direct Reduced Iron |
| EAF | Electric Arc Furnace |
| Fig | Figure |
| MPC | Model Predictive Control |
| MV | Manipulated Variable |
| NISE | Normalised Integrated Square Error |
| NILE | Normalised Integrated Limit Exceeded |
| NSS | Nominal Steady State |
| QP | Quadratic Programming |

## TABLE OF CONTENTS

# CHAPTER 1: INTRODUCTION

## 1.1 BACKGROUND

This dissertation investigates the automation of manually controlled variables such as fan speed and slip-gap length for the Electric Arc Furnace (EAF) off-gas process. The two above-mentioned variables are part of the off-gas variable set. Automation of these variables may lead to higher efficiency and greater profit. The use of the off-gas variable set in an appropriate control structure is investigated. In order to do this investigation an appropriate process model of the EAF and off-gas system is necessary. The manipulated variables in this case are the forced-draught fan power and the air-entrainment slip-gap width. The possible controlled variables in the EAF are the relative pressure of the furnace gas-phase and the liquid metal temperature. Other variables that have to be controlled are the temperature and composition of the gas that exits the cooling duct.

EAFs produce steel by melting scrap typically using a three-phase electrical supply. By oxygen blowing the concentrations of primarily carbon and silicon can be lowered, while providing an additional energy source. This is important for the type of operation under study, where hot metal (high in carbon and silicon) is charged to the furnace together with scrap. Oxygen is typically blown into the metal bath through one or more side lances, or from the bottom. With the EAF in operation, the roof is closed, and off-gas is extracted through the duct entrance in the roof. Air is entrained at a slip-gap to combust the excess carbon monoxide (CO) and to cool the off-gas. The off-gas is also cooled by forced water and air cooling, before it enters the baghouse filters.

Statistics of a two-month period in 1997 [1] gave total world crude steel production as 121 million metric tons. This translates to worldwide crude steel production of 730 million metric tons for 1997. For the same period South Africa produced approximately 7.5 million metric tons, about 1% of world production. In 1997 approximately 60% of steel production were processed with Basic Oxygen Furnaces (BOFs), and 30% through EAFs [2]. The generally accepted view [2] is that EAFs are slowly but steadily replacing BOFs worldwide. While the steel production by BOFs declines, the steel production by both EAFs and Direct Reduced Iron (DRI) operations is on the increase. The increased use of EAF operations is partly due to the combined use of electrical and oxygen steelmaking in the modern EAF, and partly due to the increased recycling of steel scrap.

During the last decade the emphasis on the operation of EAFs shifted significantly. Not only is it required to operate more efficiently, but also the demand for environmentally friendly operation of EAFs is increasing. The future development of environmental legislation shows a trend towards lower emission limits [3]. EAFs are also increasingly used for scrap recycling.

According to Jones [4] productivity increases are directly related to the increased use of oxygen in the furnace, where the exothermic reaction energy replaces a large amount of the electric energy input. While it does allow significantly shorter tap-to-tap times, it leads to greater demand on the off-gas system. The off-gas system of an EAF not only plays an important role in environmental protection, it also influences the EAF operation strongly. It is used to extract and combust hazardous gases such as carbon monoxide, and influences the steelmaking process. In particular, the rate of gas extraction has a direct influence on the furnace pressure, thus affecting air entrainment, and hence process energy requirement and nitrogen pick-up [5].

## 1.2 MOTIVATION

In order to investigate the use of the off-gas variable set in an appropriate control structure an appropriate process model of the EAF and off-gas system is necessary. There are only limited references to dynamic EAF models in the literature, as many such models tend to be proprietary. For example Petersohn *et al* [6] derived a dynamic EAF model based on mass and energy balances. They show what the principal measurement points required by a comprehensive model are. The models used in this dissertation were partly developed in Bekker, Craig and Pistorius [7,8].

Other projects on EAF control have focused mainly on electrode control. Reuter *et al* [9] discussed the impedance-based electrode control of submerged arc furnaces. The EAF type considered in this dissertation is of the open-arc type, and current-control is usually applied on this type of EAF. King and Nyman [10] show how neural networks can be used to control the electrode voltages and currents of a single-phase arc furnace. In this dissertation the assumption is made that proper control of the electrical circuits of the electrodes is in place. The choice of control structure for this dissertation stems from an indication, given by a process expert, that the gas pressure in the EAF was not well regulated, which caused several problems. For gas pressure and composition control the off-gas variable set was chosen as the manipulated variables in the control structure.

The control method that was selected for this project is Model Predictive Control (MPC) [11]. The MPC control strategy results from the optimisation of a performance index with respect to a future control sequence, using predictions of the output signals based on an internal process model. An optimisation algorithm is applied to compute a sequence of future control signals that minimises the performance index subject to the given constraints. According to Morari and Ricker [12] MPC displays it main strength when applied to problems with:

- A large number of manipulated and controlled variables;
- Constraints imposed on the manipulated variables;
- Changing control objectives or equipment failures.

## 1.3 CONTRIBUTION

The main contribution of this dissertation is to demonstrate the feasibility of using the off-gas variables for EAF process control. To do this, the following contributory steps are given:

- Development and combination of models for the off-gas system and EAF processes;
- Verification of these models with the limited plant data available;
- Linearisation of the plant model to obtain the internal model for the controller;
- Initial controller design and time domain analysis for the linearised model;
- Implementation and fine-tuning of the controller on the verified plant model;
- Evaluation of the closed loop performance with respect to the objectives.

Since many unsteady-state models are proprietary, they are not published in the literature. There are a few exceptions [7,13], which give partial model derivations for EAF processes. The model derived in this dissertation, and the publication of it, is therefore seen as an important contribution to the literature. The application of MPC to such a process is also seen as a relevant contribution.

The contributory steps that are listed above follow the guidelines of the General Control Problem (GCP) [14]. Fig.1.1 gives a graphical representation of the GCP as applied in this project.

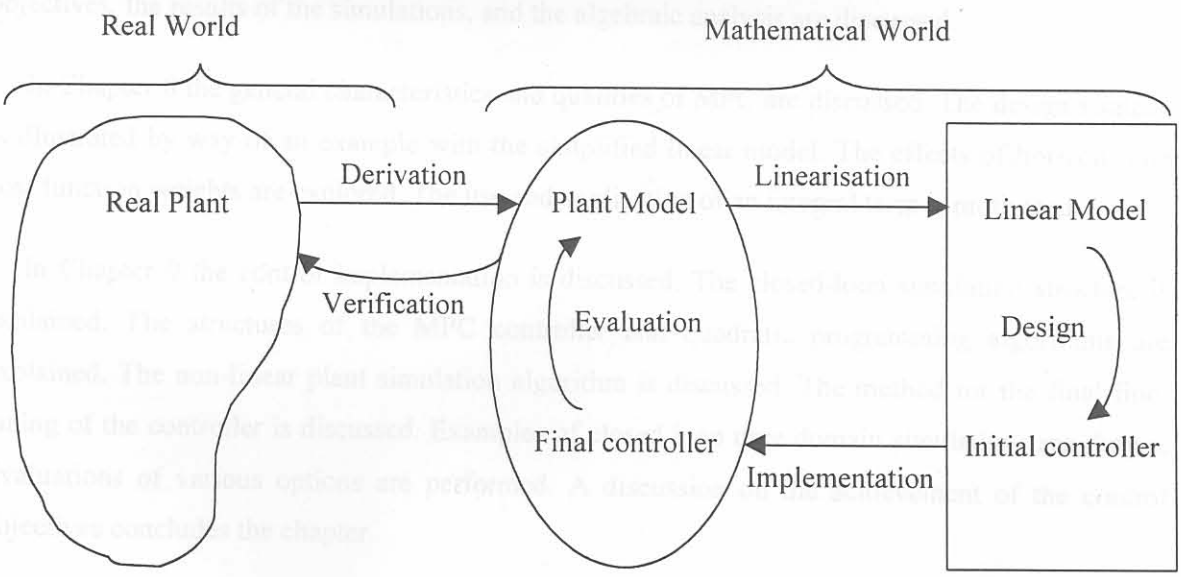


Figure 1.1 General Control Problem applied in this dissertation

## 1.4 ORGANISATION

In Chapter 2 a technical overview of the EAF process is given. The approach followed in this dissertation is briefly outlined, and the format of the project and its components are discussed.

Chapter 3 contains the derivation of the non-linear EAF plant model. The assumptions and approximations made to derive the EAF model are discussed. The incorporation of the off-gas model into the EAF model is shown. In Chapter 4 the off-gas model derivation is shown. The assumptions and approximations made to derive the off-gas model are given.

Chapter 5 discusses a time simulation of a specific EAF tap. The process conditions that correspond to a set of measured data are discussed. A disturbance model in terms of process conditions is developed. A time simulation with the combined non-linear model is shown. Model adjustment to correspond with the available data by means of parameter adjustment is discussed.

In Chapter 6 the linearisation of the plant model is shown. The approximations to derive the simplified linear state space model are discussed. An example of time simulation with the linear model is shown. The response of the linear model is compared to that of the non-linear model.

Chapter 7 discusses the control objectives in terms of EAF and off-gas parameters. An algebraic analysis of the linear system is given. The control specification, which results from the control objectives, the results of the simulations, and the algebraic analysis are discussed.

In Chapter 8 the general characteristics and qualities of MPC are discussed. The design strategy is illustrated by way of an example with the simplified linear model. The effects of horizons and cost function weights are explored. The use and application of an integral term is motivated.

In Chapter 9 the control implementation is discussed. The closed-loop simulation structure is explained. The structures of the MPC controller and quadratic programming algorithms are explained. The non-linear plant simulation algorithm is discussed. The method for the final fine-tuning of the controller is discussed. Examples of closed loop time domain simulations are shown. Evaluations of various options are performed. A discussion on the achievement of the control objectives concludes the chapter.

Chapter 10 contains a summary of the contents of the dissertation. Finally, a conclusion and recommendations are given.

# CHAPTER 2: OVERVIEW

## 2.1 INTRODUCTION

In order to relate the process and the dissertation project to each other, an overview is given in this chapter. The technical overview discusses first the off-gas system, then the water-cooled duct within the off-gas system, and then the EAF itself. The chronological order of actions performed is briefly outlined. A project overview is also given.

## 2.2 TECHNICAL OVERVIEW

### 2.2.1 Off-Gas System Overview

For a complete technical overview of EAF systems see [15]. The off-gas system under study consists of a water-cooled duct, overhead extraction canopy, three-pass air-cooled duct, six-unit baghouse filter, forced-draught fan and smoke stack. This is shown in Fig.2.1. For simplicity, elements such as the dust conveyer belt and the various emergency valves are omitted.

The baghouse of the off-gas cleaning system imposes limits on the maximum inlet temperature of the off-gas, the maximum CO content of the off-gas and the maximum differential pressure across the filters. If the temperature of the off-gas that enters the baghouse filter is too high, the baghouse may catch fire and explode. If the CO part of the gas composition that enters the baghouse filter is too high, it may also ignite and explode. If the differential pressure over the baghouse filter is too high, many of the filter bags could be ripped apart due to the high mass-flow rate in the baghouse and the resulting high stresses and pressures.

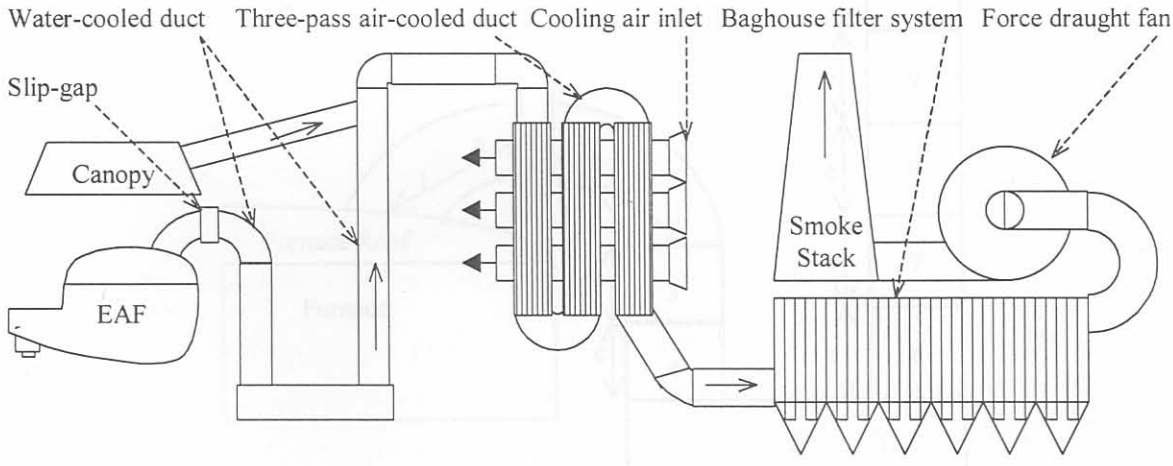


Figure 2.1 Off-gas system

A speed-controlled motor powers the force-draught fan. Due to the limitation on differential pressure over the baghouse, the operating range of the fan is limited. In general the fan has a nominal draught-force that is less than the critical limit determined by the baghouse.

Air is entrained through the slip-gap to combust CO in the EAF gas, as no combustible gases should reach the baghouse. The slip gap is situated near the EAF in the cooling duct. The slip-gap should under no circumstances be closed, because excess air is needed to combust the CO in the off-gas. Typical slip-gap widths vary from 0.1 – 0.5 m.

Valves at the top of the water-cooled duct are operated to determine the flow of gas. If the valve to the water-cooled duct is open, then the valve to the overhead canopy is closed, or *vice versa*.

### 2.2.2 Cooling Duct Overview

The off-gas water-cooled duct under study consists of 11 sections that are specially equipped with forced circulation water-cooling ribs on the inside. The dimensions of the duct are given in Fig.2.2, which is not drawn to scale. The cross section of the duct has an elliptic shape. For section one, which is fixed to the EAF roof, the cross sectional area is approximately 3.4 $m^2$, for sections two to five the cross sectional area is 4.4 $m^2$, and for sections six to eleven the cross sectional area is 5 $m^2$. An adjustable section between sections one and two can be used to regulate the slip gap. In practice this section is adjusted manually only when process requirements change.

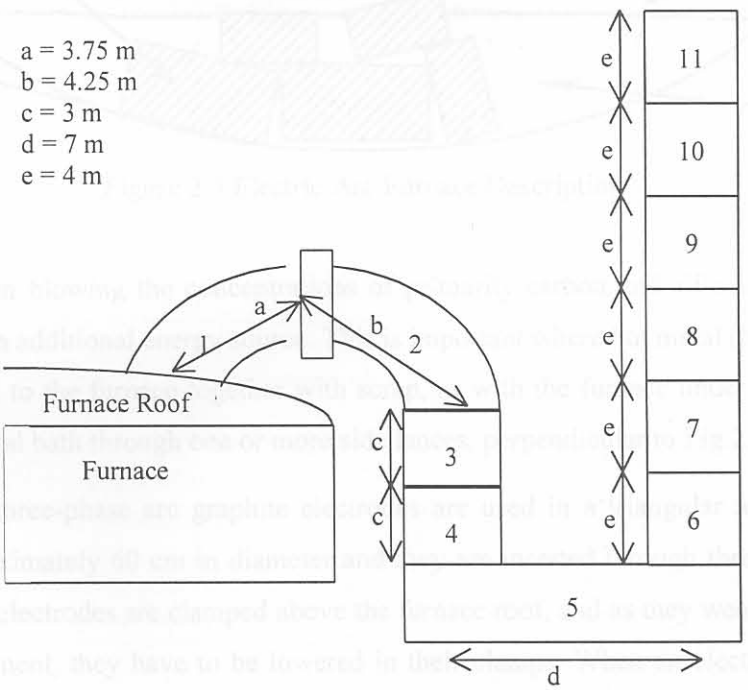


Figure 2.2 Cooling duct overview

Energy from the CO combustion reaction increases the temperature of the off-gas in the cooling duct, which requires forced circulation of cooling water. The rates of flow in the forced circulation water-cooling ribs are constant, and the water enters at 33°C. This was a nominal temperature given on the design drawings. The cooling water flow is pre-calculated for optimal cooling.

### 2.2.3 Electric Arc Furnace Overview

EAFs produce steel by melting scrap typically using a three-phase electrical supply. When the furnace is in operation, the furnace roof is closed. For the furnace under study the diameter is 10 m and the freeboard volume 175 $m^3$. Fig.2.3 gives a graphical description of the EAF with the main components and material phases shown.

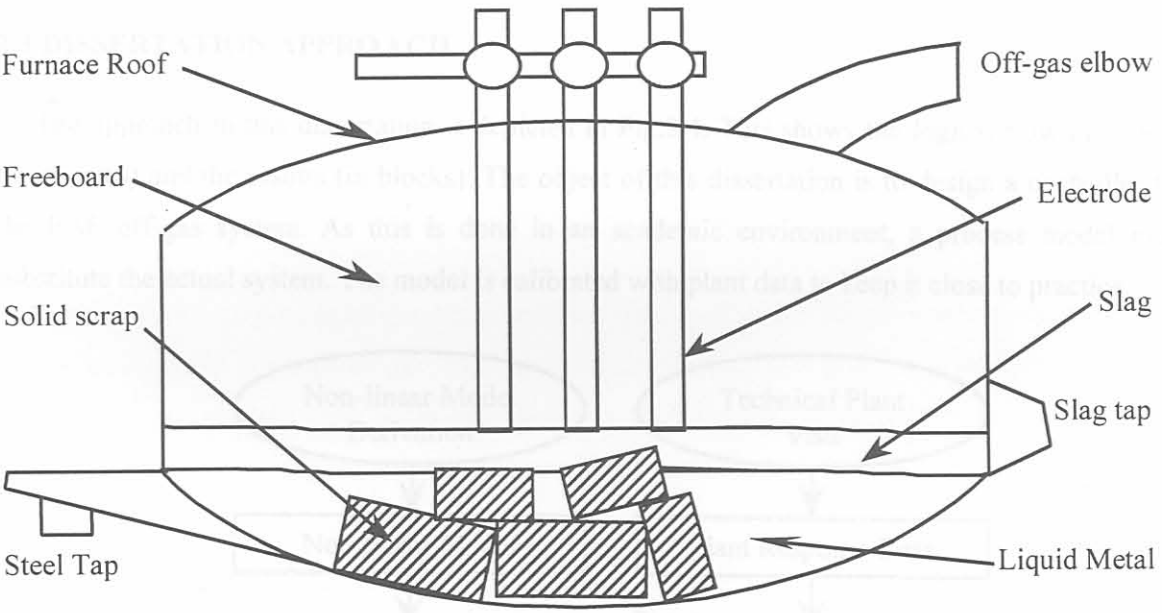


Figure 2.3 Electric Arc Furnace Description

Through oxygen blowing the concentrations of primarily carbon and silicon can be lowered, whilst providing an additional energy source. This is important where hot metal (high in carbon and silicon) is charged to the furnace together with scrap, as with the furnace under study. Oxygen is blown into the metal bath through one or more side lances, perpendicular to Fig.2.3 (into the page).

To create the three-phase arc graphite electrodes are used in a triangular arrangement. Each electrode is approximately 60 cm in diameter and they are inserted through three openings in the furnace roof. The electrodes are clamped above the furnace roof, and as they wear out in the highly corrosive environment, they have to be lowered in their clamps. When an electrode becomes too short another is joined on top of it. The electrode current is mainly controlled by means of on-load

transformer tap-changers in the high-voltage winding [15,16]. The arc is also regulated/stabilised by means of electrode position (adjustment of arc length – impedance based control) [15,17].

DRI and slag additions are charged into the furnace by means of conveyer belts in the second half of the tap. Temperature control is possible by matching the DRI addition rate to the electrical power input rate [18]. "Foaming slag" and "hot heel" practices are commonly employed in EAF operations. With the foaming slag practice graphite is blown with compressed air into the slag, where it reacts with FeO to form CO that bubbles and make the slag foam, improving the arc efficiency. With the hot heel practice about 10% of the tap weight of steel is kept in the furnace after each tap. At the end of a tap, slag is removed through the slag door and the steel is tapped through the tap door. For discussion of EAF practices see McIntyre and Landry [19].

## 2.3 DISSERTATION APPROACH

The approach in this dissertation is depicted in Fig.2.4. This shows the logical flow of actions (in ellipses) and the results (in blocks). The object of this dissertation is to design a controller for the EAF off-gas system. As this is done in an academic environment, a process model must substitute the actual system. The model is calibrated with plant data to keep it close to practice.

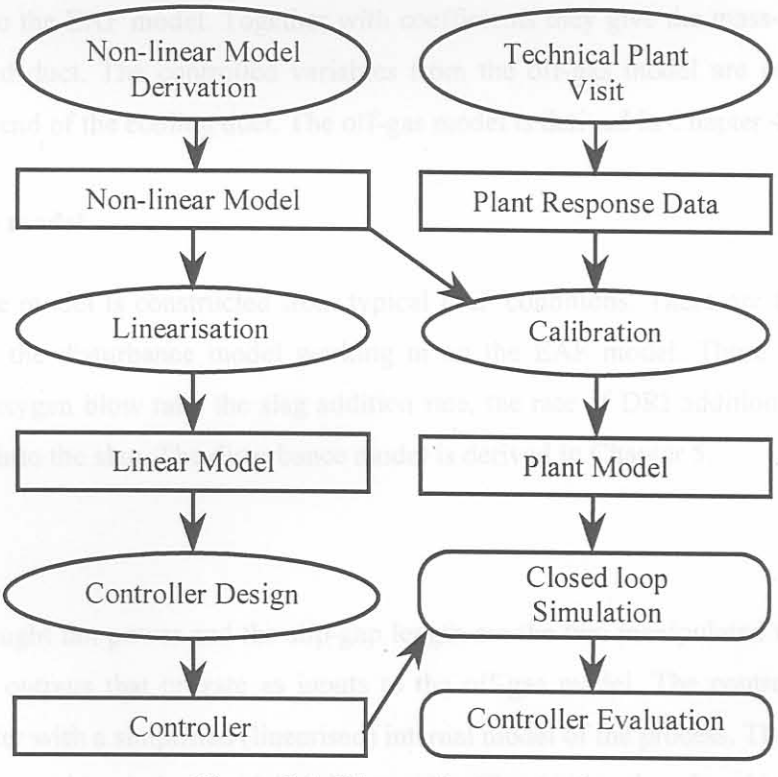


Figure 2.4. Dissertation approach

## 2.4 PROJECT OVERVIEW

There are four building blocks in the project. These are the disturbance model, the EAF model, the off-gas model and the controller. Fig.2.5 shows the interaction of the various parts in the project. The furnace model and the off-gas model are combined as a complete model for simulation-purposes. The simulation user specifies controller setpoints.

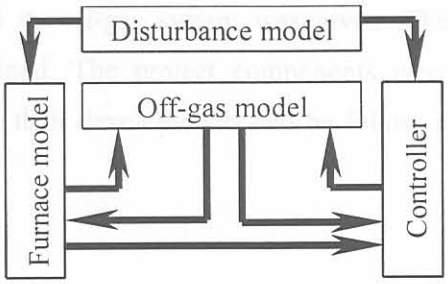


Figure 2.5 Project Overview

### 2.4.1 EAF model

The CO and $CO_2$ fractions and the temperature of the gas-phase at the slip-gap are outputs of the EAF model that operate as inputs to the off-gas model. The controlled variable from the furnace model is the pressure of the gas-phase. This is a measured variable for the controller. The EAF model is derived in Chapter 3. The EAF model and the off-gas model are combined as one model.

### 2.4.2 Off-gas model

There are two off-gas model outputs (combined with coefficients for physical significance) that operate as inputs to the EAF model. Together with coefficients they give the mass-flow of off-gas in the water-cooled duct. The controlled variables from the off-gas model are composition and temperature at the end of the cooling duct. The off-gas model is derived in Chapter 4.

### 2.4.3 Disturbance model

The disturbance model is constructed from typical EAF conditions. There are five measurable disturbances from the disturbance model working in on the EAF model. These are the electric power input, the oxygen blow rate, the slag addition rate, the rate of DRI addition and the rate of graphite injection into the slag. The disturbance model is derived in Chapter 5.

### 2.4.4 Controller

The forced-draught fan power and the slip-gap length are the two manipulated variables. These are the controller outputs that operate as inputs to the off-gas model. The controller is a model predictive controller with a simplified (linearised) internal model of the process. The internal model is derived from the combined plant model as discussed in Chapter 6 and analysed in Chapter 7. The initial controller design is in Chapter 8. The control implementation is discussed in Chapter 9.

## 2.5 CONCLUSION

In this chapter the technical overview of the EAF and its off-gas system was given. The dissertation approach and the project overview were outlined. The project components were discussed and the respective places in the dissertation where their developments can be followed were given.

# CHAPTER 3: NON-LINEAR MODEL

## 3.1 INTRODUCTION

The emphasis of this chapter is on obtaining a model that is appropriate for control system simulation and verification. A model is a mathematical abstraction of an industrial process. There are many advantages of an appropriate model for a process [20,21]. The model can improve understanding of the process, and can be used to optimise operating conditions and design a control law for a new control strategy.

The non-linear state-space model discussed in this chapter was partly derived in [7]. There are static EAF mass- and energy-balance models cited in the literature e.g. [22]. However, this model needs to approximate the physical process in terms of its dynamic response due to control and disturbance input changes. The aim is to obtain the same type of response, with the same order of magnitude as is found in an industrial furnace.

There are other groups working on dynamic models, e.g. Morales *et al* [13] are working on a complete mathematical simulator for EAF operation. In the literature only fragments of this simulator are shown. Austin *et al* [23] developed a two-dimensional model for blast furnaces that represents the major chemical reactions and physical structures. This shows that dynamic models and simulators are becoming increasingly popular for all types of furnaces, including electric arc furnaces, as process engineers are working to optimise these processes.

Sridhar and Lahiri [24] developed models to predict EAF temperature distributions. References which focus on EAF gas flow include Gardin *et al* [25], who concentrated on gas flow above the liquid steel bath, and Zhulkovsky *et al* [26], who studied in-vessel off-gas post-combustion.

Fruehan [27] has done a study on the benefits of gas stirring in an EAF. In this study interaction between the FeO in slag and the carbon in the steel melt was investigated. Sarma *et al* [28] provided experimental results of the reduction of FeO in smelting slags by solid carbon.

Section 3.2 gives all the assumptions and simplifications. Section 3.3 discusses the non-linear model derivation. Subsections 3.3.1 to 3.3.15 give the separate derivations of the state equations and auxiliary equations. Section 3.4 shows the incorporation of the off-gas model.

## 3.2 ASSUMPTIONS TO FACILITATE MODELLING

The failure to choose an appropriate set of simplifying assumptions leads to either an overly complicated model or an overly simplistic model [20]. In this section a set of assumptions is given, which yields a seventeen-state non-linear state space model that is appropriate for this dissertation.

The assumptions are given here with motivation where necessary. This set of assumptions is appropriate for an unsteady state model that is intended for controller evaluation. It facilitates the modelling effort, and allows for simplification, without making the model trivial:

1. The liquid metal, molten slag and gas-phase are all at the same temperature. These elements form the fluid group. The mass of gas-phase elements is small in relation to the other fluids.
2. The solid scrap is at the same temperature as the solid slag additions that have not yet dissolved. These elements form the solid group. The solid group melt rates and the rate of increase of the solid group temperature ($x_{13}$) are proportional to the difference between the fluid group temperature ($x_{12}$) and the solid group temperature.
3. From Plöckinger & Etterich [29] it is seen that 48% of the arc heat flows to the steel melt by means of convection. A further 17% of the arc heat flows to the steel melt by means of radiation. There can be heat transfer from the arcs to the scrap, but since the greatest fraction of heat flows to the steel melt it is more convenient to make the assumption that all heat transfer from the arcs is to the liquid metal. This avoids the problem of establishing a division of the arc heat between the separate components in the furnace. To correct for the amount of energy transferred by the arc, the power input is multiplied by an efficiency factor in the disturbance model, before the disturbance model is applied as input to the plant model.
4. A power division coefficient describes heat transfer from the fluid group to the solid group. The heat transferred to the scrap can be utilised to increase the temperature of the solid group, or to melt part of the scrap. The coefficient $\sqrt{x_{13}/x_{12}}$ is used for the melting rates of the scrap and the solid slag, while $\left(1-\sqrt{x_{13}/x_{12}}\right)$ is the coefficient used for the heating rate.
5. Fluxes added to the furnace do not melt immediately, but remain in an unmixed, solid condition until melted by the heat of the fluid group to form part of the liquid slag.
6. Because the concentration of Fe in the steel melt is very much greater than that of carbon or silicon, all oxygen blown into the steel reacts with Fe to form FeO in the slag.
7. All FeO and $SiO_2$ that form in the furnace are immediately dissolved in the molten slag.
8. A carrier gas blows graphite into the slag to reduce the FeO. The carrier gas is usually air and contains oxygen. All graphite is assumed to either react with FeO instantly or with the carrier gas during the ascent to the surface. This is based on the result that no carbon solids remain in the slag. The typical residence time of carbon particles in the slag is 8-10 seconds [13].
9. The amount of FeO that reacts with carbon and silicon is proportional to the FeO in the slag, from experimental evidence provided by Sarma *et al* [28].

10. The DRI contains 82.5% metallic iron, and when DRI is introduced into the furnace, 82.5% of the mass is added as iron to the steel melt, 4.5% as $SiO_2$ and 13% as FeO to the liquid slag.
11. The iron in the DRI melts instantaneously. This is based on the observation that the EAF temperature can be controlled by matching the DRI feed rate with the electrical power input: 33 kg/min per MW yields a constant temperature [16]. By implication the DRI effectively melts immediately upon entry, with the associated latent heat requirement effected immediately.
12. The scrap does not contain impurities that will be oxidised. In steel-making practice graded scrap is needed for low tramp element requirements in steel [30].
13. The average value (for temperatures from 600 K to 1800 K) for the specific heat of iron is used for the scrap. Cp(Fe(S)) = 0.039 kJ/(mol.K). Cp(Fe(L)) = 0.046 kJ/(mol.K) for the liquid metal.
14. Typical composition of slag additives is 2/3 burnt lime and 1/3 dolomite [30]. Burnt lime has the composition (97% CaO, 3% MgO) and doloma has the composition (57% CaO, 43% MgO) [31]. This is approximately 83% CaO and 17% MgO.
15. The CaO and MgO parts of the slag are lumped and treated as a single state variable, with an equivalent heat of fusion, heat of solution, molar mass and specific heat.
16. All elements entering the furnace are heated to the respective temperatures. Reagents are heated to 1680 K before they participate in reactions. All chemical reactions take place at an average temperature of 1680 K to prevent temperature from being a variable that determines chemical reaction power.
17. All energy is exchanged with the fluid group. The solid group receives energy from the fluid group. This means that the electric arc power is assumed to heat up the liquid metal first, which then heats up and melts the other components in the furnace.
18. The only gas-phase elements are CO, $CO_2$ and $N_2$. All $O_2$ reacts on entry, and $H_2$ is ignored.
19. The pressure in the furnace can be obtained from the ideal gas law.

## 3.3 NON-LINEAR MODEL DERIVATION

The EAF is described in a Multi-Input Multi-Output (MIMO) state space format with 17 states. There are four vectors that feature in the model: State vector **x**, manipulated variable vector **u**, measured disturbance vector **v** and unmeasured disturbance vector **w**.

The model is a vector function (**f**) of 17 ordinary differential equations (ODE) that describe the rate of change (with respect to time) of each state variable. The differential equations are mostly

non-linear, and are taken from the set that contains all functions of **x**, **u**, **v**, **w**, i.e. $\dot{\mathbf{x}} = \mathbf{f}(\mathbf{x}, \mathbf{u}, \mathbf{v}, \mathbf{w})$ where the dimensions are: $\mathbf{x} \in \Re^{17x1}, \mathbf{u} \in \Re^{2x1}, \mathbf{v} \in \Re^{3x1}, \mathbf{w} \in \Re^{2x1}$. Appendix A gives a list of symbols. Standard symbols such as molar mass ($M_x$) and specific heat (Cp(x)) are not given.

### 3.3.1 Rate of Change of Solid Scrap

The rate of change of the mass of solid scrap ($\dot{x}_1$) in the furnace is proportional to the heat transfer rate from the liquid metal to the scrap. This in turn is proportional to the temperature difference between the liquid metal and the scrap. This is an approximation, since scrap melting involves both mass transfer (diffusion of carbon) and heat transfer. However, since the main aim of this model is to characterise the off-gas system, a formulation that yields a realistic scrap-melting rate is deemed acceptable. The liquid metal temperature is denoted as $x_{12}$ and the solid scrap temperature as $x_{13}$. The heat transfer coefficient is $k_{therl} = 0.24\ kW.K^{-1}.m^{-2}$. This is an adjustable constant, depending on the observed melting time. The area of contact is assumed to be proportional to the mass of scrap in the furnace. A specific area of $k_{areal} = 0.005\ m^2.kg^{-1}$ is used, and this corresponds to sheets of thickness 0.05 m.

A partition coefficient is used to allocate power transferred to melt the scrap, as opposed to power transferred to heat the scrap, as discussed in assumption 3. The scrap that is melted must receive latent heat of fusion ($\lambda_{Fe}$ [kJ/mol]) and specific heat multiplied by the temperature difference between the liquid group and the solid group.

The equation for the scrap melt rate in units of [$kg.s^{-1}$] is given by:

$$\dot{x}_1 = \frac{-M_{Fe} k_{therl} k_{areal} (x_1)(x_{12} - x_{13})\sqrt{x_{13}/x_{12}}}{\left[\lambda_{Fe} + Cp(Fe_{(S)})(x_{12} - x_{13})\right]} \qquad (3\text{-}1)$$

### 3.3.2 Rate of Change of Liquid Metal Mass

The rate of change of liquid metal mass ($\dot{x}_2$) equation has six parts:

- Negative of equation (3-1), which gives the melt rate of steel scrap.
- Rate of oxidation of iron by oxygen to form FeO.
- Rate of iron reduced from FeO by graphite injection into the slag.
- Rate of iron reduced from FeO by dissolved carbon in the steel melt.
- Rate of iron reduced from FeO by dissolved silicon in the steel melt.
- Rate of metal added by DRI additions, which contain 82.5% metallic iron (see assumptions 10 and 11).

All oxygen blown into the steel reacts with Fe to form FeO (see assumption 6). The rate of Fe oxidation is then given by:

$$-\frac{2M_{Fe}v_1}{M_{O_2}} \tag{3-2}$$

The rate of reduction of FeO by the graphite is given by equation (3-3). It is proportional to the rate of graphite injection and the content of FeO in the slag (See assumption 8).

$$\frac{x_7 k_{gr} M_{Fe} w_2}{(x_6 + x_7 + x_8)M_C} \tag{3-3}$$

The rates of FeO reduction by dissolved carbon and dissolved silicon in the steel melt are discussed in Subsections 3.3.3 and 3.3.4. Please refer to these subsections for the development of the rate equations. Equations (3-8) and (3-9) give $X_C$ and $X_C^{eq}$ respectively and equations (3-15) and (3-16) give $X_{Si}$ and $X_{Si}^{eq}$ respectively. Thus the rate of change of liquid metal is given by:

$$\begin{aligned}\dot{x}_2 = &\frac{M_{Fe}k_{therl}k_{areal}(x_1)(x_{12}-x_{13})\sqrt{x_{13}/x_{12}}}{\left[\lambda_{Fe}+Cp(Fe_{(S)})(x_{12}-x_{13})\right]} \\ &+\frac{x_7 k_{gr} M_{Fe} w_2}{(x_6+x_7+x_8)M_C}+\left(\frac{M_{Fe}}{M_C}\right)k_{dC}\left(X_C - X_C^{eq}\right) \\ &+\left(\frac{2M_{Fe}}{M_{Si}}\right)k_{dSi}\left(X_{Si}-X_{Si}^{eq}\right)-\frac{2M_{Fe}v_1}{M_{O_2}}+0.825v_3\end{aligned} \tag{3-4}$$

### 3.3.3 Rate of Change in Dissolved Carbon

The rate of change of dissolved carbon ($\dot{x}_3$) in the steel melt is due to reaction with FeO in the slag. The reaction with FeO in the slag is driven by the deviation from equilibrium that is approximated as a hyperbolic relationship between the carbon in the steel melt and the FeO in the slag (mass percentages). For low-carbon melts ($\gamma_C=\gamma_C^{\infty}$), and for basic slags (in which $\gamma_{FeO}\approx 1$) the equilibrium product varies with temperature from 1.8 at 1500°C to 0.89 at 1700°C [31,32]. Since 1600°C is close to the final tap temperature, a constant equilibrium product was determined for 1600°C and used throughout the simulation.

The reaction between C and FeO is far from equilibrium throughout the steelmaking process, and therefore the exact value of the equilibrium constant is not critical. At 1600°C Turkdogan [31] (equation 6.6, p.183) gives equilibrium by:

$$(\%FeO)(\%C)_{equilibrium} = 1.25 = k_{C\%} \tag{3-5}$$

The relationship between $k_{C\%}$ and the molar fractions is approximated by equation (3-6). Equation (3-7) gives the relationship for the dimensionless equilibrium concentration constant $k_{XC}$.

$$k_{C\%} = X_{FeO}X_C\left(\frac{M_{FeO}M_C}{M_{slag}M_{Fe}}100^2\right) \tag{3-6}$$

$$k_{XC} = X_{FeO}X_C = k_{C\%}\left(\frac{M_{slag}M_{Fe}}{M_{FeO}M_C \cdot 100^2}\right) \tag{3-7}$$

The average molar mass of steelmaking slag is $M_{slag} = 0.0606$ kg/mol [31]. From equation (3-7) a value of $k_{XC} = 491*10^{-6}$ was obtained. $X_C$ is the molar fraction of carbon in the steel given by equation (3-8). $X_C^{eq}$ is the equilibrium molar fraction of carbon in the steel given by equation (3-9). $X_{FeO}$ is the molar fraction of FeO in the slag given by equation (3-10).

$$X_C = \frac{x_3/M_C}{x_2/M_{Fe} + x_3/M_C + x_4/M_{Si}} \tag{3-8}$$

$$X_C^{eq} = k_{XC}\left(\frac{x_6M_{FeO}}{x_7M_{slag}} + \frac{x_8M_{FeO}}{x_7M_{SiO_2}} + 1\right) \tag{3-9}$$

$$X_{FeO} = \frac{x_7/M_{FeO}}{x_6/M_{slag} + x_7/M_{FeO} + x_8/M_{SiO_2}} \tag{3-10}$$

The reaction rate is controlled by the difference of the actual carbon content from the equilibrium carbon content as in Fruehan [27] (equation 10, p.37). For this equation the rate constant was determined to give a reasonable decarburisation rate. The rate constant has units of kg/s since the differential equation for carbon is in units of kg/s.

The decarburisation rate constant was determined as $k_{dC} = 48$ kg/s. The rate of decarburisation due to reaction with FeO in the slag is given by equation (3-11) where $X_C$ and $X_C^{eq}$ are given by equations (3-8) and (3-9):

$$\dot{x}_3 = -k_{dC}\left(X_C - X_C^{eq}\right) \tag{3-11}$$

### 3.3.4 Rate of Change in Dissolved Silicon

The rate of decrease of the silicon ($\dot{x}_4$) in the steel melt is due to reaction with FeO in the slag. The reaction with FeO in the slag is driven by the deviation from equilibrium that is approximated as a hyperbolic relationship between the Si in the steel melt and the $(FeO)^2$ in the slag (mass percentages). This is similar to the treatment of the carbon in the steel melt:

$$(\%FeO)^2(\%Si) = 0.00057 = k_{Si\%} \tag{3-12}$$

The relationship between $k_{Si\%}$ and the molar fractions is approximated by equation (3-13). Equation (3-14) gives the relationship for the dimensionless equilibrium concentration constant.

$$k_{Si\%} = X_{FeO}^2 X_{Si}\left(\frac{M_{FeO}^2 M_{Si}}{M_{slag}^2 M_{Fe}} 100^3\right) \tag{3-13}$$

$$k_{XSi} = X_{FeO}^2 X_{Si} = k_{Si\%}\left(\frac{M_{slag}^2 M_{Fe}}{M_{FeO}^2 M_{Si} \cdot 100^3}\right) \tag{3-14}$$

From equation (3-14) a value of $k_{XSi} = 8.08*10^{-8}$ was obtained. $X_{Si}$ is the molar fraction of silicon in the steel given by equation (3-15). $X_{Si}^{eq}$ is the equilibrium molar fraction of silicon in the steel given by equation (3-16):

$$X_{Si} = \frac{x_4/M_{Si}}{x_2/M_{Fe} + x_3/M_C + x_4/M_{Si}} \tag{3-15}$$

$$X_{Si}^{eq} = k_{XSi}\left(\frac{x_6 M_{FeO}}{x_7 M_{slag}} + \frac{x_8 M_{FeO}}{x_7 M_{SiO_2}} + 1\right)^2 \tag{3-16}$$

The reaction rate is controlled by the difference of the actual silicon content from the equilibrium silicon content, similar to equation (3-11) for carbon. The rate constant was determined as $k_{dSi} = 144$ kg/s. The rate of change in silicon due to reaction with FeO in the slag is given by:

$$\dot{x}_4 = -k_{dSi}\left(X_{Si} - X_{Si}^{eq}\right) \tag{3-17}$$

### 3.3.5 Rate of Change of Solid Slag Mass

The rate of change of solid slag mass ($\dot{x}_5$) is dependent on the introduction of new fluxes to the furnace and the rate at which the slag is melting. Similar to the scrap melting approach the melting rate is assumed to be proportional to the heat transfer rate from the liquid metal to the solid slag, which is proportional to the temperature difference between the liquid metal and the solid slag.

The heat transfer coefficient is $k_{ther5} = 0.0125$ kW.K$^{-1}$.m$^{-2}$ which can be adjusted depending on the observed slag melting rate. The area of contact is assumed to be proportional to the mass of solid slag in the furnace, and a specific area of $k_{area5} = 0.12$ m$^2$.kg$^{-1}$ is used, corresponding to cubic blocks (density 2500 kg/m$^3$) with 0.02 m sides.

The slag that is being melted must receive latent heat of fusion ($\lambda_{Slag}$) and specific heat multiplied by the temperature difference between the liquid group and the solid group. $\lambda_{Slag}$ and $C_p(Slag_{(X)})$ has units of kJ/g-atom (kJ/(g-atom.K)) instead of kJ/g-mol (kJ/(g-mol.K)). The equation for the solid slag melt rate in units of [kg.s$^{-1}$] is given by:

$$\dot{x}_5 = \frac{-M_{Slag} k_{ther5} k_{area5} (x_5)(x_{12} - x_{13})\sqrt{x_{13}/x_{12}}}{\left[\lambda_{Slag} + Cp(Slag_{(S)})(x_{12} - x_{13})\right]} + w_1 \tag{3-18}$$

### 3.3.6 Rate of Change of Liquid Slag Mass

The rate of increase of molten slag ($\dot{x}_6$) is equal but of opposite sign to the solid slag melting rate.

$$\dot{x}_6 = \frac{M_{slag} k_{ther5} k_{area5} (x_5)(x_{12} - x_{13})\sqrt{x_{13}/x_{12}}}{[\lambda_{Slag} + Cp(Slag_{(S)})(x_{12} - x_{13})]} \tag{3-19}$$

### 3.3.7 Rate of Change of Iron-oxide Mass in Slag

The rate of change of FeO in the slag ($\dot{x}_7$) is dependent on five rate mechanisms.

- The first rate is the same as in equation (3-2), with $M_{FeO}$ replacing $M_{Fe}$;
- The second rate is the same as in equation (3-3), with $M_{FeO}$ replacing $M_{Fe}$;
- The third rate is the FeO that is introduced into the furnace with the DRI;
- The rate of FeO reduction by carbon out of the steel melt;
- The rate of FeO reduction by silicon out of the steel melt.

Equations (3-8), (3-9), (3-15) and (3-16) give $X_C$, $X_C^{eq}$, $X_{Si}$ and $X_{Si}^{eq}$ respectively. The rate of change of FeO in the slag is then given by:

$$\begin{aligned}\dot{x}_7 = {} & \frac{2M_{FeO} v_1}{M_{O_2}} - \frac{x_7 k_{gr} M_{FeO} w_2}{(x_6 + x_7 + x_8) M_C} + 0.13 v_3 \\ & - \left(\frac{M_{FeO}}{M_C}\right) k_{dC} \left(X_C - X_C^{eq}\right) - \left(\frac{2M_{FeO}}{M_{Si}}\right) k_{dSi} \left(X_{Si} - X_{Si}^{eq}\right)\end{aligned} \tag{3-20}$$

### 3.3.8 Rate of Change of Silicon-dioxide Mass in Slag

The rate of change of $SiO_2$ in the slag ($\dot{x}_8$) is equal but of opposite sign to equation (3-17) plus the $SiO_2$ introduced with DRI to the furnace. Since the molar masses are different this equation must be multiplied by the ratio of $M_{SiO2}$ to $M_{Si}$. Equations (3-15) and (3-16) give $X_{Si}$ and $X_{Si}^{eq}$ respectively. The rate of change of $SiO_2$ in the slag is then given by:

$$\dot{x}_8 = \left(\frac{M_{SiO_2}}{M_{Si}}\right) k_{dSi} \left(X_{Si} - X_{Si}^{eq}\right) + 0.045 v_3 \tag{3-21}$$

### 3.3.9 Carbon-monoxide in Furnace Gas-phase

The CO equation has 4 components:

- Rate of CO produced by decarburisation.
- Rate of CO produced by graphite injection into slag with FeO.
- Rate of CO combustion in leak-air from outside.
- Rate of CO extracted from the furnace through the off-gas door.

The rate of CO produced by decarburisation is the negative of equation (3-11). Since the molar masses are different this equation must be multiplied by the ratio of $M_{CO}$ to $M_C$. This is shown by:

$$\left(\frac{M_{CO}}{M_C}\right)k_{dC}\left(X_C - X_C^{eq}\right) \tag{3-22}$$

The rate of CO produced by injection of graphite into the slag is proportional to the rate of graphite injection ($d_5$). Following from assumption 8, all the carbon introduced by the graphite injection reacts instantly with FeO to form CO and iron. This rate of production is represented by the following equation:

$$d_5 M_{CO}/M_C \tag{3-23}$$

The rate of CO combustion is proportional to the rate of leak-air entry, which is proportional to the pressure difference between the outside atmospheric pressure and the furnace pressure. The pressure difference can be defined as the relative pressure of the furnace with respect to the atmospheric pressure. This is treated as state variable $x_{14}$, referred to here as the relative pressure. Note that the relative pressure will normally be negative because of the extraction force exercised by the off-gas extraction fan.

Air that leaks into the furnace is assumed to have the normal air composition of 79% nitrogen and 21% oxygen where other gases are ignored. This amounts to 7.3 mole $O_2$ and 27.4 mole $N_2$ per kilogram of air. Based on the assumption that all the oxygen in the leak-air combusts with CO in the furnace freeboard, the rate of CO combustion is:

$$2M_{CO}k_{AIR1}k_{PR}x_{14} \tag{3-24}$$

The rate of extraction of CO from the EAF as a fraction of the total gas extraction rate equals the CO fraction of the gas composition in the furnace. The total gas extraction rate from the EAF is given by equation (3-56). Please see Section 3.4 for an explanation. The total gas extraction rate from the EAF is then given in advance here by equation (3-25).

$$\frac{h_d\left[\left(2K_M/t_d\tau_1\tau_2\right)x_{15} - \left(K_M/\tau_1\tau_2\right)x_{16}\right]}{k_U u_2 + h_d} \tag{3-25}$$

Combining the three components as discussed, the equation for the rate of change of CO in the gas-phase within the furnace is obtained. When the relative pressure is negative, equation (3-26) is used, however when the relative pressure is positive, (3-27) is used. This takes into account that the furnace gas composition differs from the composition of air. Equations (3-8) and (3-9) give $X_C$ and $X_C^{eq}$ respectively.

$$\dot{x}_9 = \frac{M_{CO} d_5}{M_C} - \frac{[(2K_M/t_d\tau_1\tau_2)x_{15} - (K_M/\tau_1\tau_2)x_{16}]h_d x_9}{(k_U u_2 + h_d)(x_9 + x_{10} + x_{11})} + \left(\frac{M_{CO}}{M_C}\right)k_{dC}\left(X_C - X_C^{eq}\right) + 2M_{CO}k_{AIR1}k_{PR}x_{14} \quad (3\text{-}26)$$

$$\dot{x}_9 = \frac{M_{CO} d_5}{M_C} - \frac{[(2K_M/t_d\tau_1\tau_2)x_{15} - (K_M/\tau_1\tau_2)x_{16}]h_d x_9}{(k_U u_2 + h_d)(x_9 + x_{10} + x_{11})} + \left(\frac{M_{CO}}{M_C}\right)k_{dC}\left(X_C - X_C^{eq}\right) - \frac{k_{PR}x_{14}x_9}{(x_9 + x_{10} + x_{11})} \quad (3\text{-}27)$$

### 3.3.10 Carbon-dioxide in Furnace Gas-phase

The $CO_2$ equation has 2 components:

- The rate of CO combustion to $CO_2$.
- The rate of $CO_2$ extraction from the furnace through the off-gas door.

The rate of CO combustion to $CO_2$ is the negative of equation (3-24), with $M_{CO2}$ replacing $M_{CO}$. The rate of $CO_2$ extraction from the furnace is the same fraction of the total gas extraction as the $CO_2$ fraction of the gas composition in the furnace. The total gas extraction was discussed in the previous section and is explained in more detail in Section 3.4. Combining the two components as discussed, the equation for the rate of change of $CO_2$ in the gas-phase is obtained. Equation (3-28) is used for negative relative pressure and equation (3-29) for positive relative pressure.

$$\dot{x}_{10} = -\frac{[(2K_M/t_d\tau_1\tau_2)x_{15} - (K_M/\tau_1\tau_2)x_{16}]h_d x_{10}}{(k_U u_2 + h_d)(x_9 + x_{10} + x_{11})} - 2M_{CO2}k_{AIR1}k_{PR}x_{14} \quad (3\text{-}28)$$

$$\dot{x}_{10} = -\frac{[(2K_M/t_d\tau_1\tau_2)x_{15} - (K_M/\tau_1\tau_2)x_{16}]h_d x_{10}}{(k_U u_2 + h_d)(x_9 + x_{10} + x_{11})} - \frac{k_{PR}x_{14}x_{10}}{(x_9 + x_{10} + x_{11})} \quad (3\text{-}29)$$

### 3.3.11 Nitrogen in Furnace Gas-phase

The $N_2$ equation has 3 components:

- The rate of $N_2$ leaking into the furnace.
- The rate of $N_2$ blown into the furnace by the graphite injection system.
- The rate of $N_2$ extraction from the furnace through the off-gas door.

The rate of $N_2$ leaking into the furnace is proportional to the relative pressure in the furnace.

$$M_{N2}k_{AIR2}k_{PR}x_{14} \quad (3\text{-}30)$$

The rate of $N_2$ blown into the EAF by the graphite injection system is a fraction of the graphite injection rate. For every 150 kg graphite that is injected 1 kg of $N_2$ is injected as carrier gas.

The rate of $N_2$ extraction from the furnace is the same fraction of the total gas extraction as the $N_2$ fraction of the gas composition in the furnace. The total gas extraction was discussed in Subsection 3.3.9 and is explained in more detail in Section 3.4. Combining the two components, the equation for the rate of change of $N_2$ in the gas-phase is obtained. Equation (3-31) is for negative relative pressure and (3-32) for positive relative pressure:

$$\dot{x}_{11} = -\frac{[(2K_M/t_d\tau_1\tau_2)x_{15} - (K_M/\tau_1\tau_2)x_{16}]h_d x_{11}}{(k_U u_2 + h_d)(x_9 + x_{10} + x_{11})} - M_{N2}k_{AIR2}k_{PR}x_{14} + \frac{w_2}{150} \quad (3\text{-}31)$$

$$\dot{x}_{11} = -\frac{[(2K_M/t_d\tau_1\tau_2)x_{15} - (K_M/\tau_1\tau_2)x_{16}]h_d x_{11}}{(k_U u_2 + h_d)(x_9 + x_{10} + x_{11})} - \frac{k_{PR}x_{14}x_{11}}{(x_9 + x_{10} + x_{11})} + \frac{w_2}{150} \quad (3\text{-}32)$$

### 3.3.12 Temperature of Liquid Metal

The total amount of power generated in the furnace is equal to the sum of all power sources and losses. The power loss through the water-cooled furnace wall is assumed to be proportional to the temperature difference between the bath temperature and the atmospheric temperature. The total power is equal to $(p_t + v_2 - k_{VT}x_{12})$ where $p_t$ is a function of the power released by chemical reactions, power consumed by heating up the elements in the furnace, and power loss to melt scrap. Variable $v_2$ is the electric arc power. The function $p_t$ will be discussed in Subsection 4.15. The rate of temperature change of the liquid metal is the total power divided by the heat capacity of all the elements that are heated up to the liquid metal temperature. It is assumed that the heat transfer between the liquid metal and the slag is sufficiently fast that the slag and the liquid metal are at the same temperature. The equation for the rate of temperature change is then:

$$\dot{x}_{12} = \frac{p_t + v_2 - k_{VT}.(x_{12} - T_{air})}{\frac{x_2 C_p(Fe_{(L)})}{M_{Fe}} + \frac{x_3 C_p(C)}{M_C} + \frac{x_4 C_p(Si)}{M_{Si}} + \frac{(2x_6 + 2x_7 + 3x_8)}{M_{slag}} C_p(Slag_{(L)})} \quad (3\text{-}33)$$

$C_p(Slag_{(L)})$ is obtained from the enthalpy equation for liquid steelmaking slag [33].

$$H_T = -356.31 + 0.0405T \text{ kJ/g-atom} \quad (3\text{-}34)$$

### 3.3.13 Scrap and Solid Slag Temperature

The liquid metal heats the scrap and the solid slag. The heat transfer is proportional to the temperature difference between the liquid metal and the scrap. The heat transfer coefficients are $k_{therl} = 0.24$ kW.K$^{-1}$.m$^{-2}$ for scrap and $k_{ther5} = 0.0125$ kW.K$^{-1}$.m$^{-2}$ for solid slag. The constants $k_{areal} = 0.005$ m$^2$.kg$^{-1}$ for scrap and $k_{area5} = 0.12$ m$^2$.kg$^{-1}$ for solid slag are used. The heat that is transferred divided by the heat capacity gives the rate of change for the scrap and solid slag temperature:

$$\dot{x}_{13} = \frac{\left[k_{Ther1}k_{Area1}x_1(x_{12}-x_{13}) + k_{Ther5}k_{Area5}x_5(x_{12}-x_{13})\right]\left(1-\sqrt{x_{13}/x_{12}}\right)}{x_1 Cp(Fe_{(S)})/M_{Fe} + 2x_5 Cp(Slag_{(S)})/M_{Slag}} \quad (3\text{-}35)$$

$C_p(Slag_{(S)})$ is obtained from the enthalpy equation for solid steelmaking slag [33].

$$H_T = -348.35 + 0.03T \text{ kJ/g-atom} \quad (3\text{-}36)$$

### 3.3.14 Relative Pressure

To get the rate of change for the relative pressure, it is assumed that the atmospheric pressure remains constant. The rate of change of the relative pressure is then only dependent on the rate of change of the furnace pressure and is thus independent of the atmospheric pressure. One approach to obtain an equation for the rate of change of pressure is to use the ideal gas law, to solve it for pressure, and then take the first derivative with respect to time. In doing this, for simplicity it is assumed that the freeboard volume remains constant. Then only the molar quantity and the temperature rates have to be considered. Since the freeboard volume (175 $m^3$) is large with respect to the volume of the solids and liquids in the furnace, this is acceptable. For temperature variation, multiply the function $f_{12}$ by the molar quantity. When the molar quantity is considered, add the functions $f_9$, $f_{10}$ and $f_{11}$ and then multiply by the current temperature. Multiply both parts with the universal gas constant R, and divide both with the freeboard volume.

When all the components of the equation are combined, the rate of change for the relative pressure is obtained:

$$\dot{x}_{14} = \left(\frac{x_9}{M_{CO}} + \frac{x_{10}}{M_{CO_2}} + \frac{x_{11}}{M_{N_2}}\right)\frac{Rf_{12}}{Vol} + \frac{Rx_{12}}{Vol}(f_9 + f_{10} + f_{11}) \quad (3\text{-}37)$$

$f_9$ to $f_{12}$ are given in Subsections 3.3.9 to 3.3.12, they are the actual differential equation functions of the states $x_9$ to $x_{12}$.

### 3.3.15 Thermo-chemical Energy Exchange

Enthalpies of formation, molar heats of fusion, and molar heat capacities were obtained from Kubaschewski [32]. These are usually temperature dependent, and average values for the relevant temperature range are used. Square brackets indicate that the reagent/product is in solution, and for these the enthalpy of solution must be taken into account.

The average enthalpy of formation for CO is $\Delta H_{CO}$ = -117 kJ/mol, and for compositions 0% to 4% C in liquid Fe solution, $\Delta H_{C\_S}$ = 27 kJ/mol [34]. The average enthalpy of formation from elements for $CO_2$ is $\Delta H_{CO2}$ = -396 kJ/mol.

Since the activity coefficient of FeO is not a strong function of temperature [31] it can be assumed that the enthalpy of solution for FeO in the slag is sufficiently small to be ignored. The average enthalpy of formation for FeO is $\Delta H_{FeO}$ = -243 kJ/mol.

The average enthalpy of formation for $SiO_2$ is $\Delta H_{SiO2}$ = -946 kJ/mol. For low Si in liquid Fe the enthalpy of solution is $\Delta H_{Si\_S}$ = -132 kJ/mol [35]. The average enthalpy of solution for $SiO_2$ in slag is $\Delta H_{SiO2\_S}$ = -45 kJ/mol.

Equations (3-38) to (3-49) give the thermo-chemical heat equations. In each case $\Delta H_{**}$ is the enthalpy of formation from elements except where it is indicated by an underscore (_s) used for enthalpy of solution. (Elements and products are at a temperature of 1680 K, see assumption 16.)

$p_1$ = reaction ([C] + [FeO] → Fe + CO)

$$p_1 = (\Delta H_{C\_S} + \Delta H_{FeO} - \Delta H_{CO})(k_{dC}/M_C)(X_C - X_C^{eq}) \tag{3-38}$$

$X_C$ and $X_C^{eq}$ are given by equations (3-8) and (3-9) respectively.

$p_2$ = reaction (Fe + ½ $O_2$ → FeO)

$$p_2 = -(\Delta H_{FeO})2v_1/M_{O_2} \tag{3-39}$$

$p_3$ = reaction (CO + ½ $O_2$ → $CO_2$)

$$p_3 = -(\Delta H_{CO2} - \Delta H_{CO})(2k_{air1})(k_{PR}x_{14}) \tag{3-40}$$

$p_4$ = reaction ([Si] + [FeO] → Fe + [$SiO_2$])

$$p_4 = (\Delta H_{Si\_S} - \Delta H_{SiO_2} - \Delta H_{SiO_2\_S})(k_{dSi}/M_{Si})(X_{Si} - X_{Si}^{eq}) \tag{3-41}$$

Equations (3-15) and (3-16) give $X_{Si}$ and $X_{Si}^{eq}$ respectively.

$p_5$ = heating loss to oxygen stream

$$p_5 = -(v_1/M_{O2})(x_{12} - T_{O2})C_P(O_2) \tag{3-42}$$

$p_6$ = heating loss to oxygen in leak-air stream

$$p_6 = -k_{air1}k_{PR}x_{14}(x_{12} - T_{AIR})C_P(O_2) \tag{3-43}$$

$p_7$ = heating loss to nitrogen in leak-air stream

$$p_7 = -k_{air2}k_{PR}x_{14}(x_{12} - T_{AIR})C_P(N_2) \tag{3-44}$$

$p_8$ = heating loss to Slag stream

$$p_8 = -2w_1Cp(Slag_{(S)})(x_{13} - T_{Slag})/M_{slag} \tag{3-45}$$

$p_9$ = heating loss to DRI stream

$$p_9 = -0.825v_3\frac{\lambda_F(Fe) + Cp(Fe_{(S)})(x_{12} - T_{DRI})}{M_{Fe}} \tag{3-46}$$

$p_{10}$ = heating and melting loss to solid steel and solid slag

$$\begin{aligned} p_{10} &= -k_{Ther1}k_{Area1}x_1(x_{12} - x_{13}) \\ &\quad - k_{Ther5}k_{Area5}x_5(x_{12} - x_{13}) \end{aligned} \tag{3-47}$$

$p_{11}$ = heat of reaction ( C + [FeO] → Fe + CO ) from graphite injection

$$p_{11} = \frac{x_7k_{gr}w_2(\Delta H_{FeO} - \Delta H_{CO})}{(x_6 + x_7 + x_8)M_C} \tag{3-48}$$

$$p_t = p_1 + p_2 + p_3 + p_4 + p_5 + p_6 + p_7 + p_8 + p_9 + p_{10} + p_{11} \tag{3-49}$$

## 3.4 OFF-GAS MODEL INCORPORATION

The off-gas model will be treated in Chapter 4, but it is necessary to give a short description of it here, to show how it is incorporated into this model. In transfer function form, the off-gas model consists of a transfer function with two poles and dead time. The transfer function form is shown in equation (3-50).

$$\dot{m}(s) = \frac{K_M e^{-t_d s}}{(\tau_1 s + 1)(\tau_2 s + 1)}P(s) \tag{3-50}$$

After applying a Padé approximation to the dead-time function and converting the system from transfer function format to state-space format three states are added to the state space, $x_{15}$ to $x_{17}$. Their equations are given here:

$$\dot{x}_{15} = x_{16} \tag{3-51}$$

$$\dot{x}_{16} = x_{17} \tag{3-52}$$

$$\dot{x}_{17} = -2/(t_d\tau_1\tau_2)x_{15} - (2\tau_1 + 2\tau_2 + \tau_d)/(t_d\tau_1\tau_2)x_{16} - (1/\tau_1 + 1/\tau_2 + 2/t_d)x_{17} + u_1 \tag{3-53}$$

The equivalent mass-flow rate in the water-cooled duct is then given by equation (3-54):

$$\dot{m} = [2K_M/(t_d\tau_1\tau_2)]x_{15} - [K_M/(\tau_1\tau_2)]x_{16} \tag{3-54}$$

Expressed as fraction of $\dot{m}$, the rate of gas extraction from the EAF is:

$$\frac{h_d}{k_U u_2 + h_d} \tag{3-55}$$

When equations (3-54) and (3-55) are combined they give the gas extraction rate from the EAF:

$$\frac{h_d\left[(2K_M/t_d\tau_1\tau_2)x_{15} - (K_M/\tau_1\tau_2)x_{16}\right]}{k_U u_2 + h_d} \tag{3-56}$$

The complete derivation of this relationship is given in Chapter 4.

## 3.5 CONCLUSION

The set of simplifying assumptions was given to facilitate the modelling effort. The derivation of the EAF model was shown in detail. Each state variable was associated with an appropriate differential equation. The use of thermodynamic and chemical first principles was discussed. The use of empirical relations asserted by industry experts and adjustable coefficients were also discussed. The incorporation of the off-gas model into a combined model was shown.

# CHAPTER 4: OFF-GAS MODEL

## 4.1 INTRODUCTION

An excellent approach to off-gas modelling would be to make use of CFD (Computational Fluid Dynamics). This approach is rigorous, and gives very accurate results. Unfortunately it also requires much expertise in the specific field, as well as much resources in terms of computation time. The derivation of a complete CFD model is outside the scope of this dissertation. Instead, an approximate transfer function model is derived using an alternate approach. The purpose with the off-gas model is to describe the dynamic behavior of the mass-flow of gas in the off-gas duct of the electric arc furnace. Off-gas duct design drawings for the furnace under study were used in the derivation of the off-gas model. An approximate illustration of the design drawings is given in Fig.4.1. Data from the design drawings relevant to the model derivation is given in Table 4.1.

The model accepts as input the electric power applied to the force draught fan motor in the off-gas system, and also the slip-gap width in the water-cooled duct. The model then calculates the mass-flow of gas resulting from the fan power. It also divides the mass-flow into two separate flows, namely, that which enters through the slip-gap and that which enters the duct from the EAF. Based on these flows, the temperature at the end of the cooling duct is calculated, and the composition of gas (% carbon monoxide) is calculated. The cross hair in Fig.4.1 indicates the location where the off-gas composition and temperature is under study.

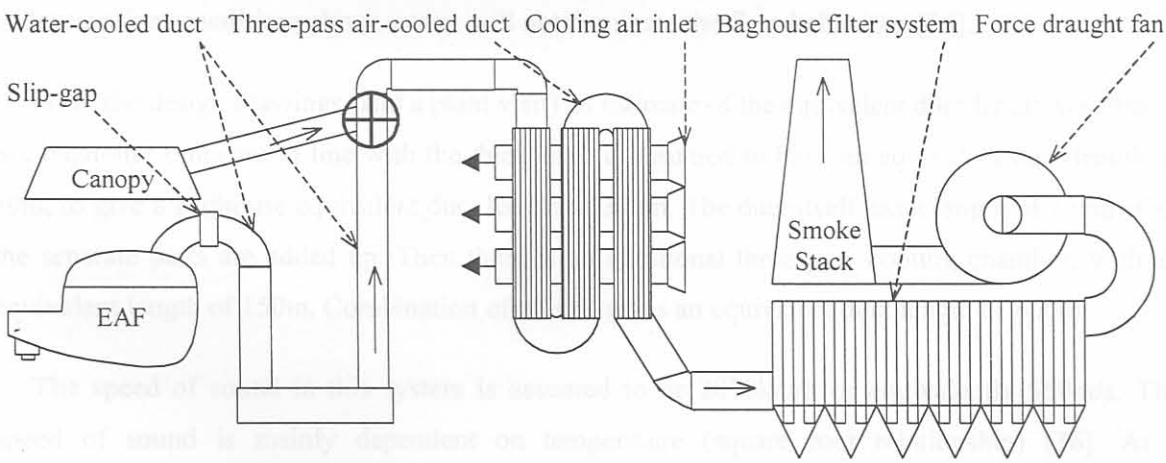


Figure 4.1 Off-gas system, with end of water-cooled duct marked

In Section 4.2 a transfer function model for the off-gas system is derived. First the necessary assumptions with respect to the steady state gain, time delay and time constants are given. Then the model approximation is discussed. In Section 4.3 the state space model is derived from the transfer function model. In Section 4.4 the mass-flow division at the slip-gap is discussed. Finally, in Section 4.5, the off-gas composition and temperature relations are derived.

## 4.2 TRANSFER FUNCTION MODEL

In the process industry, most SISO (single-input, single-output) processes can be represented by a first order transfer function (denominator is a first order polynomial) with time delay. The off-gas system is treated as two first order systems. Combination of the two systems yield a second order transfer function with time delay. One first order system relates the extraction fan power input and the relative pressure. The other first order system relates the relative pressure and the mass-flow. The time constants and the delay are related to the physical dimensions of the system.

### 4.2.1 Model Assumptions

#### *4.2.1.1 Steady-state Gain*

A constant steady-state gain from fan power input to mass-flow is assumed. The gain would vary depending on the pressure difference between the fan entrance and atmosphere, or on the condition of the baghouse. For this dissertation the steady-state gain is assumed as 11 $(kg.s^{-1})$/MW.

#### *4.2.1.2 Time Delay*

The transfer function time delay is given by the quotient of the equivalent duct length and the speed of sound in air, as the force waves travel at the speed of sound. Shock waves are not considered, because the system under consideration will normally be at steady state, and even under transient conditions shock waves will not dominate the flow behaviour [36].

From the design drawings (and a plant visit) an estimate of the equivalent duct length was made. Six baghouse units are in line with the duct, each is assumed to have an equivalent duct length of 50m, to give a baghouse equivalent duct length of 300m. The duct itself has a length of 150m if all the separate parts are added up. Then there is an additional three-pass cooling chamber, with an equivalent length of 150m. Combination of all this gives an equivalent duct length of 600m.

The speed of sound in this system is assumed to be 2070km/h or equivalently 550m/s. The speed of sound is mainly dependent on temperature (square root relationship) [36]. At a temperature of 800K the speed of sound is 568.5m/s (2047km/h) while at 300K it is 348m/s (1253km/h). With the velocity of sound 550m/s and the equivalent duct length 600m the corresponding time delay is then equal to 1.09s.

*4.2.1.3 Time Constants*

For the time constant relating the extraction fan force to the duct relative pressure the same dimensions are considered as with the time delay. Due to the inertia and friction in the off-gas system, the gas in the off-gas duct flows with a velocity of eighteen times slower than the speed of sound. The motivation for this assumption stems from the worst case steady state analysis given in the design drawings. The applicable data is given in Table 4.1:

Table 4.1: Off-gas flow data

| Location | Water-cooled duct entrance | Water-cooled duct exit |
|---|---|---|
| Mass Flow | 143674 kg/h = 39.9 kg/s | 143674 kg/h = 39.9 kg/s |
| Temperature | 1425 K | 879 K |
| Density | 0.23 kg/m$^3$ | 0.37 kg/m$^3$ |
| Volume Flow | 173.48 m$^3$/s | 107.84 m$^3$/s |
| Duct Area | 4.3 m$^2$ | 5.8 m$^2$ |
| Flow Velocity | 40.3 m/s | 18.6 m/s |

The data given in Table 4.1 is regarded as a worst case scenario. As is apparent from the data, the average flow velocity is 29 m/s. This is about 18 times slower than the speed of sound in this environment. This justifies the assumption that under steady state conditions the flow velocity is eighteen times slower than the speed of sound. The corresponding time constant is then assumed to be eighteen to twenty times as large as the time delay. For a first order transfer function without time delay, the time constant is the time that the output response takes to reach 63% of its final value in reaction to a step input change. Using an average time delay of 1.09s the time constant is assumed to be 19.6s. Where the time delay was determined from the speed of sound, the time constant is determined from the speed of flow.

The time constant that relates the relative pressure to the mass-flow is much shorter since the cooling duct length is much shorter. As can be calculated from Fig.2.2 the length of the cooling duct is approximately 45m. The time constant corresponding to this length is 1.5s.

### 4.2.2 Model Approximation

The transfer function model has two factors in the denominator, a steady state gain and a time delay function as in equation (4-1):

$$\dot{m}(s) = \frac{K_M e^{-t_d s}}{(\tau_1 s + 1)(\tau_2 s + 1)} u_1(s) \qquad (4\text{-}1)$$

A first order Padé approximation [21] is made to approximate the time delay. Since one of the time constants will always be at least ten times larger than the time delay, this is deemed to be an acceptable approximation. The first order Padé approximation for time delay is:

$$e^{-t_d s} = \frac{1-0.5t_d s}{1+0.5t_d s} \tag{4-2}$$

This approximation is substituted into equation (4-1) to obtain the approximated transfer function:

$$\dot{m}(s) = \frac{K_M(1-0.5t_d s)}{(1+0.5t_d s)(\tau_1\tau_2 s^2 + (\tau_1+\tau_2)s+1)} u_1(s) \tag{4-3}$$

When the factors in the numerator and denominator are multiplied out, the result is:

$$\dot{m}(s) = \frac{K_M - 0.5K_M t_d s}{((0.5t_d\tau_1\tau_2)s^3 + (0.5t_d(\tau_1+\tau_2)+\tau_1\tau_2)s^2 + (\tau_1+\tau_2+0.5t_d)s+1)} u_1(s) \tag{4-4}$$

When the coefficient of the $s^3$-term in the denominator is divided out, the result is:

$$\dot{m}(s) = \frac{(2K_M/t_d\tau_1\tau_2) - (K_M/\tau_1\tau_2)s}{(s^3 + (1/\tau_1 + 1/\tau_2 + 2/t_d)s^2 + ((2\tau_1+2\tau_2+t_d)/(t_d\tau_1\tau_2))s + 2/(t_d\tau_1\tau_2))} u_1(s) \tag{4-5}$$

## 4.3 STATE SPACE MODEL

Since the main model in the previous chapter is derived as a state-space model it is logical to convert this transfer function model to an equivalent state-space model. The desired state space model is given in equation (4-6):

$$\begin{aligned} \frac{d(\delta \mathbf{x}(t))}{dt} &= \mathbf{A}.\delta\mathbf{x}(t) + \mathbf{B}.\delta\mathbf{u}(t) \\ \mathbf{y}(t) &= \mathbf{C}.\delta\mathbf{x}(t) + \mathbf{D}.\delta\mathbf{u}(t) \end{aligned} \tag{4-6}$$

The matrices are in the companion (Luenberger's second controllable canonical-) form [37]:

$$\mathbf{A} = \begin{bmatrix} 0 & 1 & 0 \\ 0 & 0 & 1 \\ -a_1 & -a_2 & -a_3 \end{bmatrix} \quad \mathbf{B} = \begin{bmatrix} 0 \\ 0 \\ 1 \end{bmatrix} \quad \mathbf{C} = [c_1 \;\; c_2 \;\; c_3] \quad D = 0 \tag{4-7}$$

The plant SISO transfer function can be obtained from the state space model in companion form. The output y is the mass flow $\dot{m}$ in equation (4-1). Then the SISO equation is:

$$y = G_p(s)u_1 \tag{4-8}$$

which is the same as equation (4-1). The transfer function $G_p(s)$ is obtained from the state space companion form as in equation (4-9):

$$G_p(s) = \mathbf{C}[s\mathbf{I}-\mathbf{A}]^{-1}\mathbf{B}+D \tag{4-9}$$

After matrix inversion and matrix multiplication the result is:

$$G_p = \frac{c_1 + c_2 s + c_3 s^2}{s^3 + a_3 s^2 + a_2 s + a_1} \tag{4-10}$$

Now equation (4-10) and equation (4-5) are equated and the various coefficients are determined:

$c_1 = 2K_M/(t_d\tau_1\tau_2)$; $c_2 = -K_M/(\tau_1\tau_2)$; $c_3 = 0$;

$a_1 = 2/(t_d\tau_1\tau_2)$; $a_2 = (2\tau_1 + 2\tau_2 + t_d)/(t_d\tau_1\tau_2)$; $a_3 = (1/\tau_1 + 1/\tau_2 + 2/t_d)$.

A similar derivation is given in [38]. In order to incorporate this into the model, three states, $x_{15}$ to $x_{17}$, are added to the state space. The output of these three state equations is the mass flow given by $y = c_1x_{15}+c_2x_{16}$. The equations for $x_{15}$ to $x_{17}$ are:

$$\dot{x}_{15} = x_{16} \tag{4-11}$$

$$\dot{x}_{16} = x_{17} \tag{4-12}$$

$$\dot{x}_{17} = -2/(t_d\tau_1\tau_2)x_{15} - (2\tau_1 + 2\tau_2 + \tau_d)/(t_d\tau_1\tau_2)x_{16} - (1/\tau_1 + 1/\tau_2 + 2/t_d)x_{17} + u_1 \tag{4-13}$$

The equivalent mass flow in the cooling duct is then given by equation (4-14):

$$\dot{m} = (2K_M/(t_d\tau_1\tau_2))x_{15} - (K_M/(\tau_1\tau_2))x_{16} \tag{4-14}$$

## 4.4 MASS-FLOW DIVISION

At the slip-gap air is entrained from the atmosphere to combust the CO remaining in the extracted EAF gas, and to cool the off-gas. The duct area at the slip gap has a characteristic dimension $h_d$. The slip gap width ($u_2$) is the other manipulated variable and is the characteristic dimension of the slip-gap area. Fig.4.2 gives a close look at the slip-gap structure:

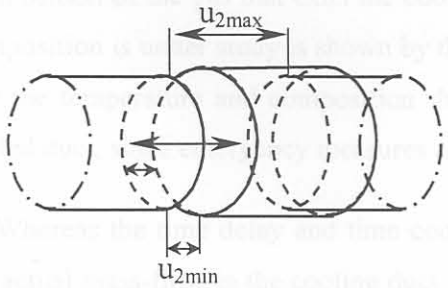


Fig.4.2 Slip-gap Structure

The flow rate through each area is proportional to the ratio of the respective characteristic dimension to the sum of the characteristic dimensions. Expressed as a fraction of $\dot{m}$, the rate of gas extraction from the EAF is:

$$\frac{h_d}{k_U u_2 + h_d} \tag{4-15}$$

To improve the approximation a dimensionless constant $k_U$ is used to adjust the influence of $u_2$. The mass-flow through the EAF gas exit is then given by equation (4-16), while the mass-flow through the slip-gap is given by equation (4-17).

$$\dot{m}_{EAF} = \frac{h_d\left((2K_M/t_d\tau_1\tau_2)x_{15} - (K_M/\tau_1\tau_2)x_{16}\right)}{k_U u_2 + h_d} \tag{4-16}$$

$$\dot{m}_{air} = \frac{k_U u_2\left((2K_M/t_d\tau_1\tau_2)x_{15} - (K_M/\tau_1\tau_2)x_{16}\right)}{k_U u_2 + h_d} \tag{4-17}$$

## 4.5 OFF-GAS TEMPERATURE AND COMPOSITION

In the duct the off-gas from the furnace mixes with the air from the atmosphere that enters at the slip-gap. The carbon monoxide combusts with oxygen that enters with the air. The fraction of carbon monoxide that combusts is determined by the temperature, pressure and concentrations of oxygen and carbon monoxide in the mixed gas in the cooling duct [39].

The temperature of the gas at the end of the cooling duct is determined by the amount of air that is mixed with the EAF gas. It is also determined by the initial EAF gas temperature, the combustion of carbon monoxide in the duct and the amount of cooling done by the cooling water in the walls of the duct. Since the cooling duct has a length of approximately 45m there is a time delay between when gas enters and exits the cooling duct. This time delay is not determined by the velocity of sound, but by the velocity of the gas flow in the cooling duct.

Note that the cooling duct temperature and gas composition refer to the temperature and composition of the gas that exits the cooling duct. The location where the off-gas temperature and composition is under study is shown by the cross hair in Fig.4.1. The motivation for this location is that the temperature and composition should be monitored and controlled in advance of the air-cooled duct, since emergency measures are available to operators to prevent baghouse explosions.

Whereas the time delay and time constants derived in Section 4.2 were necessary to calculate the actual mass-flow in the cooling duct, the time delay in this case is dependent on the magnitude of mass-flow in the cooling duct. Previously approximations to determine the mechanism that

causes mass-flow had to be relied on. In this case the time delay can be calculated precisely from the knowledge of the actual mass-flow, the geometry of the cooling duct and the state (pressure and temperature) of the gas in the cooling duct. In the following three sub-sections algebraic equations will be developed to give the time delay resulting from the actual mass-flow, and then the composition and temperature of the gas that exits the cooling duct.

### 4.5.1 Composition and Temperature Time Delay

To calculate the off-gas temperature at the entrance of the water-cooled duct, an average between the air temperature and the EAF temperature is taken, based on the ratio of mass-flows:

$$T_{mixed} = \frac{T_{air} k_U u_2 + x_{12} h_d}{k_U u_2 + h_d} \tag{4-18}$$

The cross sectional area of the cooling duct is $5.2m^2$ on average. The density ($\rho$) of the gas [$kg/m^3$] is calculated using equation (4-19), where $M_{Gas}$ is an average molar mass of the gas in the duct and $T_{mixed}$ is the average temperature of the mixed gas before combustion. P is the absolute pressure, and R is the universal gas constant:

$$\rho = \frac{M_{Gas} P}{R T_{mixed}} \tag{4-19}$$

The velocity of flow (v) can be calculated from the density, mass-flow and cross sectional area. This is shown in equation (4-20):

$$v = \frac{\dot{m}}{\rho A} \tag{4-20}$$

Substitute equations (4-19) and (4-14) into equation (4-20) to get the equation for the actual velocity of flow:

$$v = \left(R T_{mixed} \left((2 K_M / t_d \tau_1 \tau_2) x_{15} - (K_M / \tau_1 \tau_2) x_{16}\right)\right) / A M_{Gas} P \tag{4-21}$$

The time delay is equal to the length of the cooling duct divided by the velocity of flow:

$$t_{tcd} = L / v \tag{4-22}$$

Substitute equation (4-21) into (4-22) to obtain the final equation for the time delay:

$$t_{tcd} = A L M_{Gas} P / \left(R T_{mixed} \left((2 K_M / t_d \tau_1 \tau_2) x_{15} - (K_M / \tau_1 \tau_2) x_{16}\right)\right) \tag{4-23}$$

### 4.5.2 Cooling Duct Exit Composition

The composition of the off-gas at the cooling duct exit is determined by the amount of CO that combusted since the off-gas was mixed with air. The rate of reaction is dependent on the temperature, mol-fraction CO and mol-fraction $O_2$. The time delay limits the time the reaction has to take place. The assumption here is that no combustion can occur after the gas exits the cooling-duct. Once again, this is a worst case approximation.

The mol-fractions of CO and $O_2$ are given by equations (4-24) and (4-25):

$$X_{CO} = \frac{x_9 h_d / M_{CO}}{(x_9/M_{CO} + x_{10}/M_{CO2} + x_{11}/M_{N2})(k_U u_2 + h_d)} \tag{4-24}$$

$$X_{O2} = \frac{0.2 k_U u_2}{(k_U u_2 + h_d)} \tag{4-25}$$

The fraction of CO ($QC_{CO}$) that will then combust in the cooling duct is given by equation (4-26) where $\gamma$ is given by equation (4-27). The natural exponential decay relationship is typical for this type of chemical reaction process.

$$QC_{CO} = 1 - e^{-\gamma} \tag{4-26}$$

$$\gamma = k_{combust} X_{CO} X_{O2} T_{mixed} t_{tcd} \tag{4-27}$$

To determine the rate constant $k_{combust}$ the values of the four variables were given their limiting values, and $QC_{CO}$ was set equal to 0.95, which is the highest value it should reach.

The limiting values (according to a steady state calculation) for the four variables were:

- $T_{mixed} = 1250$ K
- $t_{tcd} = 6$ s
- $X_{CO} = 0.28$
- $X_{O2} = 0.14$

This resulted in a value of $k_{combust} = 0.01\ K^{-1}s^{-1}$. The final CO fraction can be derived from equations (4-23) to (4-27). Note that the temperature in equation (4-23) is the same as $T_{mixed}$, and therefore cancels out. The final exit CO fraction is then:

$$FX_{CO} = \frac{x_9 h_d e^{-\gamma}}{(x_9 + x_{10} + x_{11})(k_U u_2 + h_d)} \tag{4-28}$$

Where $\gamma$ is given by:

$$\frac{0.2k_{combust}k_U u_2 x_9 h_d M_{Gas} L_{CD} A_{CS} P_{ABS}}{\left(R\left(\left(\frac{2K_M}{t_d\tau_1\tau_2}\right)x_{15}-\left(\frac{K_M}{\tau_1\tau_2}\right)x_{16}\right)\right)\left(\frac{x_9}{M_{CO}}+\frac{x_{10}}{M_{CO2}}+\frac{x_{11}}{M_{N2}}\right)M_{CO}(k_U u_2+h_d)^2} \quad (4\text{-}29)$$

### 4.5.3 Cooling Duct Exit Temperature

The cooling entrance temperature is given by equation (4-18). After the gas enters the cooling duct, it mixes and the carbon monoxide combusts with the oxygen which leads to an increase in the enthalpy. At the same time the forced circulation of cooling water through the duct walls extracts some of the heat. Both of these process rates are proportional to the temperature difference between the off-gas and the atmosphere (cooling water) and inversely proportional to the mass-flow. Since their mechanics are approximately the same, they can be treated in a single relationship. To justify this approximation, recall that in addition to the water-cooled duct, there is also a three-pass air-cooled duct before the off-gas enters the baghouse filter. Thus the water-cooled duct is not the last cooling stage, and the exit temperature is not critical, and an approximation suffices.

The temperature change of gas that flows from the cooling duct entrance to the exit is related to the heat rate of change (DH) in the cooling duct as in equation (4-30). (Units: [K])

$$DT = \frac{DH\, M_{gas}}{\dot{m}\, C_p(gas)} \quad (4\text{-}30)$$

The heat change is a combination of the cooling and combustion heats. The cooling heat ($DH_1$) and combustion heat rates ($DH_2$) are approximated as follows (Units: kJ/s):

$$DH_1 = k_{\Delta C1}\Delta T \quad (4\text{-}31)$$

$$DH_2 = k_{\Delta C2}\Delta T \quad (4\text{-}32)$$

These rate constants are determined for a specific example, and the two equations are then combined to give the effect of the cooling-duct conditions (cooling as well as combustion) on the off-gas temperature. For this purpose the data in Table 4.1 is used again.

Additional information is obtained from the design drawings. The heat removed between the duct entrance and exit was $DH_1$ = 39.8 MW = 39800 kJ/s. This value is given in the design drawing. The mass-flow rate is given in Table 4.1 (39.9 kg/s). The atmosphere (and also cooling water) is assumed to be at a temperature of 33°C. The off-gas temperature at the cooling duct entrance is identical with $T_{mixed}$ and is 1425 K = 1152°C. The temperature difference is then 1119 K. Substitute the necessary variables into equation (4-31), and the rate constant is $k_{\Delta C1}$ = -35.57 (kJ)/(sK). If only the cooling heat extraction is considered, the temperature change is:

$$DT = \frac{(39800\,kJ/s)}{(39.9\,kg/s)(0.034\,kJ/molK)}(0.032\,kg/mol) = 939\,K \quad (4\text{-}33)$$

Here the $C_p$ and M values of oxygen were used, since the gas is heavier after some combustion, and the average is comparable to oxygen. At the cooling entrance, the mixed gas has a temperature of 1152°C = 1425 K. If the combustion heat is ignored, then the temperature at the exit is supposed to be $T_{exit}$ = 1425 K – 939 K = 486 K = 213°C. However, this is not the case. The exit temperature (according to the limiting case in the design drawings) is 606°C, indicating that the combustion heat may not be ignored. The temperature change due to the combustion heat is then calculated as 606°C – 213°C = 393 K. The corresponding heat change is:

$$DH_2 = \frac{(393\,K)(39.9\,kg/s)(0.034\,kJ/molK)}{(0.032\,kg/mol)} = 16661\,kJ/s \quad (4\text{-}34)$$

From this the second rate constant can be obtained as $k_{\Delta C2}$ = 14.89 (kJ)/(sK). The combined rate constant is then $k_{\Delta C}$ = 14.89 – 35.57 = -20.68 (kJ)/(sK). The final equation for the temperature change is then given here in (4-35):

$$DT = \frac{k_{\Delta C}\Delta T\, M_{gas}}{\dot{m}\, C_p(gas)} \quad (4\text{-}35)$$

## 4.6 CONCLUSION

In this chapter the transfer function model for the off-gas system was derived. The necessary assumptions with respect to the steady state gain, time delay and time constants were given and then the model approximation was discussed. The state space model was derived from the transfer function model and the mass-flow division at the slip-gap was discussed. Finally, the off-gas composition and temperature relations were derived.

# CHAPTER 5: MODEL SIMULATION AND VERIFICATION

## 5.1 INTRODUCTION

The aim of this chapter is to verify the combined model with data from an actual tap. Data that was obtained from measurements at Iscor Vanderbijlpark works can be used to do this in two ways. Firstly, model input trajectories of supply materials and energy sources can be matched exactly to that of the actual tap. Secondly, parameters within the state space model can be adjusted to give comparable results. The applicable data is given in Appendix B.

As elements such as phosphorus and manganese are omitted from the model, the carbon and silicon impurities are slightly increased to account for the mass balance of oxidising reagents that would have reacted with the omitted elements had they been included. The same applies to FeO and $SiO_2$ since products such as $Fe_2O_3$ or $Al_2O_3$ are not included in the model.

In Section 5.2 the EAF operation is discussed. In Section 5.3 the disturbance model is developed. In Section 5.4 a simulation without model adjustment is shown. In Section 5.5 the method for model adjustment is discussed. In Section 5.6 the adjusted model simulation is compared to the actual tap data as well as the unadjusted model simulation.

## 5.2 EAF OPERATION

Conditions for the actual tap under consideration are described in this section. At the end of the previous tap 20 ton hot heel was left in the furnace, with negligible impurities. The following materials were added from two large vessels: (T = 0 when the arc is switched on for the first time.)

- 53.5 ton scrap of high purity type, with less than 0.5% impurities, added at T = -1 min;
- 8 ton burnt lime and 3.5 ton doloma, added together with the scrap at T = -1 min;
- 65 ton hot metal (Liquid), with 4.4% carbon and 1.1% silicon, added at T = 10 min.

The following materials were added continuously throughout the process at constant feed rates by means of conveyer belts (total values are given):

- 35 ton DRI in total, with 82.5% metalization, 4.5% $SiO_2$ and 13% FeO;
- 2.5 ton burnt lime in total, 1.5 ton doloma in total and 0.5 ton anthracite in total.

The following feeds were injected continuously throughout the process at constant feed rates by means of injection lances (total values are given):

- 0.1 ton graphite in total, with air used as the carrier gas;
- 4220 $Nm^3$ oxygen in total.

The total energy input was 70605 kWh. The total iron content of the added inputs is 144 ton, 53.5 ton from the scrap, 61.5 ton from the hot metal and 29 ton from the DRI. The hot heel is not taken into account, because at the end of this tap the same mass of hot heel will be left in the furnace. To verify that this particular tap is typical, the specific energy and oxygen consumption are compared to the industry average. This particular tap used 490.3 kWh/ton electrical energy and 29.3 $Nm^3$/ton oxygen which is close to the industry average (500 kWh/ton, 30 $Nm^3$/ton) [30,40].

The following is a selected list of events that describe the tap. Rates have been converted from their units in the data sheets to units of kg/s or MW:

- T = -1 min: Scrap, lime and doloma added;
- T = 0 min: Arc switched on, 48.9 MW;
- T = 4 min: Arc switched off;
- T = 10 min: Hot metal added;
- T = 15 min: Oxygen injection started, 2.1 kg/s;
- T = 17 min: Arc switched on, 48.9 MW;
- T = 22 min: Slag conveyer belt started, 1.21 kg/s slag and 0.15 kg/s anthracite;
- T = 33 min: Graphite injection started, 0.42 kg/s;
- T = 35 min: DRI conveyer belt started, 11.2 kg/s;
- T = 37 min: Graphite injection stopped;
- T = 56 min: DRI feed rate increased to 33.6 kg/s;
- T = 59 min: Oxygen injection stopped;
- T = 61 min: DRI feed rate reduced to 11.2 kg/s;
- T = 73 min: DRI feed rate increased to 22.4 kg/s;
- T = 75 min: DRI conveyer belt stopped;
- T = 77 min: Slag conveyer belt stopped;
- T = 82 min: Arc switched off;
- T = 83 min: Steel tapped.

## 5.3 DISTURBANCE MODEL

The simulation starts when the furnace roof is closed for the last time. On the event-list given above, this is done at T = 15 minutes, when the oxygen injection is started. Before this the furnace roof is pivoted open to allow the hot metal charge. During the charge the valve to the water-cooled duct is closed, while the valve to the overhead canopy is opened in order to capture gas escaping from the open EAF. While the overhead canopy is in use, it is not possible to do any control on the off-gas at all. In addition, the model does not apply to times when the EAF roof is open. Consequently, the simulation is only started at T = 15 minutes, when the furnace roof is closed and

the oxygen injection is started. At this time the valve to the water-cooled duct is opened, and the overhead canopy is no longer used. The total simulation time is 65 minutes (until T = 80 above).

The anthracite is added to the slag to react with the FeO and make the slag foam [30] in order to limit the nitrogen pickup in the steel. In this regard it has exactly the same role as the graphite injection. The anthracite is not pure carbon however, but consists of approximately 80% carbon and 15% ash. It also contains small percentages of oxygen, hydrogen and water. To accommodate this input in the model (the model assumes pure graphite injection), the anthracite is multiplied by a coefficient of 0.8 and added to the graphite injection. The ash and other impurities are ignored.

The power efficiency of the electrical system is assumed to be 80% [29], i.e. 80% of the energy input from the transformer reaches the steel melt. Consequently, the arc power is multiplied by a factor of 0.8 in the disturbance model. The disturbance model consists of the profiles for the disturbance inputs that are the same as for the actual EAF tap. Note that the simulation time is 15 minutes less than the actual tap time. The profiles for those inputs that are treated as disturbances in this dissertation are as follow:

- Fig.5.1 shows the profile for the electrical power (multiplied by efficiency factor, $\eta = 0.8$);
- Fig.5.2 shows the oxygen injection profile;
- Fig.5.3 shows the DRI charge rate profile;
- Fig.5.4 shows the slag charge rate profile;
- Fig.5.5 shows the equivalent carbon feed rate profile.

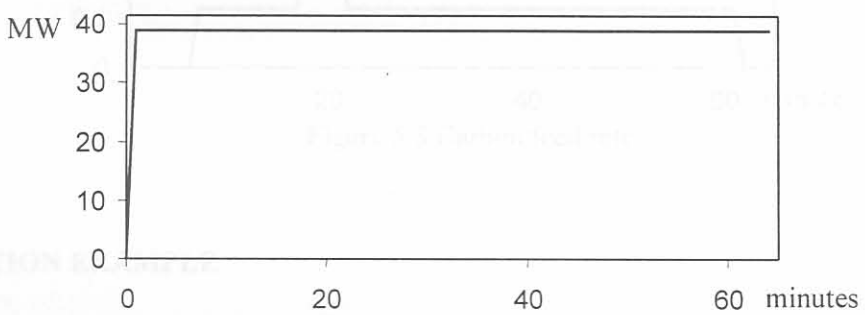


Figure 5.1 Arc electrical power input

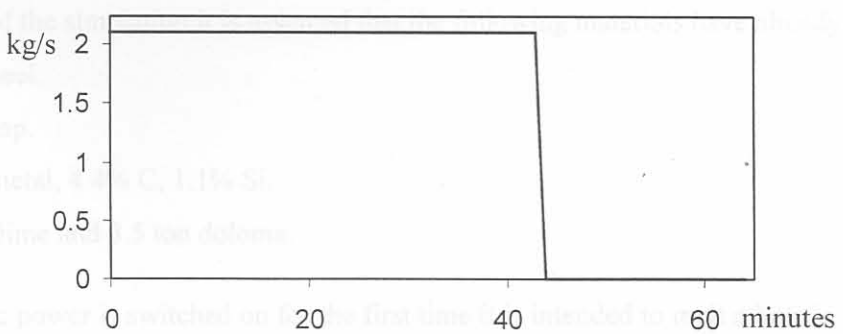


Figure 5.2 Oxygen injection

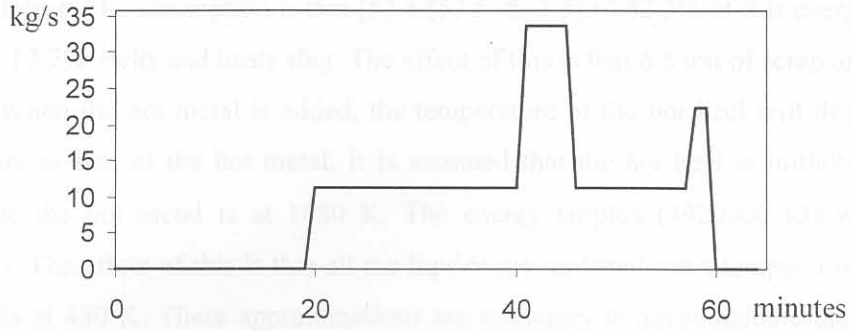


Figure 5.3 DRI charge rate

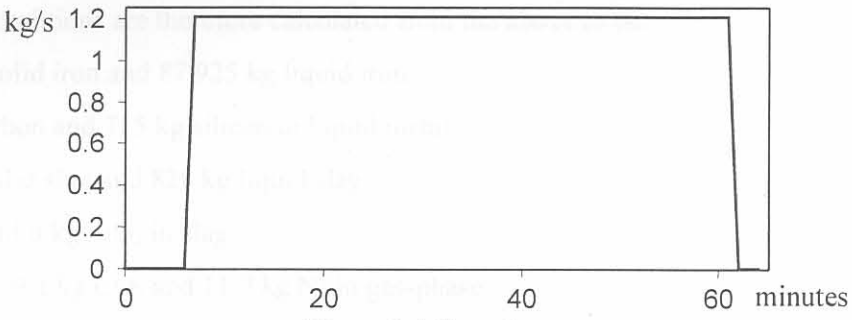


Figure 5.4 Slag charge rate

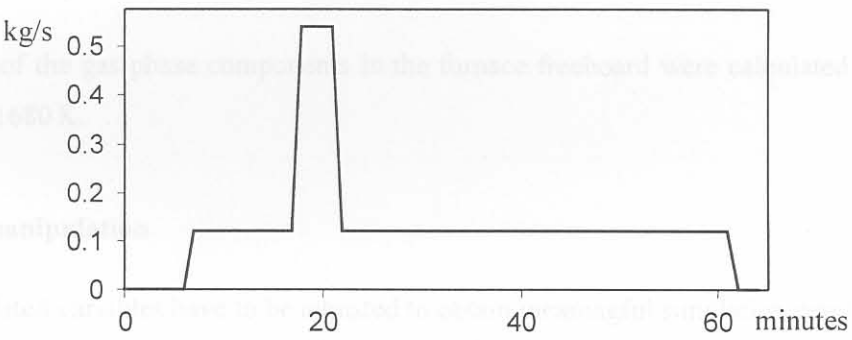


Figure 5.5 Carbon feed rate

## 5.4 SIMULATION EXAMPLE

### 5.4.1 Initial Conditions

At the start of the simulation it is assumed that the following materials have already been added:

- 20 ton hot heel.
- 53.5 ton scrap.
- 65 ton hot metal, 4.4% C, 1.1% Si.
- 8 ton burnt lime and 3.5 ton doloma.

When the arc power is switched on for the first time it is intended to melt a hole in the scrap. At this stage 9360000 kJ is delivered. The arc efficiency is already accounted for by using an

efficiency coefficient. The assumption is that (53.5/(53.5+8+3.5) =) 82.3% of this energy melts and heats scrap, and 17.7% melts and heats slag. The effect of this is that 6.5 ton of scrap and 820 kg of slag will melt. When the hot metal is added, the temperature of the hot heel will decrease to the same temperature as that of the hot metal. It is assumed that the hot heel is initially at 1980 K (~1707°C) while the hot metal is at 1680 K. The energy surplus (4920000 kJ) will heat the remaining solids. The effect of this is that all the liquids are uniformly at a temperature of 1680 K and all the solids at 480 K. These approximations are necessary to accommodate the actual EAF conditions within the framework of the model.

The initial conditions are therefore calculated from the above to be:

- 47 000 kg solid iron and 87 925 kg liquid iron
- 2860 kg carbon and 715 kg silicon in liquid metal
- 10680 kg solid slag and 820 kg liquid slag
- 0 kg FeO and 0 kg $SiO_2$ in slag
- 17.4 kg CO, 9.1 kg $CO_2$ and 11.7 kg $N_2$ in gas-phase
- Liquids at 1680 K and solids at 480 K
- Relative furnace pressure starting at 0 Pa.

The masses of the gas-phase components in the furnace freeboard were calculated assuming a temperature of 1680 K.

### 5.4.2 Off-gas manipulation

The manipulated variables have to be adjusted to obtain meaningful simulation results. The slip-gap size is kept constant at a value of 0.33 m. The fan power is kept at 0.8 MW until simulation time t = 50 minutes, when it is decreased to 0.4 MW.

### 5.4.3 Simulation results

Fig.5.6 shows the liquid metal mass and the scrap mass on the same graph. Note that the addition of DRI (t=41) directly increases the liquid metal mass. Before DRI addition it is evident that the rate of increase of liquid metal mass is equal to the rate of decrease of the scrap mass.

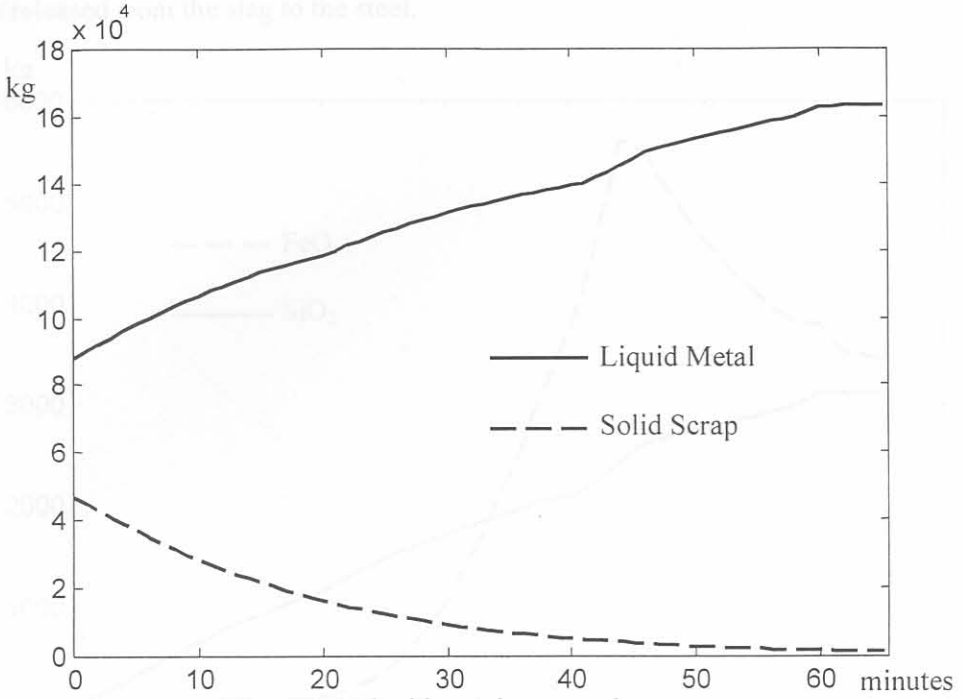


Figure 5.6 Liquid metal mass and scrap mass

Fig.5.7 shows the mass of carbon and silicon in solution in the liquid metal. Note that the silicon reaches the equilibrium concentration much quicker than the carbon. The explanation for this is simply that silicon is much more reactive in a basic slag environment.

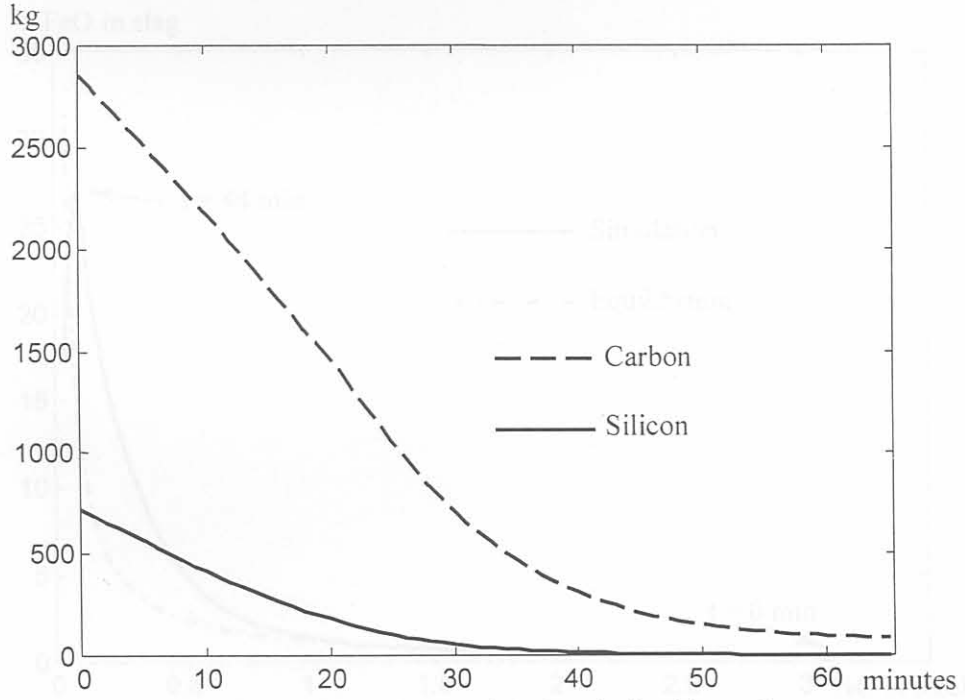


Figure 5.7 Silicon and Carbon in liquid metal

Fig.5.8 shows the $SiO_2$ and FeO in solution in the liquid slag. Note that the $SiO_2$ does not react with anything after it entered the slag-phase as the basic slag environment prevents silicon from re-entering the steel. However, the FeO reacts with carbon in the steel and in the graphite injection,

and iron is released from the slag to the steel.

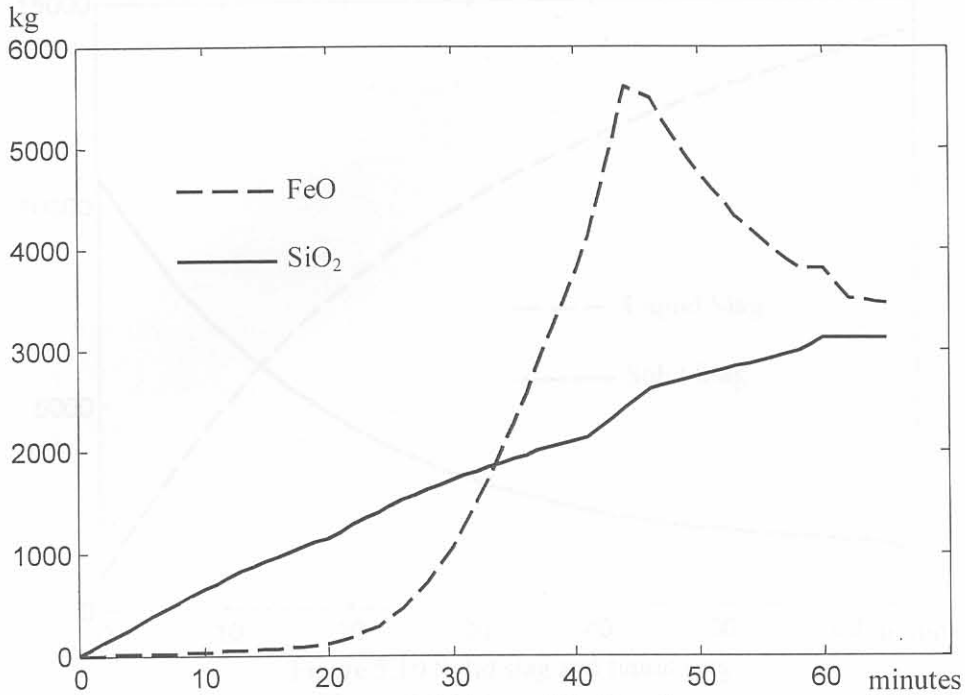


Figure 5.8 $SiO_2$ and FeO in slag

Fig.5.9 shows the relationship between the FeO mass percentage in the slag and the carbon mass percentage in the steel melt. The equilibrium relationship is shown on the same graph.

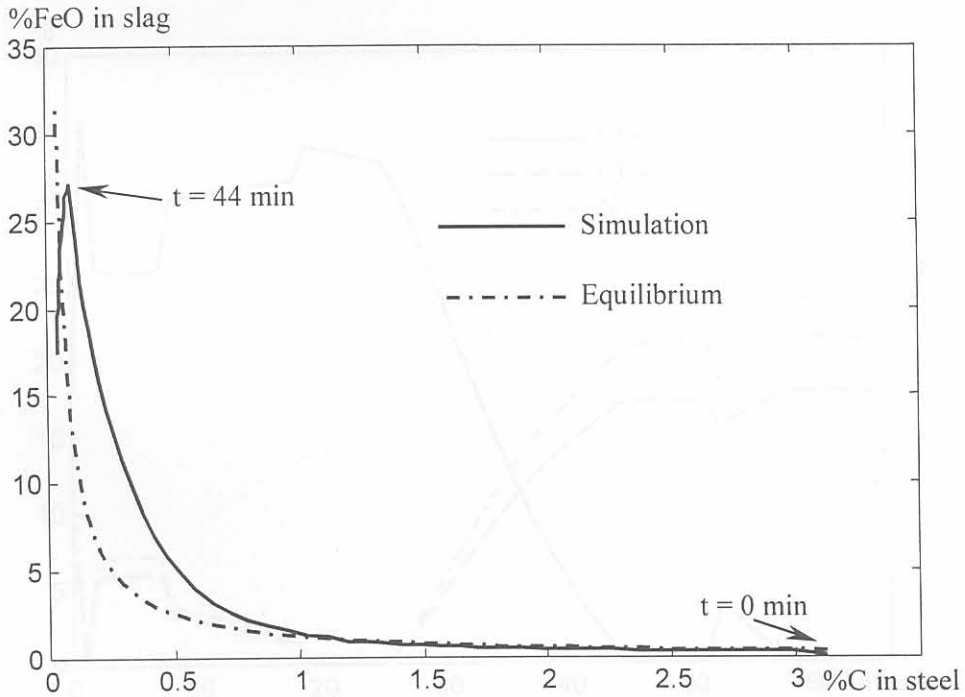


Figure 5.9 %FeO in slag against %C in steel

Fig.5.10 shows the masses of the solid and liquid slag. Note that in this dissertation the FeO and $SiO_2$ components are excluded from the liquid slag mass, although they are accounted for in thermo-chemical calculations. This means that the liquid slag mass denotes CaO and MgO only.

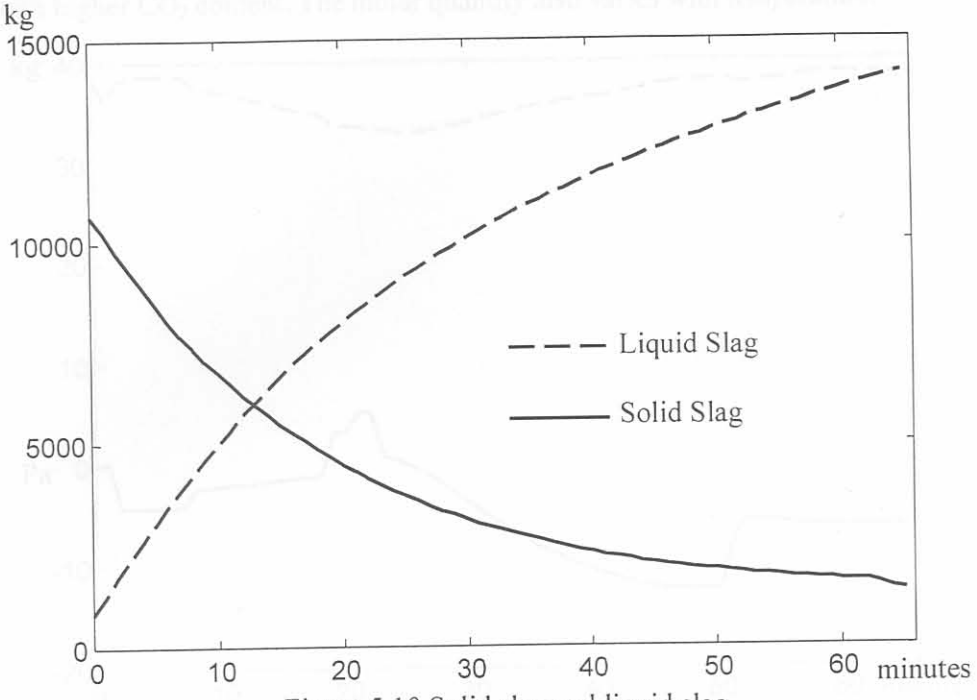


Figure 5.10 Solid slag and liquid slag

Fig.5.11 shows the three gas components together. In the first half of the simulation (t<30), the oxygen injection causes carbon monoxide production. When the oxygen injection stops, the conditions in the furnace are more favourable for carbon to combust directly to carbon dioxide.

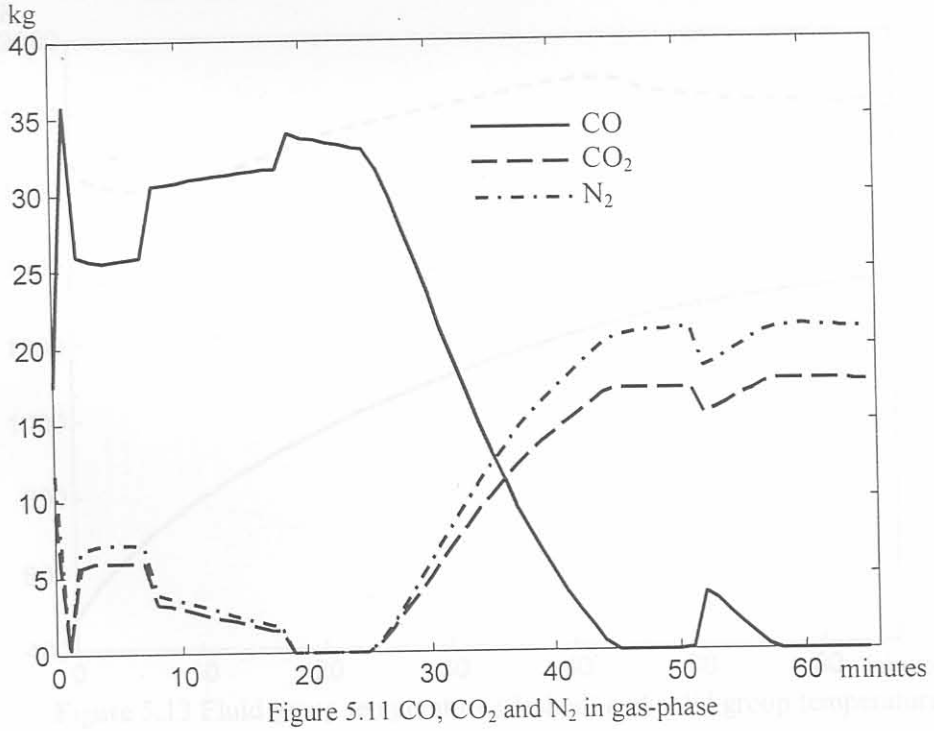


Figure 5.11 CO, $CO_2$ and $N_2$ in gas-phase

Fig.5.12 shows the sum of the gas-masses, together with the relative pressure of the furnace. Although the ideal gas law determines that the total molar quantity remains constant in the furnace, the mass will vary due to gas composition changes. $CO_2$ is a heavy gas and the total gas mass thus

increases with higher $CO_2$ content. The molar quantity also varies with temperature.

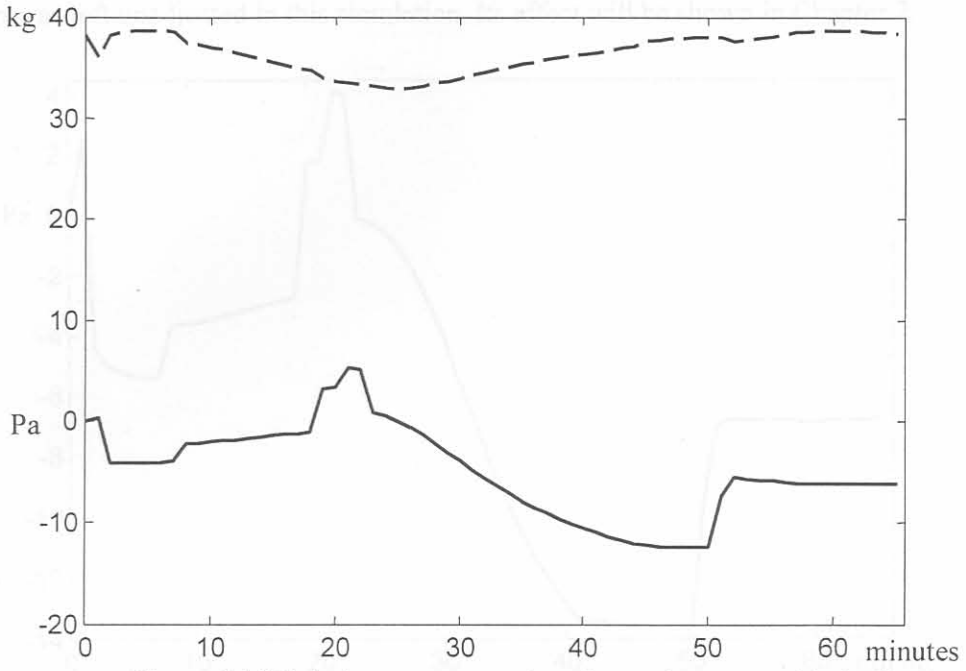


Figure 5.12 Relative pressure and total gas-phase mass (dashed)

Fig.5.13 shows the liquid metal temperature and the scrap temperature. Note that the scrap temperature approaches the liquid metal temperature gradually as the scrap is melted away.

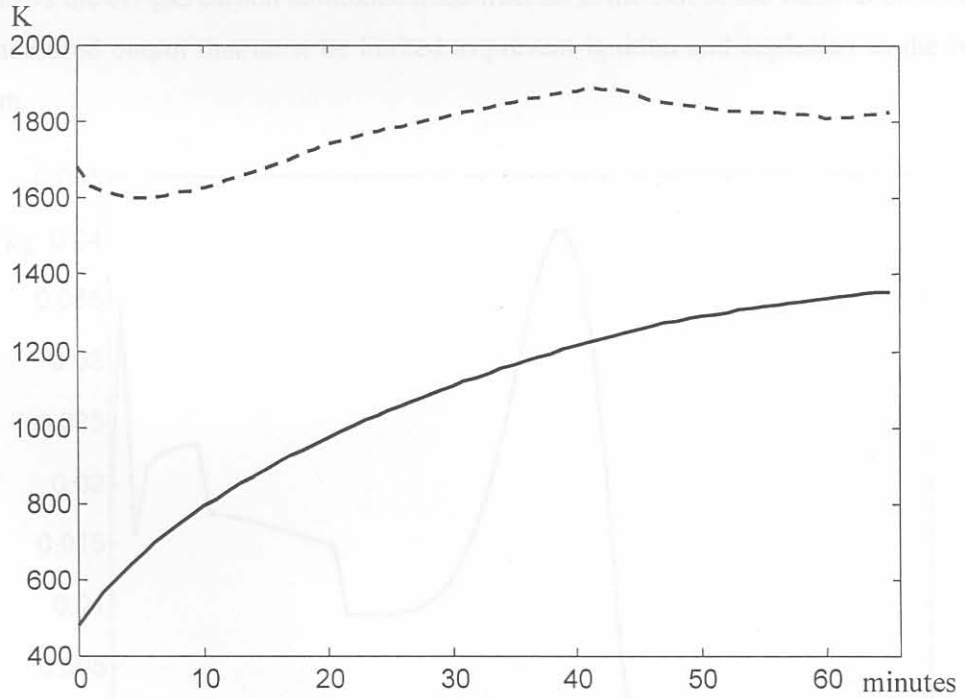


Figure 5.13 Fluid group temperature (dashed) and solid group temperature

Fig.5.14 gives a closer look at the relative pressure, which is also a measured output. Note that the slip-gap was left unadjusted in this simulation. Its effect will be shown in Chapter 7.

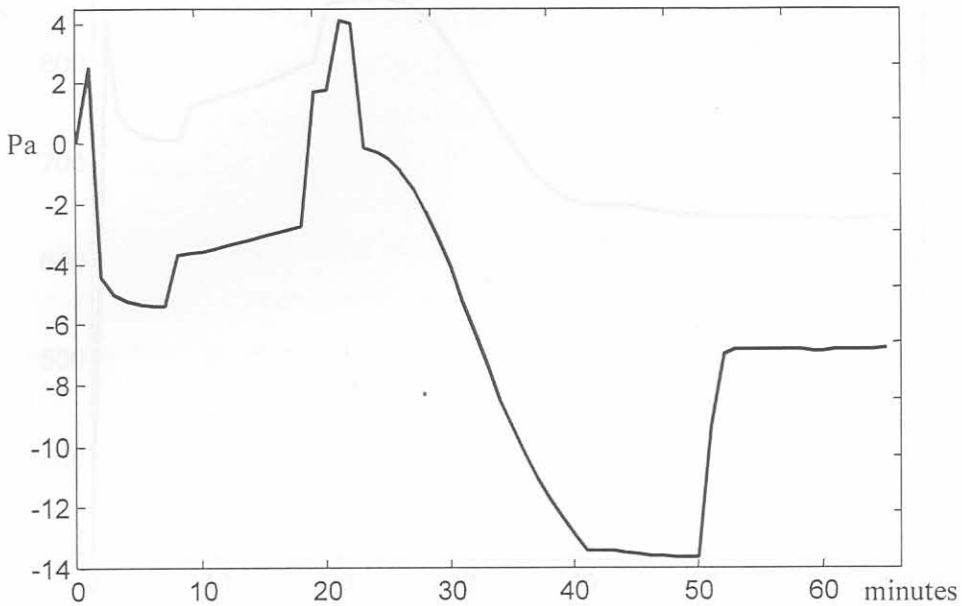


Figure 5.14 Relative Pressure

Another measured output is the steel temperature. Although it cannot be effectively controlled by means of the off-gas parameters, it is measured to adjust the model as discussed in Section 5.6. Fig.5.15 shows the off-gas carbon monoxide mass fraction at the exit of the water-cooled duct. This is also a measured output that must be limited to prevent ignition and explosion in the baghouse filter system.

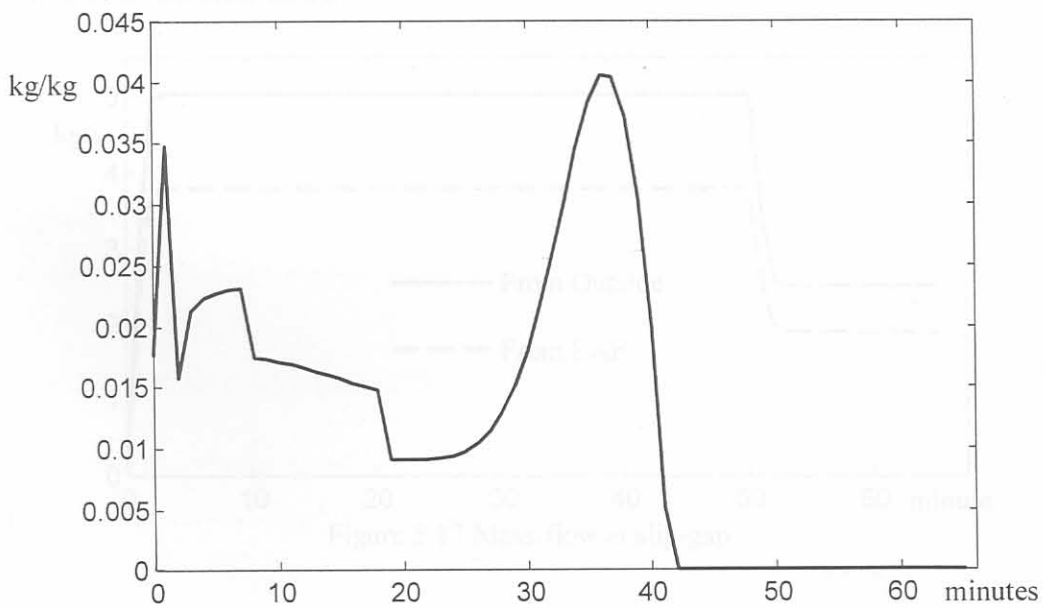


Figure 5.15 CO mass fraction in off-gas

Fig.5.16 shows the off-gas temperature, that must be limited for the same reason.

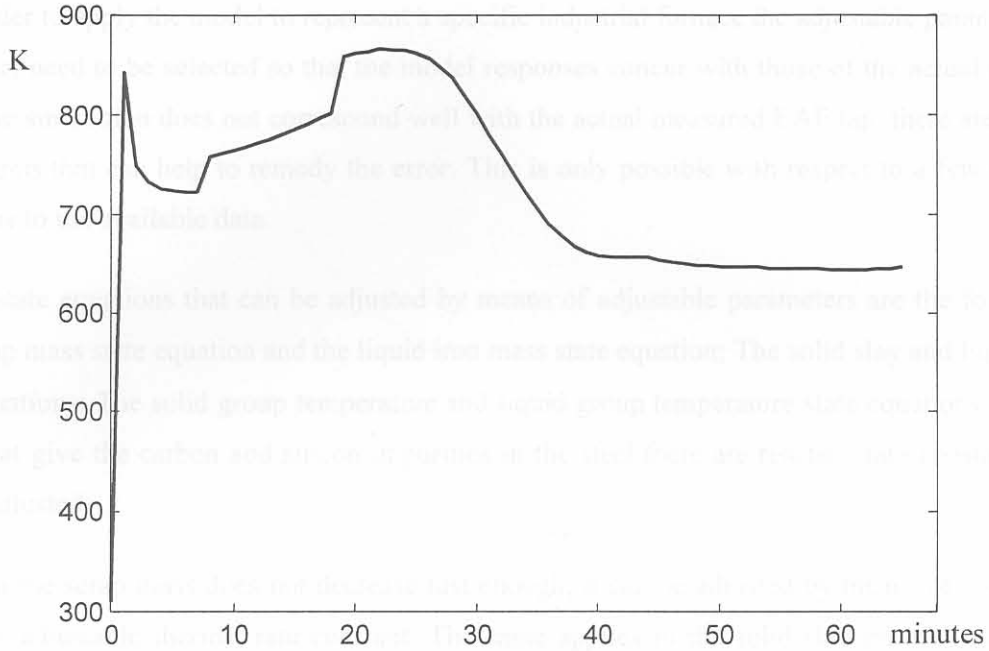


Figure 5.16 Off-gas Temperature

The mass-flow through the slip-gap and the mass-flow out of the EAF are also considered as measured outputs. Although these are not controlled variables, they can serve as model correction measurements. By means of venturi flow meters or diaphragm flow metres it is possible to measure the actual mass-flow on a plant [41]. The mass-flow measurements together with the steel temperature and furnace pressure measurements could then be used to correct the model errors. Fig.5.17 shows the two mass-flows:

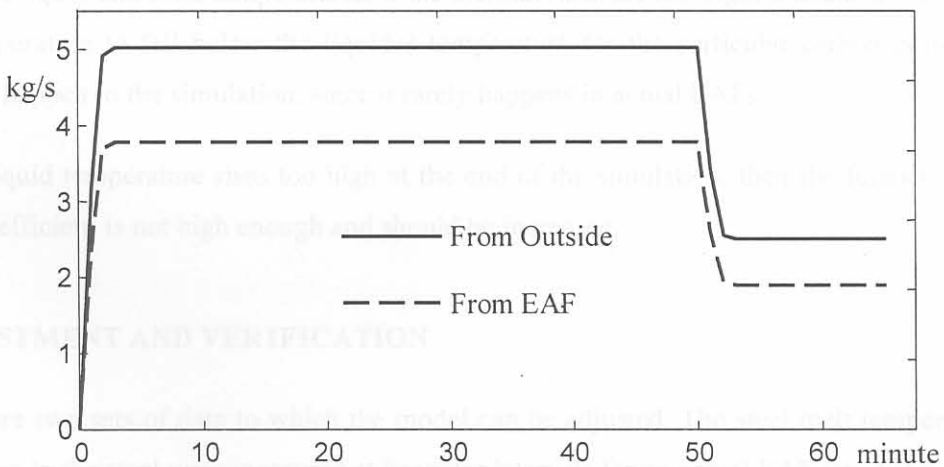


Figure 5.17 Mass-flow at slip-gap

## 5.5 METHOD FOR MODEL ADJUSTMENT

In order to apply the model to represent a specific industrial furnace the adjustable parameters in the model need to be selected so that the model responses concur with those of the actual furnace. When the simulation does not correspond well with the actual measured EAF tap, there are certain adjustments that can help to remedy the error. This is only possible with respect to a few selected states due to the available data.

The state equations that can be adjusted by means of adjustable parameters are the following: The scrap mass state equation and the liquid iron mass state equation; The solid slag and liquid slag state equations; The solid group temperature and liquid group temperature state equations. For the states that give the carbon and silicon impurities in the steel there are reaction rate constants that can be adjusted.

When the scrap mass does not decrease fast enough, it can be adjusted by means of increasing $k_{ther1}$, the adjustable thermal rate constant. The same applies to the solid slag mass ($k_{ther5}$). Care must however be taken not to force the solid slag mass to decrease to zero, since slag is continually charged to the furnace and the solid slag should not decrease to zero until the very last minutes of the simulation.

Increasing the thermal rate constants has the effect of raising the rates of increase of the liquid masses. Care must be taken not to increase the thermal rates too much, since it also has a direct effect on the temperatures, especially that of the liquid group. In the first minute, when the electrical power is not yet switched on, the temperature falls quickly due to the large difference between the liquid and solid temperatures. If the thermal rates are too high, it could cause the liquid group temperature to fall below the liquidus temperature for the particular carbon content. This should not happen in the simulation, since it rarely happens in actual EAFs.

If the liquid temperature rises too high at the end of the simulation, then the furnace wall heat transfer coefficient is not high enough and should be increased.

## 5.6 ADJUSTMENT AND VERIFICATION

There are two sets of data to which the model can be adjusted. The steel melt temperature and the %carbon in the steel were measured at irregular intervals for an actual EAF tap. Fig.5.18 shows the comparison of the %C in the steel and Fig.5.19 shows the comparison of the temperatures. These are simulations that were done before model adjustment.

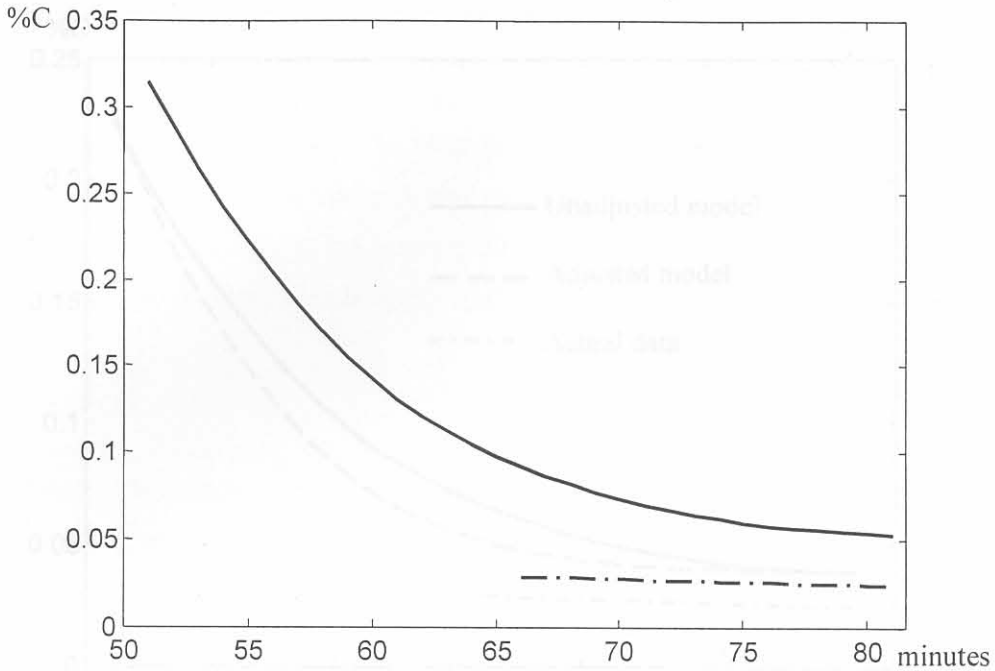


Figure 5.18 Comparison of %C given by model and actual data (dashed)

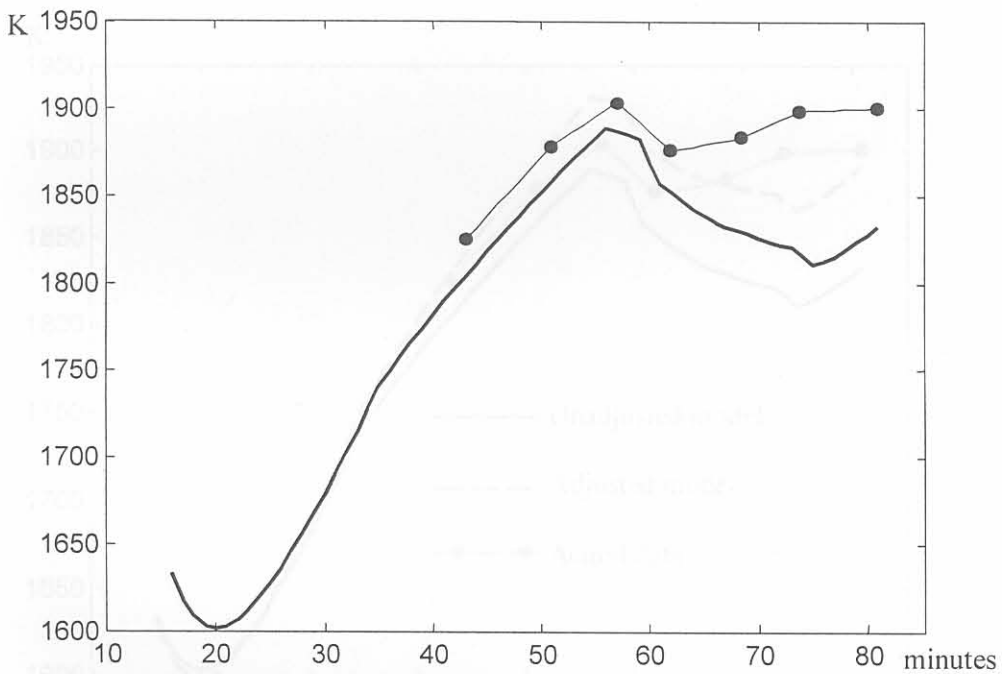


Figure 5.19 Comparison of unadjusted model temperature against actual EAF tap data temperature (dotted). Note: actual instead of simulation time

To improve the temperature correlation with the actual tap data the heat-loss coefficient for the EAF wall must be decreased. To adjust the %C the reaction rate coefficient for the C-FeO reaction must be increased. The two adjustments were done separately in that order, namely first heat-loss coefficient and then reaction rate coefficient. The heat-loss coefficient was initially 15, and was adjusted to a final value of 13.1. The reaction rate coefficient was initially 48, and was adjusted to a final value of 72. Fig.5.20 compares the adjusted model %C and Fig.5.21 the adjusted temperature.

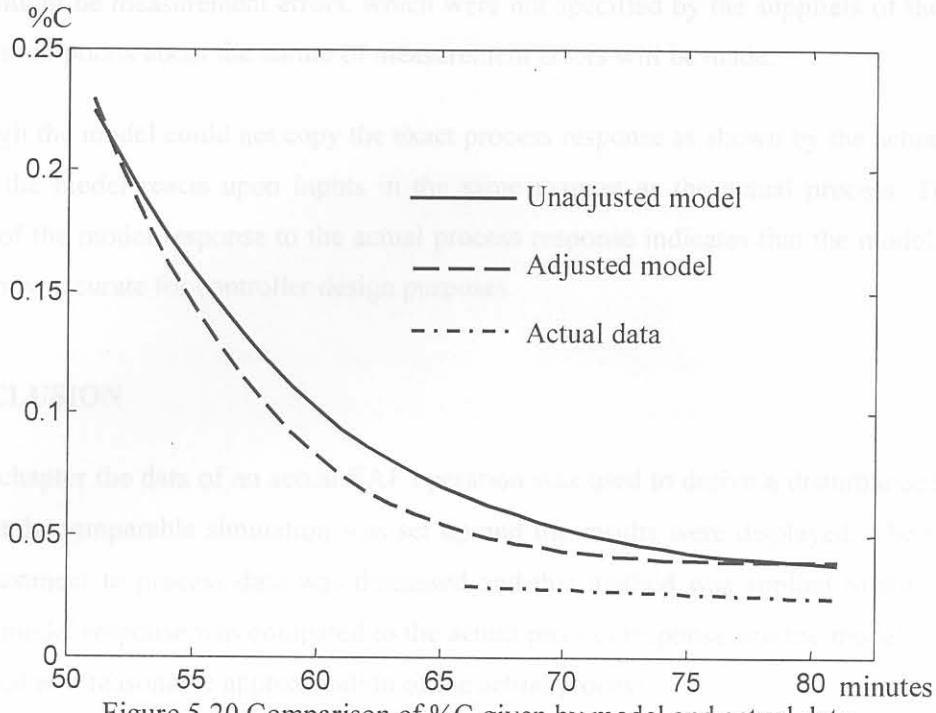


Figure 5.20 Comparison of %C given by model and actual data

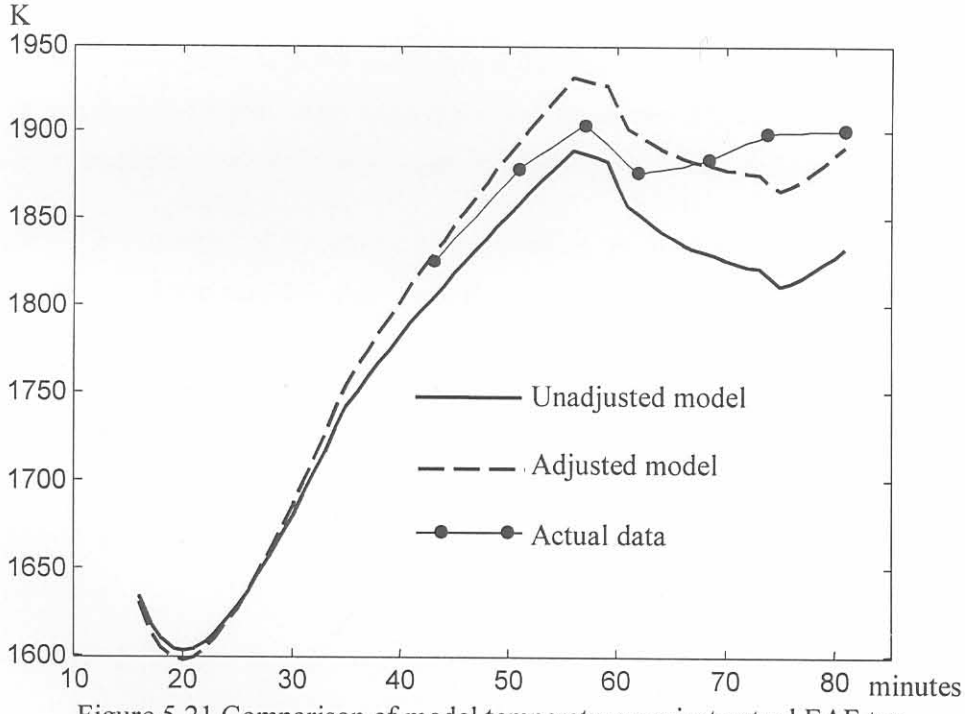


Figure 5.21 Comparison of model temperature against actual EAF tap data temperature.

The adjusted model reaches the same final temperature and achieves good correlation with the actual data. The carbon content fails to correlate as well.

While it is important that any meaningful model should represent the actual process as closely as possible, the inadequacies of the available process data must also always be taken into account.

There might be measurement errors, which were not specified by the suppliers of the data used here. No assumptions about the nature of measurement errors will be made.

Although the model could not copy the exact process response as shown by the actual data, it is clear that the model reacts upon inputs in the same manner as the actual process. The relative closeness of the model response to the actual process response indicates that the model derivation is sufficiently accurate for controller design purposes.

## 5.7 CONCLUSION

In this chapter the data of an actual EAF operation was used to derive a disturbance model. An approximately comparable simulation was set up and the results were displayed. The method for model adjustment to process data was discussed and this method was applied to the example at hand. The model response was compared to the actual process response and the model was verified and accepted as a reasonable approximation of the actual process.

# CHAPTER 6: LINEAR MODEL DEVELOPMENT

## 6.1 INTRODUCTION

In this dissertation a model based controller design method is used which requires a linear plant model. The control law is then developed for the linear model and verified after which it is applied to the actual process, which might not be linear at all. Despite the difference between the process and the linear model, the control law should perform well for the same set of operating conditions. It is with the controller design in mind that a linear model is developed in this chapter.

The linear model is derived from the combined furnace and off-gas non-linear model. In itself it introduces no new assumptions other than the assumptions and approximations necessary to perform the linearization. In order to do the linearisation a nominal steady state set of conditions must be chosen. The linearisation then determines the gradients of all the differential equations for the specific set of conditions. A state-space set of matrices is then composed of all the gradients.

In this context the product of linearisation is a set of linear differential equations. With any linearisation the assumption is that the non-linear differential equations are sufficiently linear (in the region of the nominal steady state (NSS)) that the linearized differential equations will give state trajectories that approximate the state trajectories of the non-linear differential equations.

In Section 6.2 the method of linearisation is illustrated. In Section 6.3 the method for model adjustment is discussed. Section 6.4 shows that the linearized model approximates the non-linear model sufficiently close to be used for control design or as an internal model for a controller.

## 6.2 LINEARISATION

The required form for a linear state-space representation of the off-gas system model is:

$$\begin{aligned} \frac{d(\delta x(t))}{dt} &= A.\delta x(t) + B.\delta u(t) + E.\delta d(t) \\ y(t) &= C.\delta x(t) + D.\delta u(t) + F.\delta d(t) \end{aligned} \tag{6-1}$$

Where the following vector and matrix dimensions are used:

$$\mathbf{x}(t) \in \Re^{17x1}, \mathbf{u}(t) \in \Re^{2x1}, \mathbf{d}(t) \in \Re^{5x1}, \mathbf{y}(t) \in \Re^{6x1}$$

$$\mathbf{A} \in \Re^{17x17}, \mathbf{B} \in \Re^{17x2}, \mathbf{C} \in \Re^{6x17}$$

$$\mathbf{D} \in \Re^{6x2}, \mathbf{E} \in \Re^{17x5}, \mathbf{F} \in \Re^{6x5}$$

Linear system fundamentals are discussed by Reid [38].

The linearisation is done about a steady-state condition denoted by $x^*$, $u^*$, $d^*$. The numerical values for this particular steady-state condition can be determined from industrial furnace practice.

The next step in the linearisation is to determine the elements of the matrices A, B, C, D, E and F. This can be done using a Taylor series expansion and is illustrated by example. The state equation for silicon in liquid steel is:

$$\dot{x}_4 = f_4(x(t), d(t)) = -k_{dSi}\left(\frac{x_4/M_{Si}}{x_2/M_{Fe} + x_3/M_C + x_4/M_{Si}} - k_{XSi}\left(\frac{x_6 M_{FeO}}{x_7 M_{slag}} + \frac{x_8 M_{FeO}}{x_7 M_{SiO_2}} + 1\right)\right) \quad (6\text{-}2)$$

The relevant elements in **A** are obtained as:

$$A_{42} = \frac{\partial \dot{x}_4}{\partial x_2} = \frac{k_{dSi} x_4^* / (M_{Si} M_{Fe})}{\left(x_2^*/M_{Fe} + x_3^*/M_C + x_4^*/M_{Si}\right)^2} \quad (6\text{-}3)$$

$$A_{43} = \frac{\partial \dot{x}_4}{\partial x_3} = \frac{k_{dSi} x_4^* / (M_{Si} M_C)}{\left(x_2^*/M_{Fe} + x_3^*/M_C + x_4^*/M_{Si}\right)^2} \quad (6\text{-}4)$$

$$A_{44} = \frac{\partial \dot{x}_4}{\partial x_4} = \frac{-\frac{k_{dSi}}{M_{Si}}\left(\frac{x_2^*}{M_{Fe}} + \frac{x_3^*}{M_C}\right)}{\left(\frac{x_2^*}{M_{Fe}} + \frac{x_3^*}{M_C} + \frac{x_4^*}{M_{Si}}\right)^2} \quad (6\text{-}5)$$

$$A_{46} = \frac{\partial \dot{x}_4}{\partial x_6} = \frac{k_{dSi} k_{XSi} M_{FeO}}{x_7^* M_{slag}} \quad (6\text{-}6)$$

$$A_{47} = \frac{\partial \dot{x}_4}{\partial x_7} = -k_{dSi} k_{XSi}\left(\frac{x_6^* M_{FeO}}{(x_7^*)^2 M_{slag}} + \frac{x_8^* M_{FeO}}{(x_7^*)^2 M_{SiO_2}}\right) \quad (6\text{-}7)$$

$$A_{48} = \frac{\partial \dot{x}_4}{\partial x_8} = \frac{k_{dSi} k_{XSi} M_{FeO}}{x_7 M_{SiO_2}} \quad (6\text{-}8)$$

With $A_{4N} = 0$ if $N \neq \{2\text{-}4\}$ or $\{6\text{-}8\}$; $B_{4N} = 0$ for $N = \{1\text{-}2\}$; $E_{4N} = 0$ for $N = \{1\text{-}4\}$

The same calculations can be done for all elements of all matrices, using the same method as above. The required form as given in (6-1) is then obtained and the result is given in Appendix C.

## 6.3 METHOD OF MODEL ADJUSTMENT

The aim is to maximise the range over which the linear model is valid, so that the model based controller will perform good over a wide range. To begin with it is necessary to explain how the initial linear model version was obtained. A nominal steady state (NSS) was determined by taking

the time-average (by integration) of the various states, as given by the non-linear simulation. Then the NSS was used to determine the linear model matrix element values and adjusted such that the differential equation gradient conforms to the gradient obtained from the non-linear model (for deviation from the initial conditions). Since the NSS was determined by time-average over the full non-linear simulation, it is an approximation for an actual steady state over a wide range.

The NSS and the initial conditions for the linear model do not have to be the same. The NSS selection is manipulated to adjust the simulation response, while the initial conditions are merely the same as that for the non-linear model simulation. The NSS adjustment is done to achieve good correlation between the non-linear model simulation and the linear model simulation for the whole tap. After the NSS was adjusted to its final value a number of states compared exceptionally well with the non-linear simulation. These were in particular the liquid metal mass, solid scrap mass, fluid group temperature, and solid group temperature. The liquid and solid slag masses of the linear simulation did not agree exactly with the non-linear simulation, but were deemed acceptable.

Most of the other states also compared satisfactorily, although the linear simulation failed to follow the exact trends of the non-linear simulation. The linear simulation was inaccurate with respect to those states where the mass transfer is determined partly or completely by chemical reactions. These are the dissolved masses of carbon and silicon in the liquid metal, and the dissolved masses of FeO and $SiO_2$ in the liquid slag. The rates of change for these states are mainly determined by the reaction of FeO in the liquid slag with carbon and silicon in the liquid metal. The linear simulation at one stage allowed the FeO mass to go to a negative value. From a physical point of view, this is absurd. This is due to the fact that the linear model is a much-simplified model, and is unable to account for chemical reaction rates, while the non-linear model can. With the non-linear model, if there is no FeO to react, then there will be no reaction. Not so for the linear model, since it simply follows the trends dictated by the matrix-multiplication as in equation (6-1).

An attempt was made to correct the negative error in the FeO mass by means of adjustment to the NSS, as well as by means of adjustment of individual matrix elements. It was found that no NSS could remedy this problem, and that adjustment of individual matrix elements was just as futile. In addition, whenever the FeO mass followed a different trend, it influenced other states too, and almost invariably in an undesired manner, causing other states to behave completely erroneous. The best compromise was finally obtained, as shown in Section 6.4.

Finally the only states that could still not compare satisfactorily with those of the non-linear simulation were the gas-phase component masses and the relative pressure. These were then corrected by means of adjustments to individual matrix elements, without much effect on the other

states. Here the same problem of chemical reaction kinetics appears, due to the chemical reaction of the CO with oxygen from the leak-air. The relative pressure also causes trouble for the linear model: Where it is possible to place switches in the non-linear model, to determine whether the relative pressure is positive or negative, and act accordingly, it is not possible with the linear model. This explains the inaccuracy with respect to gas-phase components. Adjustment to individual matrix elements was limited to relations that were exaggerated by the linear model.

## 6.4 SIMULATION RESULTS

The linear model is now used in a pure simulation (not 1-step ahead simulation). With the same initial conditions given in Chapter 5 and the same disturbance model of Chapter 5 the following simulation results were obtained. Fig.6.1 shows the liquid metal and solid scrap masses. Fig.6.2 and Fig.6.3 show the carbon and silicon in solution in the liquid metal.

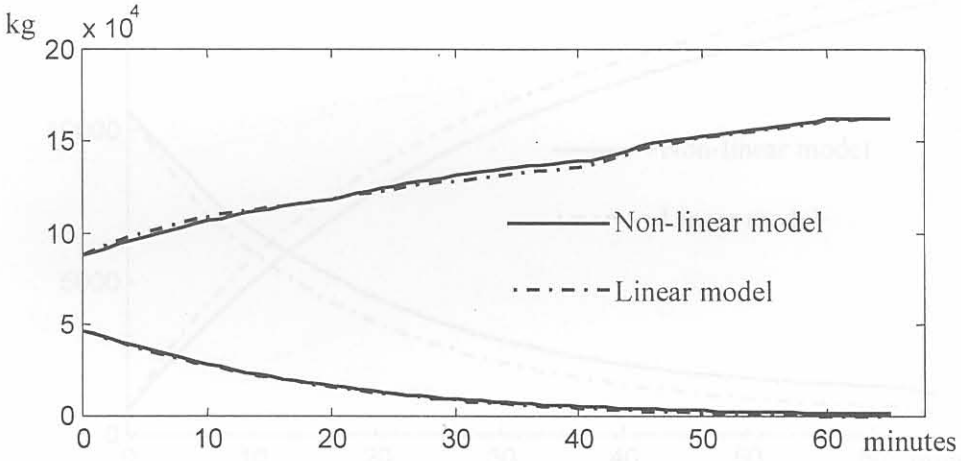


Figure 6.1 Liquid metal mass and solid scrap mass

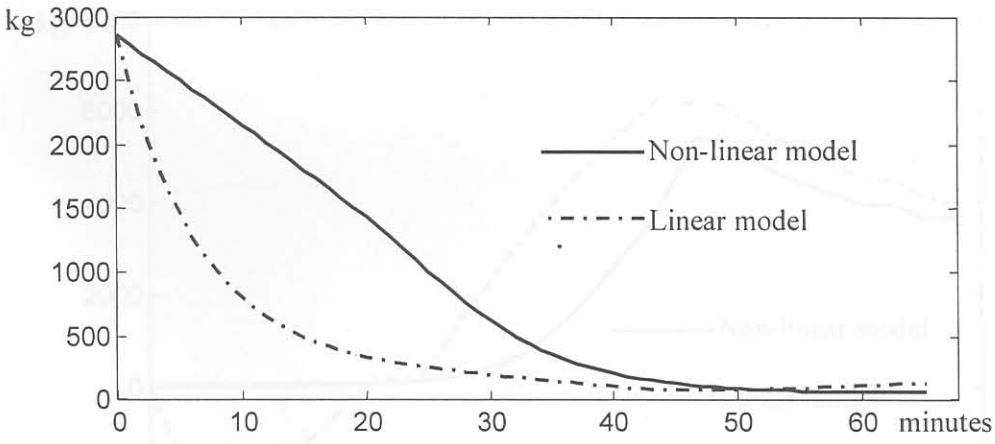


Figure 6.2 Mass of carbon in solution in liquid metal

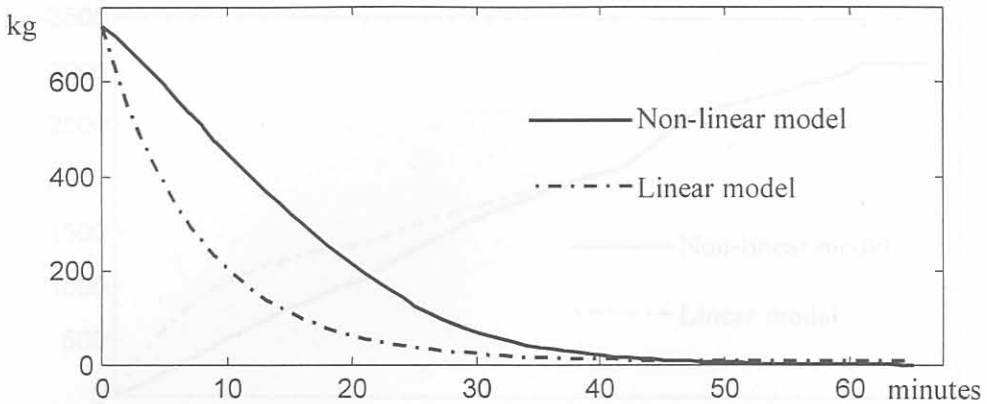


Figure 6.3 Mass of silicon in solution in liquid metal

In Fig.6.4 the comparison of the liquid and solid slag masses are shown. In Fig.6.5 the FeO in solution in the liquid slag is shown (the negative behaviour is discussed in Section 6.3). In Fig.6.6 the $SiO_2$ in solution in the liquid slag is shown.

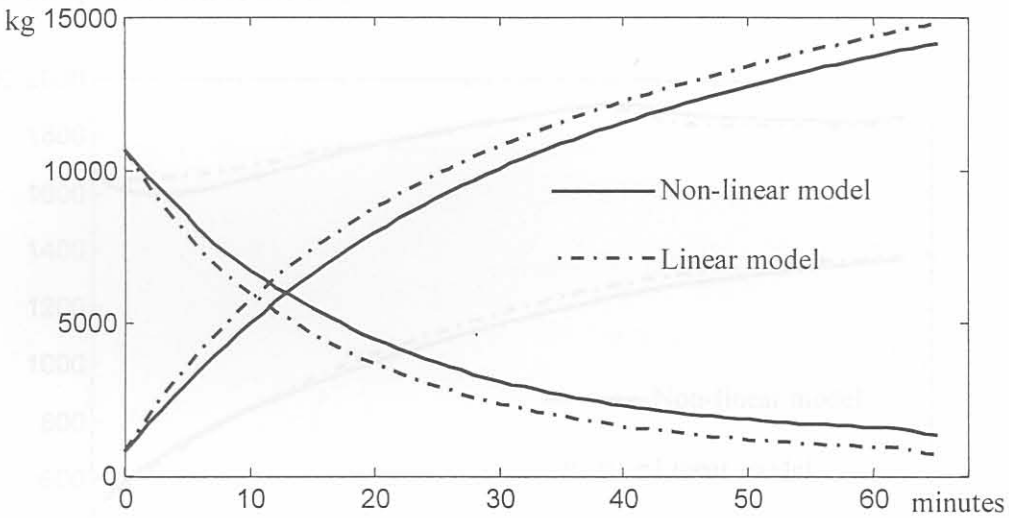


Figure 6.4 Liquid slag mass and solid slag mass

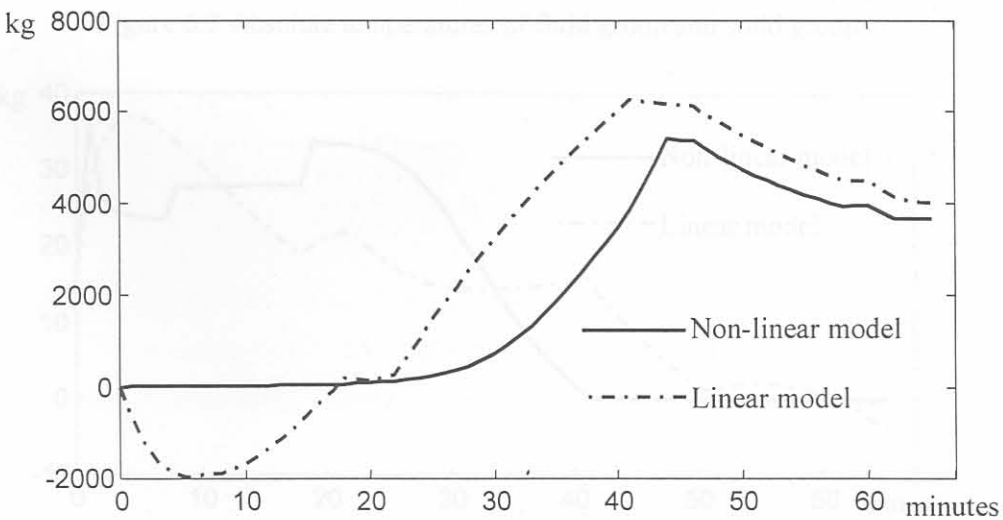


Figure 6.5 Mass of FeO in solution in liquid slag

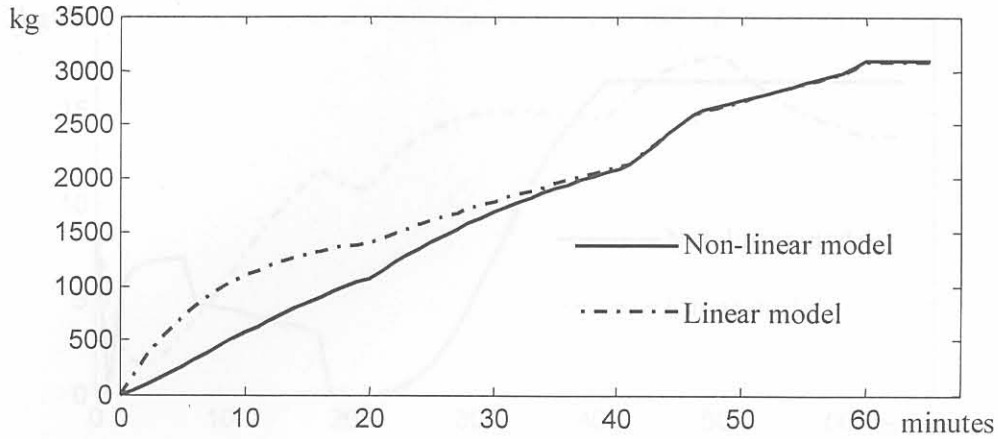


Figure 6.6 Mass of $SiO_2$ in solution in liquid slag

In Fig.6.7 the fluid group and solid group temperature are shown. In Fig.6.8 the mass of CO in the gas-phase is shown. Fig.6.9 shows the $CO_2$ mass in the gas-phase. The nitrogen in the gas-phase behaves quite similar to the $CO_2$.

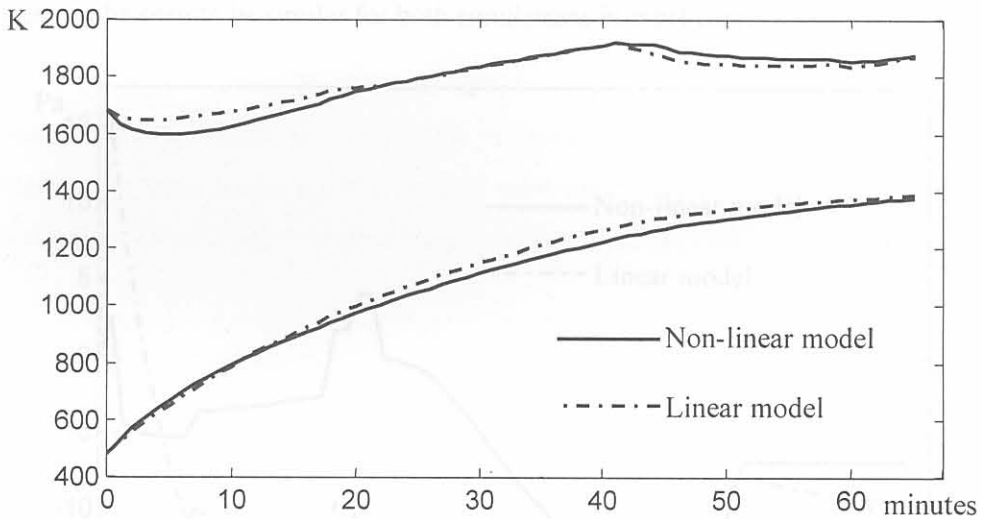


Figure 6.7 Absolute temperatures of fluid group and solid group

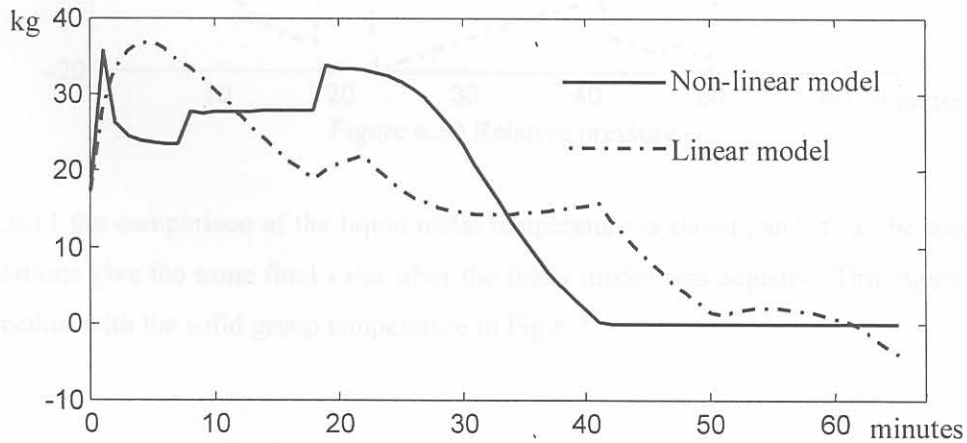


Figure 6.8 Mass of carbon-monoxide in gas-phase

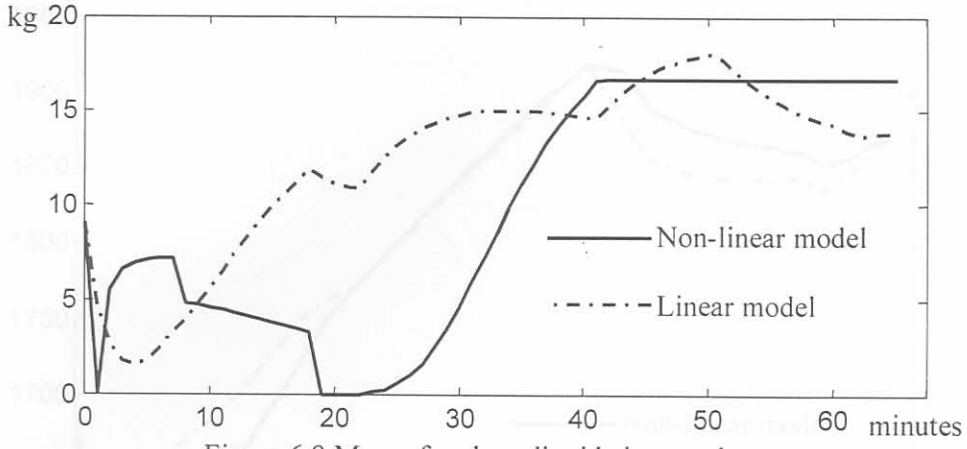


Figure 6.9 Mass of carbon-dioxide in gas-phase

There are four outputs that are considered here: The relative pressure, liquid metal temperature, off-gas CO mass-fraction and the off-gas temperature. The relative pressure is shown in Fig.6.10. Although the linear simulation diverges from the non-linear simulation, the effects of external disturbances can be seen to be similar for both simulations in most cases.

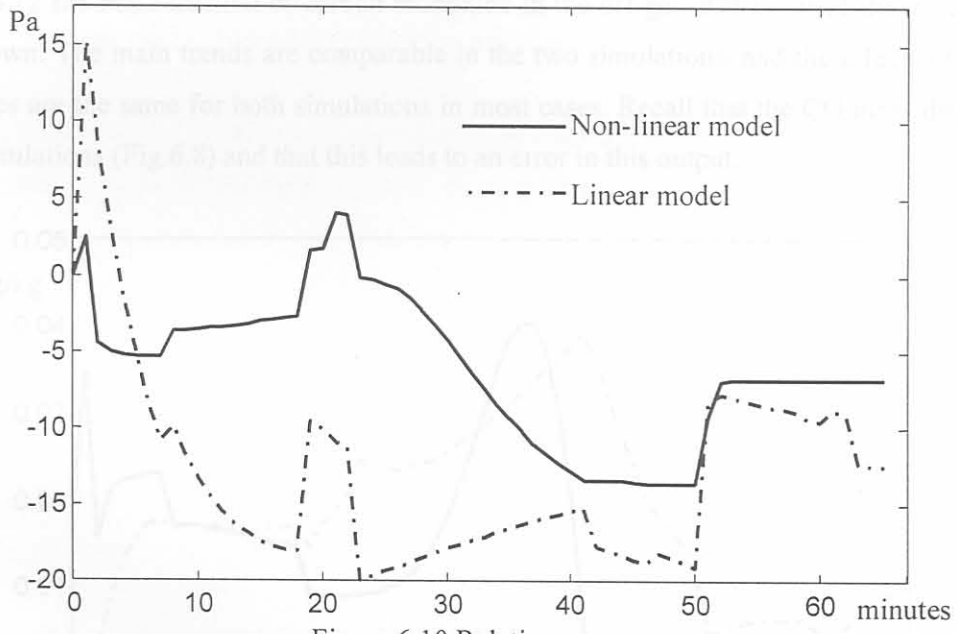


Figure 6.10 Relative pressure

In Fig.6.11 the comparison of the liquid metal temperature is shown, and it can be seen that the two simulations give the same final value after the linear model was adjusted. This figure was also shown together with the solid group temperature in Fig.6.7.

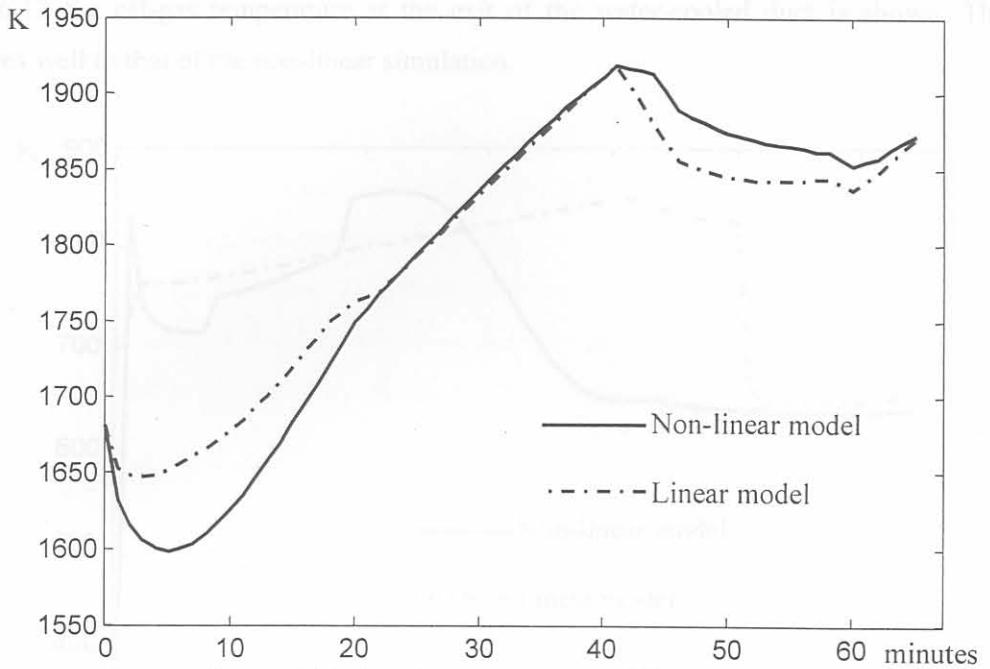


Figure 6.11 Absolute temperature of liquid metal

In Fig.6.12 the mass fraction of carbon monoxide in the off-gas at the exit of the water-cooled duct is shown. The main trends are comparable in the two simulations, and the effects of external disturbances are the same for both simulations in most cases. Recall that the CO mass differed for the two simulations (Fig.6.8) and that this leads to an error in this output.

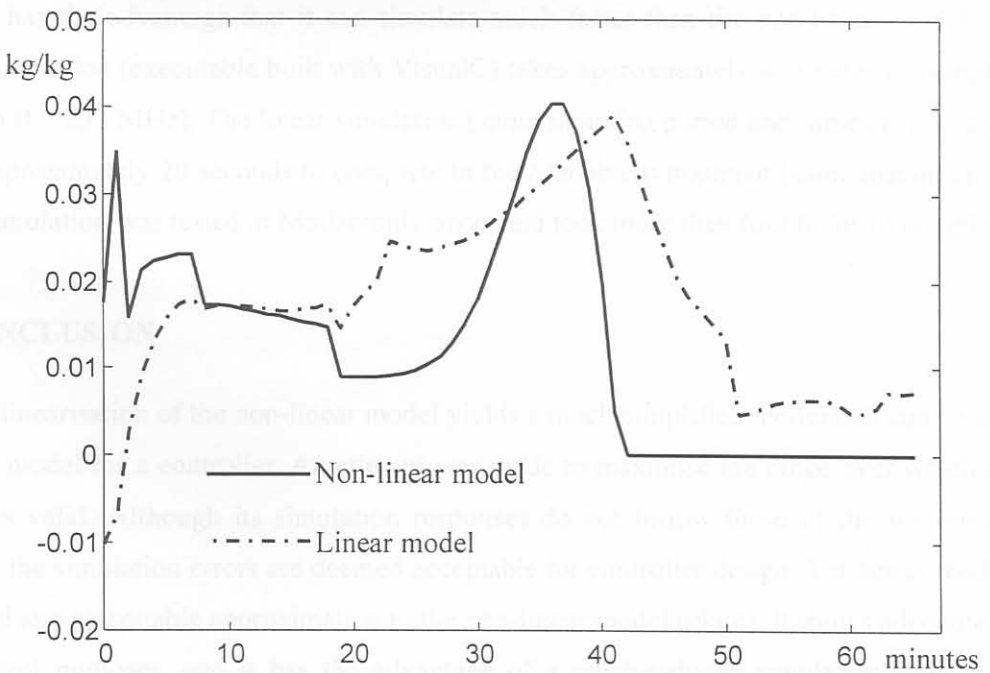


Figure 6.12 Mass fraction of CO in off-gas at water-cooled duct exit

In Fig.6.13 the off-gas temperature at the exit of the water-cooled duct is shown. This output compares well to that of the non-linear simulation.

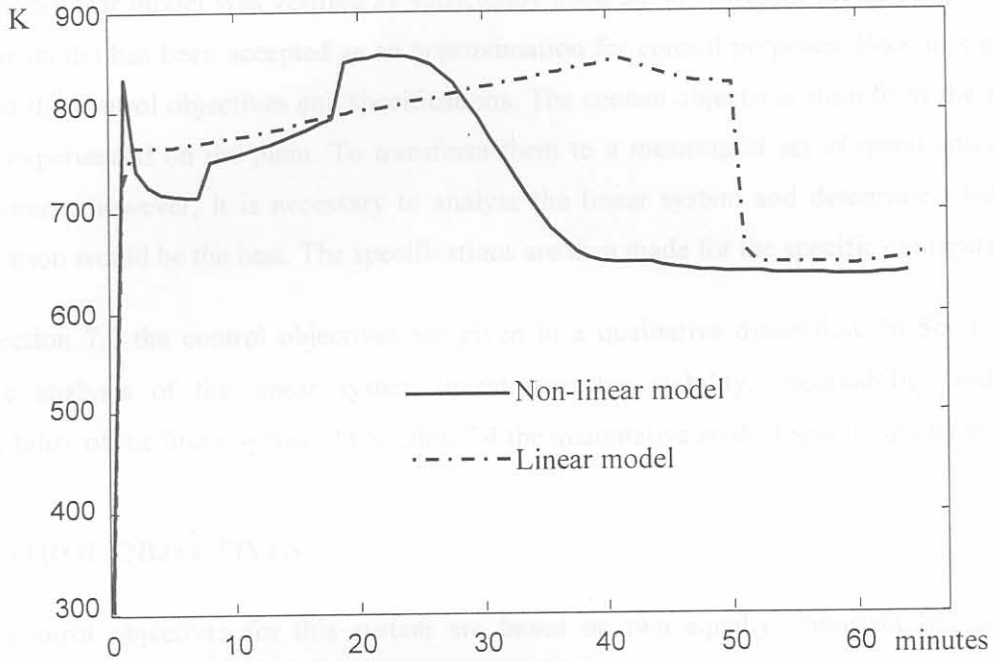


Figure 6.13 Absolute temperature of off-gas at water-cooled duct exit

Although a very good linear model approximation is always desired, it is not critical for control design purposes, since output-feedback will be employed. The linear model presented in this chapter has the advantage that it can simulate much faster than the non-linear model. The non-linear simulation (executable built with VisualC) takes approximately 4 minutes to complete (on a Pentium II – 233 MHz). The linear simulation (same sampling period and same process conditions) takes approximately 20 seconds to complete in the Matlab environment (same machine). The non-linear simulation was tested in Matlab only once, and took more than four hours to complete.

## 6.5 CONCLUSION

The linearisation of the non-linear model yields a much-simplified model that can be used as an internal model for a controller. An attempt was made to maximise the range over which the linear model is valid. Although its simulation responses do not follow those of the non-linear model exactly, the simulation errors are deemed acceptable for controller design. The linear model is then accepted as a reasonable approximation to the non-linear model (plant). It shows adequate accuracy for control purposes, and it has the advantage of a much-reduced simulation time. These two characteristics make it ideal for an internal model in Model Predictive Control.

# CHAPTER 7: CONTROL OBJECTIVES AND SPECIFICATIONS

## 7.1 INTRODUCTION

The non-linear model was verified as sufficiently accurate to represent the actual process, and the linear model has been accepted as an approximation for control purposes. Now it is necessary to look at the control objectives and specifications. The control objectives stem from the problems that are experienced on the plant. To transform them to a meaningful set of quantitative control specifications, however, it is necessary to analyse the linear system and determine what control configuration would be the best. The specifications are then made for the specific configuration.

In Section 7.2 the control objectives are given in a qualitative discussion. In Section 7.3 an algebraic analysis of the linear system investigates the stability, observability and output-controllability of the linear system. In Section 7.4 the quantitative control specifications are given.

## 7.2 CONTROL OBJECTIVES

The control objectives for this system are based on two equally important but conflicting agendas. They are process efficiency improvement and environmental protection.

Since the EAF cannot be entirely sealed off, there is always a hazard of pollution in the workshop. Gas, loaded with dust, can exit the EAF through any unsealed openings if the negative relative pressure of the EAF is not large enough. The gas contains high levels of CO at a high temperature, and can thus cause a severe safety hazard in the workshop. As a result the EAF is required to operate at a negative relative pressure.

The negative relative pressure causes a loss of energy, as a large amount of heat is extracted with the off-gas, since a powerful forced draught has to be applied to maintain the negative relative pressure. The agenda of process efficiency improvement calls for lower energy waste, which would lead to shorter tap-to-tap times, since the steel would reach the required tap temperature quicker. One benefit of improved control would be that the negative relative pressure would be kept consistently smaller, resulting in less energy being wasted.

Besides the negative relative pressure, the agenda of environmental protection also requires that the off-gas must be cleaned by an appropriate filter system. The carbon monoxide content in the gas that is emitted in the atmosphere must be sufficiently low, and all dust must be removed from the gas before it is emitted into the atmosphere. The system under study makes use of post-combustion in the water-cooled duct to reduce the carbon monoxide level. It then uses a baghouse filter system to filter out the dust.

The baghouse can ignite and explode if the carbon monoxide content of the off-gas entering it is too high, or if the off-gas temperature is too high. Should this happen, the regulatory authorities can require the entire EAF operation to cease until the baghouse filter system is repaired. To avoid this the carbon monoxide level in the off-gas and the off-gas temperature must be limited to safe levels.

## 7.3 LINEAR SYSTEM ANALYSIS

There are three objectives for this analysis. Firstly to take a look at stability of the linear model. Secondly to look into observability of the model, and thirdly to analyse output-controllability.

### 7.3.1 Stability

The simplest stability analysis is a look at the eigenvalues of the A-matrix, see Table 7.1:

Table 7.1 Eigenvalues of A-matrix

| Real Part | Imaginary Part |
|---|---|
| -8.5991 | |
| -1.1111 | |
| -1 | |
| -0.083333 | |
| -0.0027321 | |
| -0.0026838 | |
| -0.0026838 | |
| -0.002153 | |
| -0.00096723 | |
| -0.00087352 | +3.8408e-005 |
| -0.00087352 | -3.8408e-005 |
| -0.00054087 | |
| -2.1531e-005 | |
| -1.8119e-017 | +4.0619e-014 |
| -1.8119e-017 | -4.0619e-014 |
| -1.278e-019 | |
| -4.5671e-020 | |

Since $Re[\lambda_j(A)]<0$ for all j, the linear system is stable for finite inputs [42]. The simulations support this indication, since no sign of instability was found in any of the simulations.

### 7.3.2 Observability

For the internal states of the system to be completely observable from the output-measurements, the observability matrix have to be of maximum rank [42,43]. The observability matrix (Ob) is given by equation (7-1) (where $\mathbf{Ob} \in \Re^{102x17}$ ):

$$Ob = [C; CA; CA^2; CA^3; \ldots; CA^{16}; CA^{17}] \quad (7\text{-}1)$$

For a tolerance of 1 the rank of the observability matrix was 5, and for a tolerance of $10^{-7}$ the rank was 12. This indicates that the internal states of the system are not completely observable from the outputs. This is expected, since the C-matrix contain only seven columns with nonzero elements. The states corresponding to zero-columns in the C-matrix are not observable. This is also confirmed by an eigenvector analysis, as described by [44].

### 7.3.3 Output-Controllability

In this dissertation, the aim is to control outputs rather than internal states. It therefore makes more sense to also look at output-controllability [37]. Output-controllability for a system such as equation (6-1) is guaranteed if the output-controllability matrix has full rank.

In the system under study there are only two manipulated variables, but there are four outputs. One task of the control-designer is to determine which outputs should be controlled, and which should be left alone. Since the output-controllability analysis is based on conventional methods, it would yield meaningful results only if the analysis is done on at most two outputs at a time. In contrast, the control law that will be given in the next chapter is capable of using two manipulated variables (MVs) to control three or four controlled variables (CVs). However, if the CVs are more than the MVs, their control is interdependent. For the present analysis, however, it is necessary to consider only two outputs at a time, so that they can be controlled independently. Four combinations will be investigated:

- Relative pressure ($y_1$) and liquid metal temperature ($y_2$) – C1;
- Relative pressure ($y_1$) and off-gas composition ($y_3$) – C2;
- Relative pressure ($y_1$) and off-gas temperature ($y_4$) – C3;
- Off-gas composition ($y_3$) and off-gas temperature ($y_4$) – C4.

Each time the respective rows were extracted from the C-matrix, and placed in a reduced substitute, C1 to C4. Then the output-controllability matrices $Q_1$ to $Q_4$ were computed, according to equation (7-2) (where $\mathbf{Q}_x \in \Re^{2x34}$ ):

$$Q_x = [C_xB, C_xAB, C_xA^2B, C_xA^3B, \ldots, C_xA^{16}B, C_xA^{17}B] \tag{7-2}$$

To determine the rank of each output-controllability matrix, the Matlab® function "rank" was used. "Rank" determines the number of singular values of the argument matrix "$Q_x$" that are larger than the tolerance "tol". This is equivalent to estimating the number of rows that are linearly independent. If $Q_x$ has a rank of two, it is of full rank, and output-controllability for that specific configuration is guaranteed. Six different tolerances were used to determine the rank of each of the matrices. Table 7.2 shows the tolerances and the rank of each matrix at each tolerance:

Table 7.2 Output-controllability matrices: tolerances and ranks

| Tolerance | Rank(Q1) | Rank(Q2) | Rank(Q3) | Rank(Q4) |
|---|---|---|---|---|
| 50.0 | 1 – deficient | 1 – deficient | 2 – full | 1 – deficient |
| 10.0 | 1 – deficient | 1 – deficient | 2 – full | 2 – full |
| 3.5 | 1 – deficient | 1 – deficient | 2 – full | 2 – full |
| 1.5 | 1 – deficient | 2 – full | 2 – full | 2 – full |
| 1.0 | 1 – deficient | 2 – full | 2 – full | 2 – full |
| 0.7 | 2 – full | 2 – full | 2 – full | 2 – full |

From Table 7.2 the following deductions can be made:

- The common factor between C1, C2 and C3 is the relative pressure, and as it is always controllable in C3, it is assumed that it is also always controllable in C1and C2.
- The common factor between C3 and C4 is the off-gas temperature, and as it is always controllable in C3, it is assumed that it is also always controllable in C4.
- A further analysis on each output alone is done to extract additional knowledge about the linear system. The same output-controllability matrix is calculated as in equation (7-2). The difference is now that the C matrix used consists of only one row. The tolerance at which the rank of each output-controllability matrix becomes deficient was determined and normalised. The tolerance of the relative pressure is three orders of magnitude larger than any of the other tolerances, indicating that it is much more controllable.
- The order of controllability is C3, C4, C2, and C1. It may therefore be assumed that the order of output-controllability is $y_1$, $y_4$, $y_3$ and $y_2$.
- The least controllable output is the liquid metal temperature, which makes sense, since no controller can be expected to have much effect on the temperature of a 160-ton liquid metal pool, by manipulating an off-gas stream in the order of 10 kg/s.
- The off-gas CO mass-fraction is a controllable output, but from the analysis it is clear that it is less controllable than the relative pressure or the off-gas temperature. It would probably require much stronger control actions to regulate or limit.

## 7.4 CONTROL SPECIFICATIONS

The control specification stems from the control objectives given in Section 7.2, as well as from the linear system analysis given in Section 7.3.

The control objectives require that the relative pressure should be regulated at a negative pressure, yet close to atmospheric pressure. The control objectives also require that the controller strive for higher energy efficiency as embodied in the liquid metal temperature (integration of energy). It is also required that the off-gas CO content and off-gas temperature must both be limited to protect the baghouse filter system.

The output-controllability analysis shows that the relative pressure and the off-gas temperature are both controllable. It also shows that the off-gas CO content is controllable, although it will probably require much stronger control actions to effect a meaningful response.

The analysis also shows that it will probably be futile to attempt to control the liquid metal temperature. Preliminary experiments confirmed this deduction [11]. In industry the DRI feed rate is used to control the liquid metal temperature, with the electric arc providing the main energy input. The oxygen injection also strongly influences the liquid metal temperature.

Based on these findings a set of meaningful controlled variables for the off-gas system are then the relative pressure, and the off-gas composition and temperature. The relative pressure is first priority, unless the other variables exceed acceptable limits.

A number of excursions were made to steel manufacturers, to gain insight into the problem. In conversations with process experts a few guidelines were obtained, and the specifications given here are influenced by those guidelines. The worst case scenario given in the design drawings also influences the specifications. In order to accommodate the conflicting control objectives within the specifications a compromise is necessary.

- Regulate the relative pressure at –5 Pa;
- Limit the CO mass fraction in the off-gas to 0.01 kg/kg = 1%;
- Limit the off-gas temperature to 500°C = 773 K;
- Do not attempt to regulate or control the liquid metal temperature, but take it into account as a measure of the energy-efficiency.

Fig.7.1 gives a more exact description of the process input-output relationships.

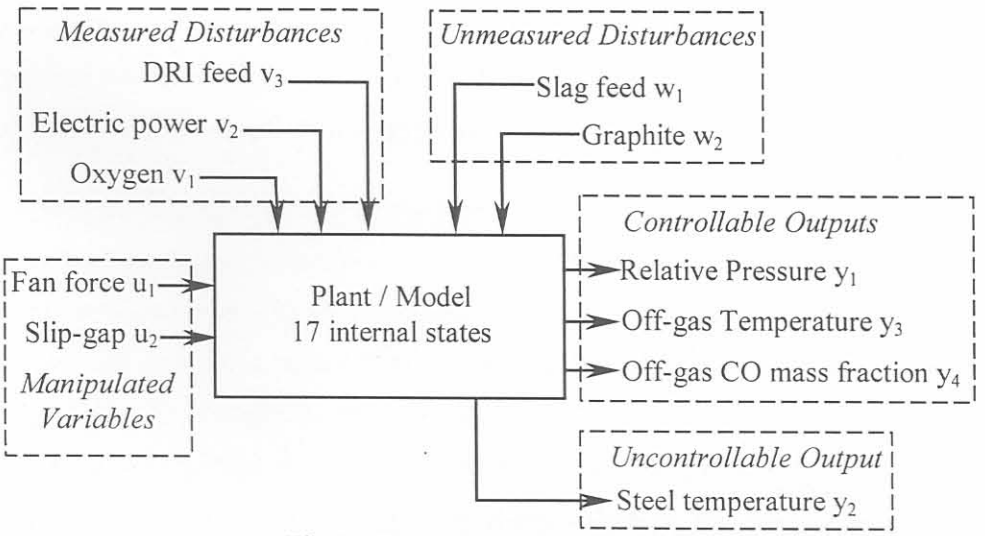


Figure 7.1 Input – Output diagram

## 7.5 CONCLUSION

The control objectives were given in a qualitative discussion. A linear system analysis showed that the linear system is stable. It was also determined that the relative pressure and the off-gas composition and temperature are all controllable outputs, but that the liquid metal temperature is not, since it is controlled by variables that are regarded as measurable disturbances for this dissertation. Based on the qualitative control objectives and the linear system analysis, and also based on guidelines from the industry, the necessary quantitative control specifications were given.

# CHAPTER 8: CONTROLLER DESIGN

## 8.1 INTRODUCTION

In this chapter the basic controller design is done on the simplified linear model. This design is done in the Matlab® environment with the MPC toolbox [12]. This toolbox enables the user to design a controller with various options. The design tools are the cost function weight multipliers, for the inputs and the outputs, the input and output limits and the manipulation and prediction horizons. An increase in the input cost function weights smooth the manipulator signals, while an increase in the output cost function weights forces the outputs closer to their setpoints. The manipulation (M) and prediction (P) horizons affect the optimisation of the cost function. It may appear that controller design with MPC is done by trial and error, but the effects of each parameter can be determined from repeated experiments. The design method will be shown step by step. The controller is tested for the same operating conditions as in Chapters 5 & 6.

In Section 8.2 the properties of Model Predictive Control (MPC) are discussed. Section 8.3 gives the basic design procedure for MPC. Section 8.4 shows the inclusion of an integrator in the controller, and motivates the choice of integral cost function weight.

## 8.2 MODEL PREDICTIVE CONTROL

The control method that was selected for this project is MPC [11]. The MPC strategy results from the optimisation of a performance index with respect to a future control sequence, using predictions of the output signals based on an internal process model. An optimisation algorithm is applied to compute a sequence of future control signals that minimises the performance index subject to the given constraints. MPC uses the receding horizon principle. This means that after computation of the optimal control sequence, only the first control is implemented. The horizon is shifted one time step and the optimisation is repeated with new information of the measurements. Clarke and Scattolini [45] give a discussion of the receding horizon principle.

It is assumed that a proper furnace control system is already in place. This control system uses MVs such as the electric arc current and voltage, the DRI feed-rate and the oxygen injection rate. This dissertation treats those MVs as disturbances. Those MVs that are operator controlled through the furnace control system is regarded as unmeasurable disturbances, since operator control is frequently applied with override mechanisms. Those MVs that are automatically controlled by the furnace controller are regarded as measurable disturbances, since the control system generates their command values and can simultaneously relay those values to any other control system. MPC makes use of the measurement of measured disturbances in its optimisation.

Under certain conditions, the future trajectories for some of the MVs are also known. This leads to the observation that MPC combines feed-forward and feedback control. Feed-forward control is done because MPC can predict undesired behaviour in response to disturbances, and is capable of correcting for such behaviour in advance (for measured disturbances). Feedback control is done in that MPC recalculates each control with the newest measurement of the outputs. For a comparison of the advantages and disadvantages of feed-forward and feedback control see [21].

The use of an internal model makes MPC very attractive. When a very good internal model is available, feed-forward control performs better than feedback control, because it is not affected by process lag and does not introduce instability in the closed loop response. The linearised model is not that good that it can be used in pure feed-forward control, but combined with MPC it will compensate for the lack of measurable data. The use of real-time optimisation also makes MPC attractive. Optimisation enables a controller to control a larger number of controlled variables (CVs) than the number of available manipulated variables (MVs). This is achieved by the selection of cost function weights and limits. While all the CVs are within their specified limits, the cost function is minimised with the ordinary cost function weights. When a CV is predicted to exceed a specified limit, the controller attempts to prevent it by selection of MVs, to obtain feasible optimal control. Therefore, by the optimisation of the cost of internal model predictions, MPC can use two MVs to control three CVs, depending on the feasibility due to the constraints.

For a Generalised Predictive Control [46] performance index (a quadratic cost function), and linear constraints, the solution can be found using quadratic programming algorithms. For this dissertation a quadratic-programming algorithm formulated by G.B. Dantzig is used, as this algorithm displays fast convergence [47]. According to Morari and Ricker [12] MPC displays its main strength when applied to problems with:

- A large number of manipulated and controlled variables;
- Constraints imposed on the manipulated variables;
- Changing control objectives or equipment failures.

Although MPC is in fact a time-variant system (due to real-time optimisation) it is possible to design a much-simplified pre-computed (time-invariant) controller, on the condition that no constraints may be applied. Bordons and Camacho [48] illustrate a practical example of this, where they show that the pre-computed MPC is computationally much less demanding, and can therefore work at a much shorter sampling time than MPC with real-time optimisation (on the same machine). In this system however, the constraints are crucial, since they are actual physical constraints. Thus only MPC with true real-time optimisation will be considered.

## 8.3 CONTROLLER DESIGN

### 8.3.1 Design Tools

The MPC toolbox of Matlab® was used [12]. The toolbox Mod-format is used, and to obtain it, the matrices B&E and D&F are combined. The "A" and "B" matrices are converted to the discrete time format. The internal and plant models are the same, except that the unmeasured disturbances affect the plant, while the internal model is not affected by the unmeasured disturbances. The effects of the unmeasured disturbances are only detected in the measured outputs.

The controller design parameters are the prediction and manipulation horizons and the cost function weights, for outputs and inputs. An increase in the input cost function weights smooth the manipulator signals, while an increase in the output cost function weights forces the outputs closer to their setpoints. The manipulation and prediction horizons affect the optimisation of the cost function. The use of each is shown step by step towards the best controller design. First the initial parameter selection is discussed, and then the changes are shown step by step.

### 8.3.2 Initial parameter selection

The initial output cost function weight selection was based on a semi-normalised cost for the three controlled variables (relative pressure, off-gas temperature, off-gas %CO). The cost function takes the following general form where $\bar{\gamma} = \bar{r} - \bar{y}$ is the error vector, the difference between the controlled variables and setpoints.

$$\psi(\bar{\gamma}, \bar{u}) = \frac{1}{2}\bar{\gamma}' \mathbf{Y}\bar{\gamma} + \frac{1}{2}\bar{u}' \mathbf{U}\bar{u} \qquad (8\text{-}1)$$

The errors for the outputs were approximated as the absolute values of the setpoints or CV limits. For the three controlled variables this translates to $\gamma_a$ = [5, 1, 773]. A completely normalised output cost weight matrix would then yield diag(Y) = [0.04, 1, 1.67E-6]. It was found that this cost function weight selection is completely biased in favour of the off-gas composition.

The off-gas composition is less controllable than either of the other controlled variables, and in addition its linear model estimate is worse than the others are (see Fig.6.10-13). A completely normalised output cost is thus not preferred. Even when the output cost weight matrix elements are simply made equal to the inverse of the corresponding error estimates, the same bias toward the off-gas composition was experienced, which resulted in poor or no control of all three variables at all. The output cost weight matrix elements are therefore made equal to the square root of the corresponding error estimate inverse: diag(Y) = [0.45, 1, 0.036].

The input ranges are approximately the same and the input cost weight matrix is therefore made a unity matrix. The horizons are initially M = 1 and P = 2, which is a minimum requirement for this system, as P=1 results in an infeasible Quadratic Programming (QP) problem. This minimum requirement is the initial selection, since it results in the smallest computational requirement.

For the design procedure, the output limits will not be applied, since they only make the design procedure more difficult (infeasible QP), while the outputs are not yet satisfactorily controlled. The output limits will only be applied in the plant simulation, which will be demonstrated in the next chapter. For the design procedure, and for all time-domain analysis, the input limits will be applied. In the case where hard constraints are imposed, the resulting control law is generally non-linear. The performance of such a control system has to be evaluated by time-simulation [12]. In the solution of the problem at hand there were important physical constraints as shown in Table 8.1. The rate constraints are expressed as a percentage of the maximum range of the MVs. Due to these constraints the control law had to be evaluated by means of time simulations.

Table 8.1: Constraints on manipulated variables

| Fan Power: $u_1$ | | | Slip-gap width: $u_2$ | | |
|---|---|---|---|---|---|
| Min | Rate | Max | Min | Rate | Max |
| 0 MW | 1% / s | 1 MW | 0.1 m | 1% / s | 0.5 m |

Table 8.2 gives a summary of the initial parameter selection (Y,U,M,P) and the output reference (R) signals. The reference signals for the outputs are chosen lower than the limits (where there are limits, although not applied), in order to prevent "Bang-bang control" in the implementation phase:

Table 8.2: Initial parameter selection summary C8.0

| Y(1) | r̄ (1) | Y(2) | r̄ (2) | Y(3) | r̄ (3) | U(1) | U(2) | M | P |
|---|---|---|---|---|---|---|---|---|---|
| 0.45 | -5 Pa | 1 | 0.5 % | 0.036 | 753 K | 1 | 1 | 1 | 2 |

### 8.3.3 Initial controller test

The fan power control signal is shown in Fig.8.1, and the slip-gap in Fig.8.2:

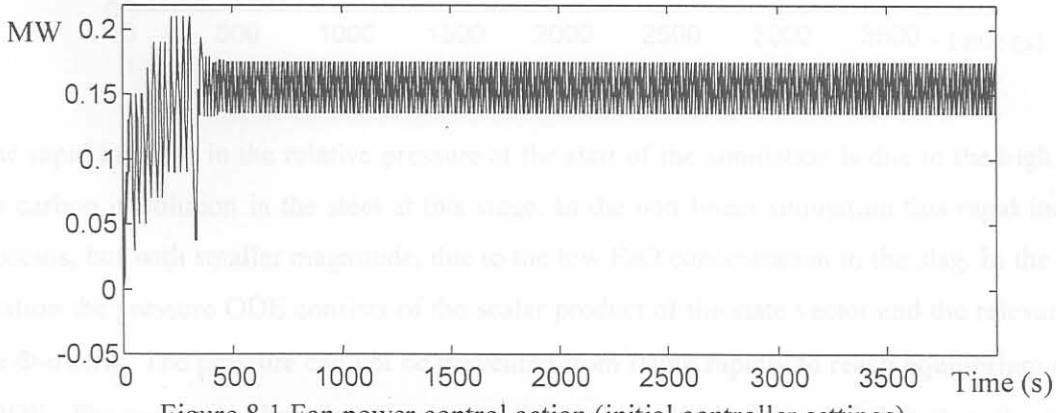


Figure 8.1 Fan power control action (initial controller settings)

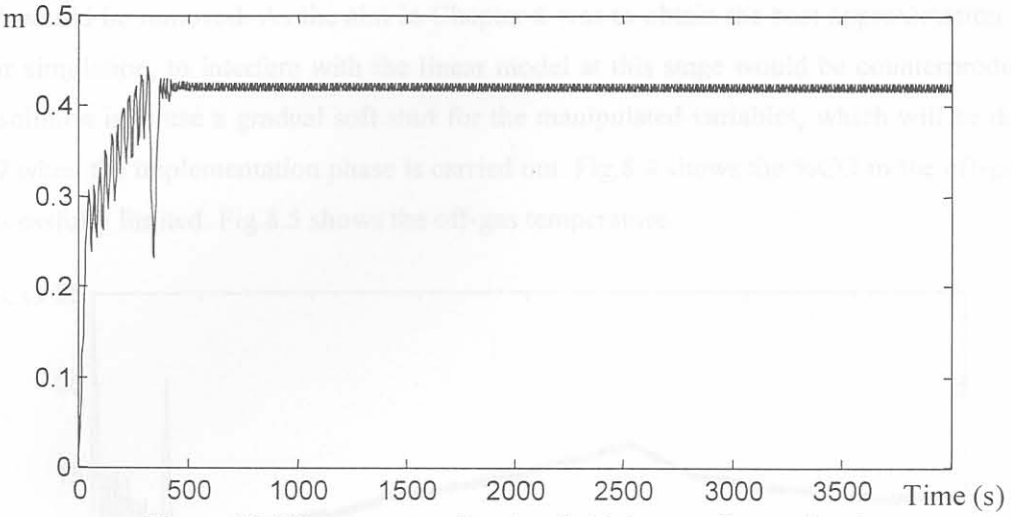


Figure 8.2 Slip-gap control action (initial controller settings)

It is seen from the preceding two figures that both control signals enter a limit cycle, also known as "ringing" [12]. In general this is undesirable in a controller as it adds unnecessary high frequency components that wear out actuators. The time step (sampling time) is one second. The initial controller is not successful as shown in the next three figures. Fig.8.3 shows the relative pressure, which does not even achieve a negative value.

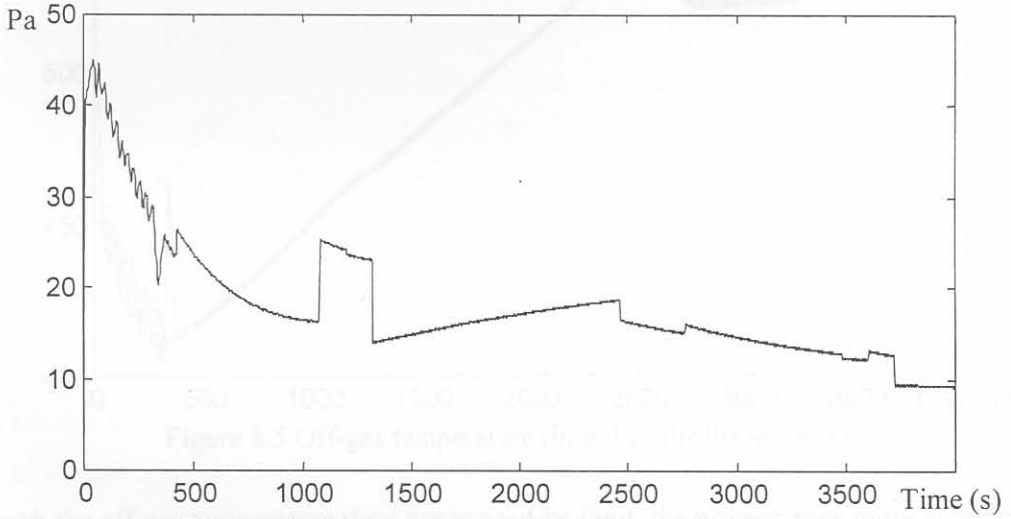


Figure 8.3 Relative pressure (initial controller settings)

The rapid increase in the relative pressure at the start of the simulation is due to the high value of the carbon in solution in the steel at this stage. In the non-linear simulation this rapid increase also occurs, but with smaller magnitude, due to the low FeO concentration in the slag. In the linear simulation the pressure ODE consists of the scalar product of the state vector and the relevant row of the Φ-matrix. The pressure can not be prevented from rising rapidly to reach equilibrium due to the ODE. The corresponding elements in the Φ-matrix could be removed, but then the aim of

Chapter 6 would be removed. As the aim in Chapter 6 was to obtain the best approximation to the non-linear simulation, to interfere with the linear model at this stage would be counterproductive. Another solution is to use a gradual soft start for the manipulated variables, which will be done in Chapter 9 when the implementation phase is carried out. Fig.8.4 shows the %CO in the off-gas that is not successfully limited. Fig.8.5 shows the off-gas temperature.

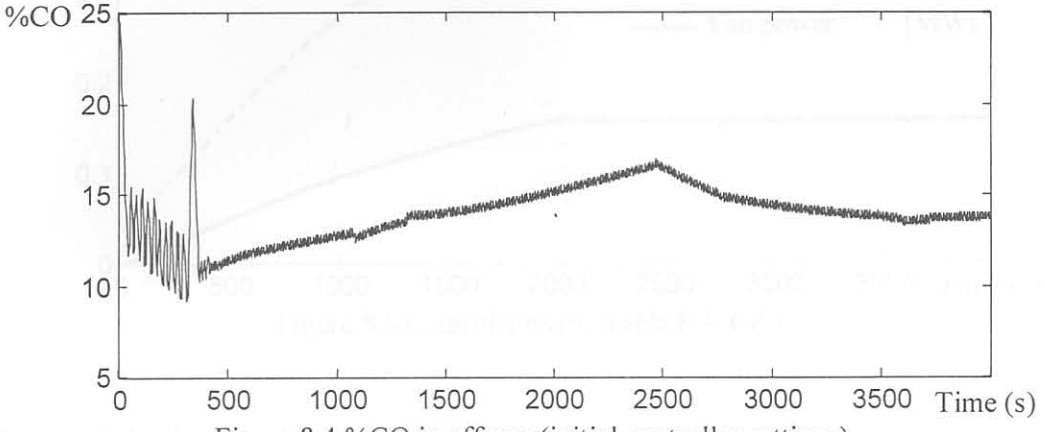


Figure 8.4 %CO in off-gas (initial controller settings)

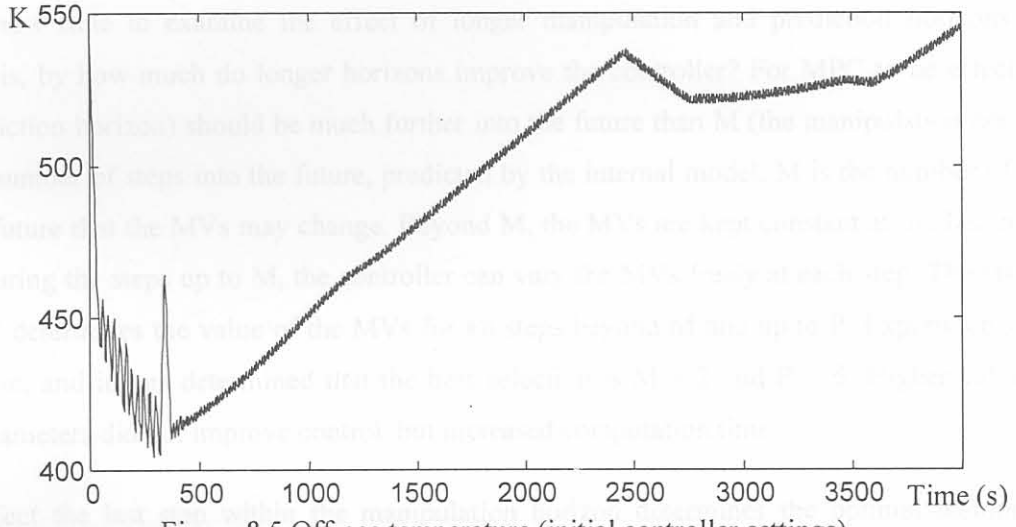


Figure 8.5 Off-gas temperature (initial controller settings)

Although the off-gas temperature does not exceed its limit, the process runs more economically if it is closer to its limit. In conclusion, the initial controller settings yield a noisy, unsuccessful controller. Before an attempt is made to improve the control, the manipulator noise must be reduced. Increasing the input cost weights, in the matrix **U** equation (8-1) can achieve this. Experiments were carried out to determine the input cost weight selection. The final result is shown here, with the input cost weights at 400 each. The new controller settings are in Table 8.3:

Table 8.3: Controller settings C8.1

| Y(1) | Y(2) | Y(3) | U(1) | U(2) | M | P |
|---|---|---|---|---|---|---|
| 0.45 | 1 | 0.036 | 400 | 400 | 1 | 2 |

The control responses shown in Fig.8.6 are much smoother than those in Fig.8.1 and Fig.8.2.

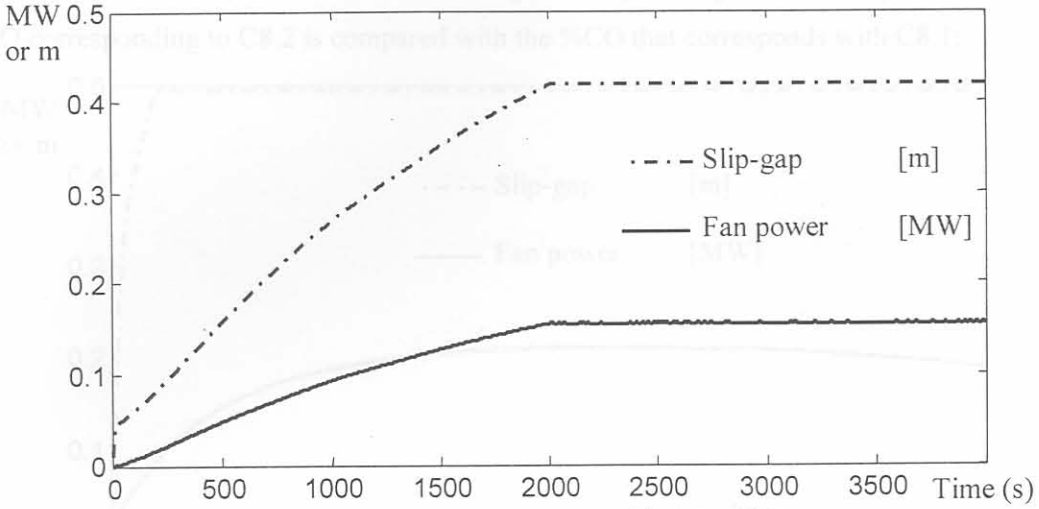


Figure 8.6 Control signals: Table 8.3: C8.1

### 8.3.4 Horizon Selection

It is now time to examine the effect of longer manipulation and prediction horizons. The question is, by how much do longer horizons improve the controller? For MPC to be effective P (the prediction horizon) should be much further into the future than M (the manipulation horizon). P is the number of steps into the future, predicted by the internal model. M is the number of steps into the future that the MVs may change. Beyond M, the MVs are kept constant at the last control value. During the steps up to M, the controller can vary the MVs freely at each step. The last step before M determines the value of the MVs for all steps beyond M and up to P. Experiments were carried out, and it was determined that the best selection is M = 2 and P = 6. Higher values for these parameters did not improve control, but increased computation time.

In effect the last step within the manipulation horizon determines the optimal manipulated variables in quasi-steady state. The time duration of this quasi-steady state (P-M) should preferably be an order of magnitude larger than M, to make it an approximation to steady state. Another way to see it is in terms of the dead time of the process response to the manipulated variables. The prediction horizon should extend beyond the manipulation horizon by more than the process dead time [49] (which is 1.09 s for the reaction time plus 1-2 s for the transport delay). If (P-M) is shorter than the dead time, the effect of the manipulation changes will not be seen in the prediction. The new controller settings are shown in Table 8.4:

Table 8.4: Controller settings C8.2

| Y(1) | Y(2) | Y(3) | U(1) | U(2) | M | P |
|---|---|---|---|---|---|---|
| 0.45 | 1 | 0.036 | 400 | 400 | **2** | **6** |

The control signals for C8.2 are shown in Fig.8.7. The horizon selection mainly caused an improvement in the %CO, which was reduced significantly throughout the simulation. In Fig.8.8 the %CO corresponding to C8.2 is compared with the %CO that corresponds with C8.1:

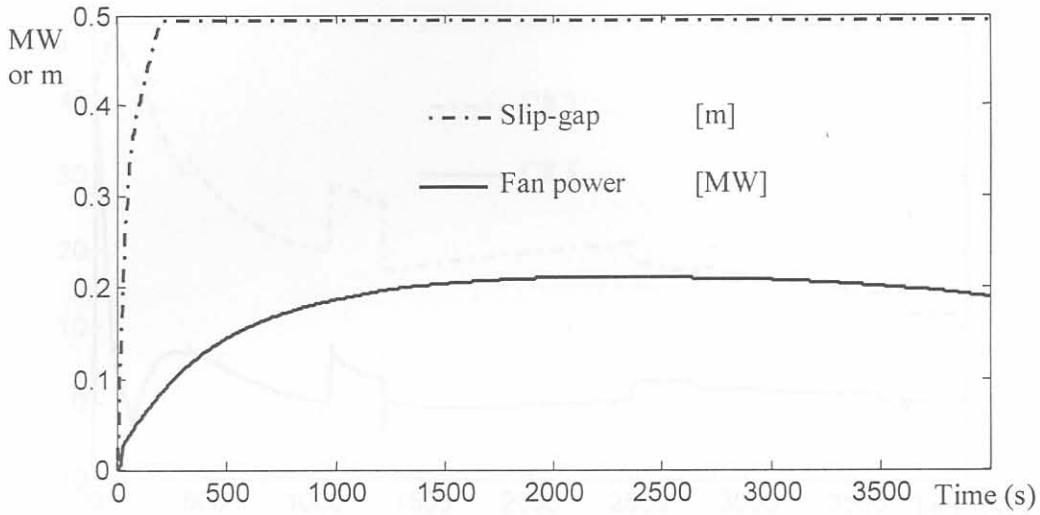


Figure 8.7 Control signals: Table 8.4: C8.2

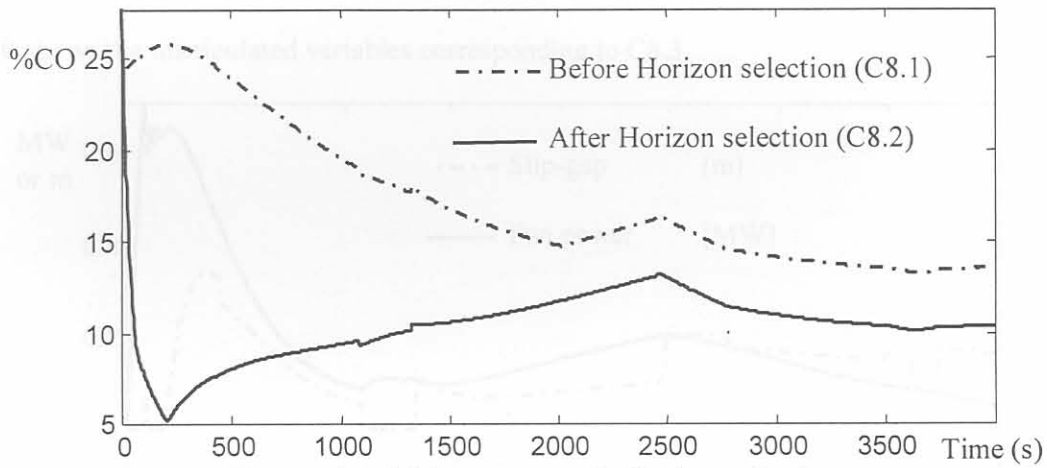


Figure 8.8 %CO improvement by horizon selection

### 8.3.5 Output Weight Selection

In the previous subsection, better horizon selection remarkably improved the controlled variable with the highest output cost weight, namely the %CO. The relative pressure was neglected though, and it still remains positive for the entire duration of the simulation. This introduces a severe safety hazard, as discussed in the previous chapters. To improve the relative pressure regulation, its output cost weight should be increased relative to the other cost weights. Experiments show that the particular cost weight directly improves the relative pressure regulation when it is multiplied by a factor up to a maximum of ten. When it is multiplied by a factor larger than ten the improvement is not enough to justify the increase in cost weight. The controller settings are shown in Table 8.5. Fig.8.9 compares the relative pressure regulation with the settings of C8.3 to that of C8.2.

Table 8.5: Controller settings C8.3

| Y(1) | Y(2) | Y(3) | U(1) | U(2) | M | P |
|---|---|---|---|---|---|---|
| **4.5** | 1 | 0.036 | 400 | 400 | 2 | 6 |

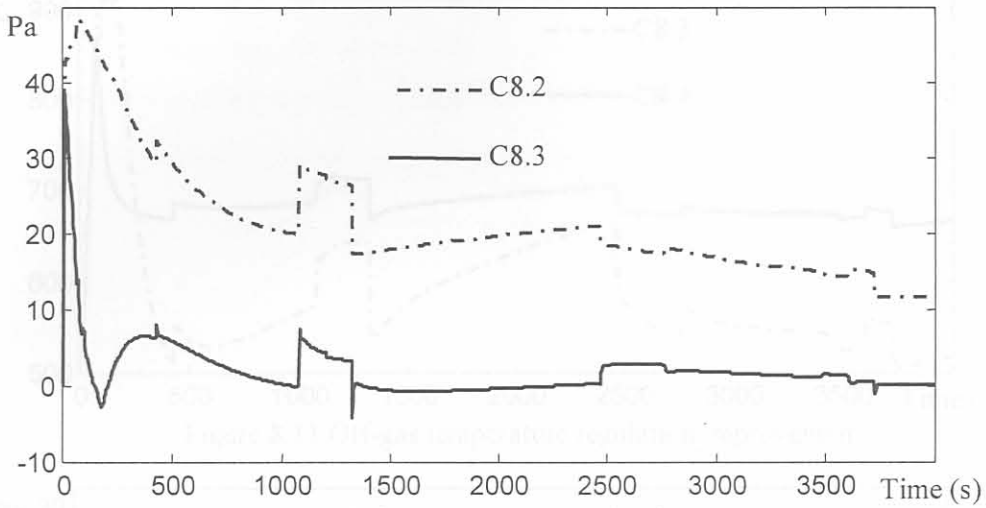


Figure 8.9 Relative pressure regulation improvement

Fig.8.10 shows the manipulated variables corresponding to C8.3.

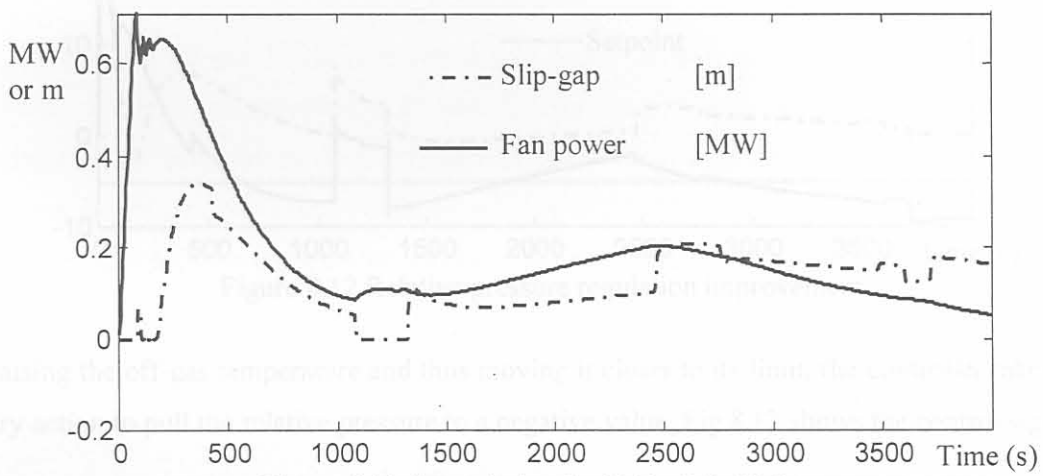


Figure 8.10 Control signals: Table 8.5: C8.3

The next adjustment made is to the output cost weight of the off-gas temperature. Experiments show that increase in the off-gas temperature cost weight brought the off-gas temperature closer to its limit and at the same time the relative pressure was made negative (setpoint = -5), although the regulation on the pressure was relaxed slightly. The off-gas temperature cost weight was multiplied by a factor of ten. A larger factor made the relative pressure too far negative and the off-gas %CO was also adversely affected. Table 8.6 indicates the new controller settings.

Table 8.6: Controller settings C8.4

| Y(1) | Y(2) | Y(3) | U(1) | U(2) | M | P |
|---|---|---|---|---|---|---|
| 4.5 | 1 | **0.36** | 400 | 400 | 2 | 6 |

Fig.8.11 compares the off-gas temperature between C8.4 and C8.3, while Fig.8.12 compares the relative pressure. It is clear from the figures that the emphasis shifted from regulating the pressure towards regulating the off-gas temperature (two conflicting agendas).

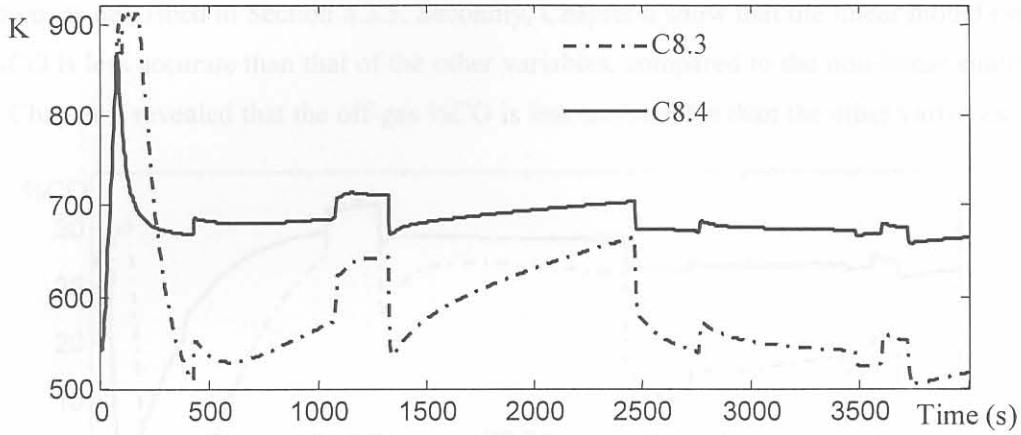


Figure 8.11 Off-gas temperature regulation improvement

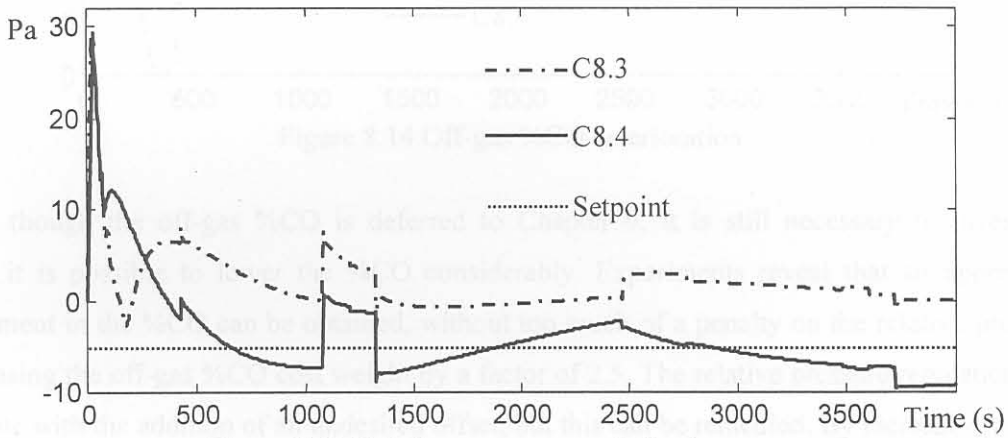


Figure 8.12 Relative pressure regulation improvement

By raising the off-gas temperature and thus moving it closer to its limit, the controller takes the necessary action to pull the relative pressure to a negative value. Fig.8.13 shows the control signals.

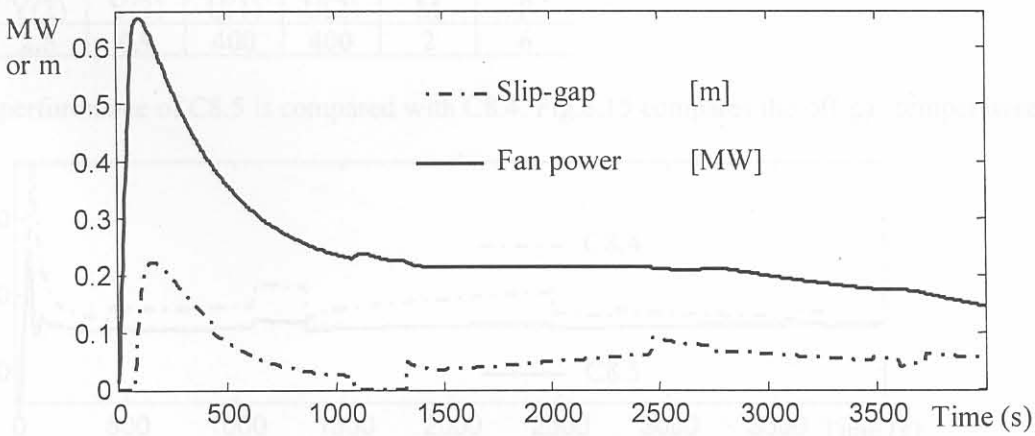


Figure 8.13 Control signals: Table 8.6: C8.4

As shown in Fig.8.14, this last controller tuning had a detrimental effect on the off-gas %CO, as it increases along with the off-gas temperature. There are three reasons why the off-gas %CO limit is not regarded as critically important here: Firstly, the off-gas %CO could not be brought below its limit before, as described in Section 8.3.5. Secondly, Chapter 6 show that the linear model estimate of the %CO is less accurate than that of the other variables, compared to the non-linear simulation. Thirdly, Chapter 7 revealed that the off-gas %CO is less controllable than the other variables.

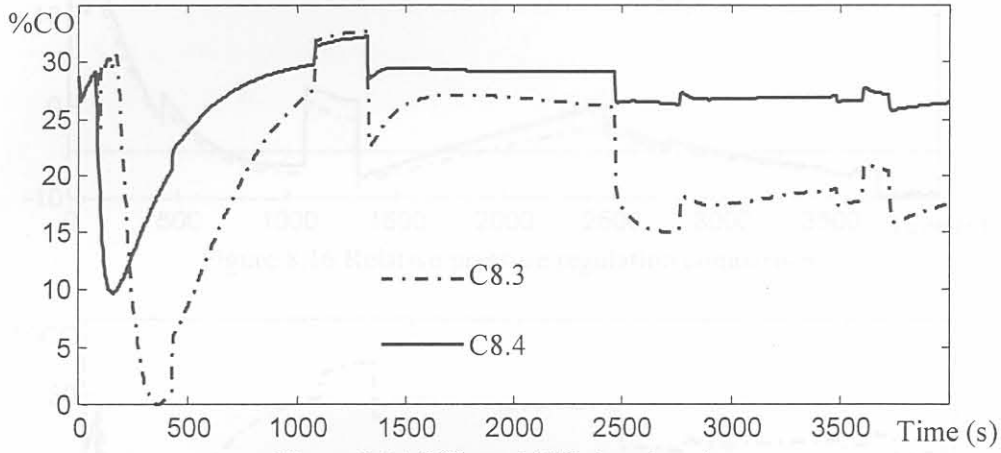


Figure 8.14 Off-gas %CO deterioration

Even though the off-gas %CO is deferred to Chapter 9, it is still necessary to investigate whether it is possible to lower the %CO considerably. Experiments reveal that an appreciable improvement in the %CO can be obtained, without too much of a penalty on the relative pressure, by increasing the off-gas %CO cost weight by a factor of 2.5. The relative pressure regulation does deteriorate with the addition of an undesired offset, but this can be remedied. By increasing the off-gas temperature cost weight by a factor of 2.5 as well, the pressure is brought back to its negative reference value. Table 8.7 summarises these controller settings.

Table 8.7: Controller settings C8.5

| Y(1) | Y(2) | Y(3) | U(1) | U(2) | M | P |
|---|---|---|---|---|---|---|
| 4.5 | **2.5** | **0.9** | 400 | 400 | 2 | 6 |

The performance of C8.5 is compared with C8.4. Fig.8.15 compares the off-gas temperature.

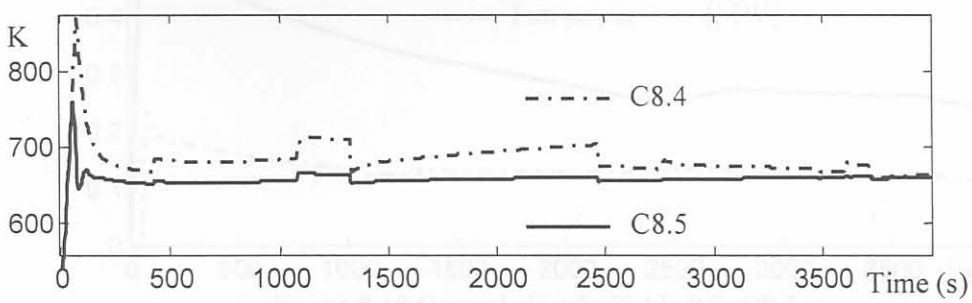


Figure 8.15 Off-gas temperature regulation comparison

Fig.8.16 compares the relative pressure regulation, which is slightly more relaxed for the final controller. Fig.8.17 compares the off-gas %CO, where the benefit of C8.5 is clearly seen.

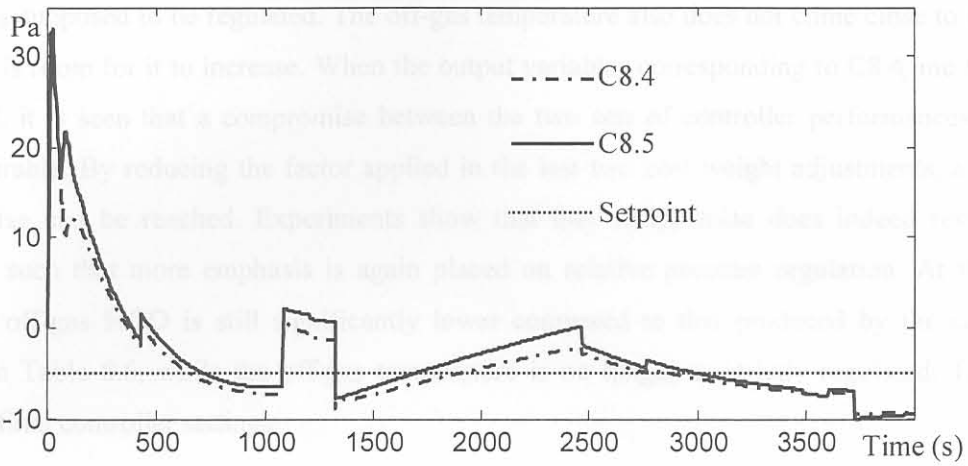


Figure 8.16 Relative pressure regulation comparison

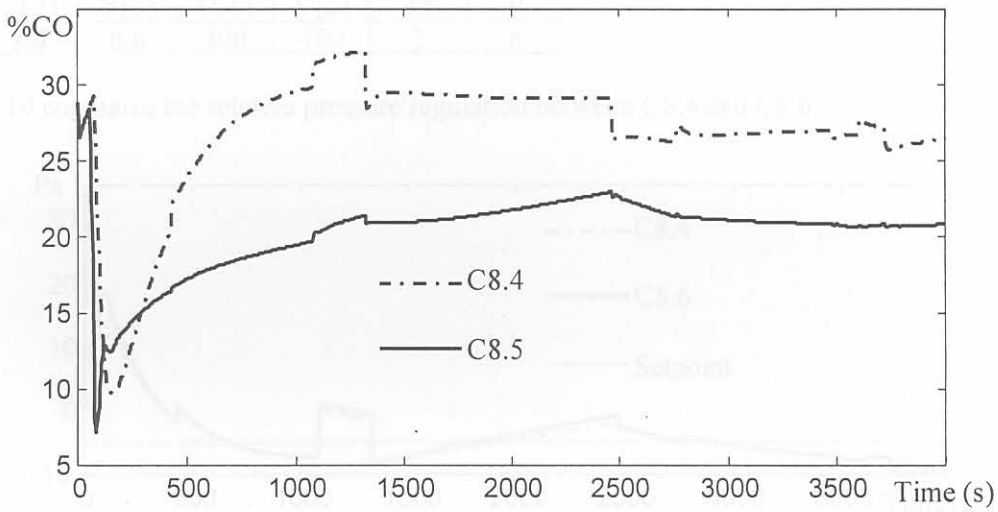


Figure 8.17 Off-gas %CO comparison

With C8.5 more emphasis is now placed on temperature regulation than on relative pressure regulation. Fig.8.18 shows the control signals corresponding to C8.5.

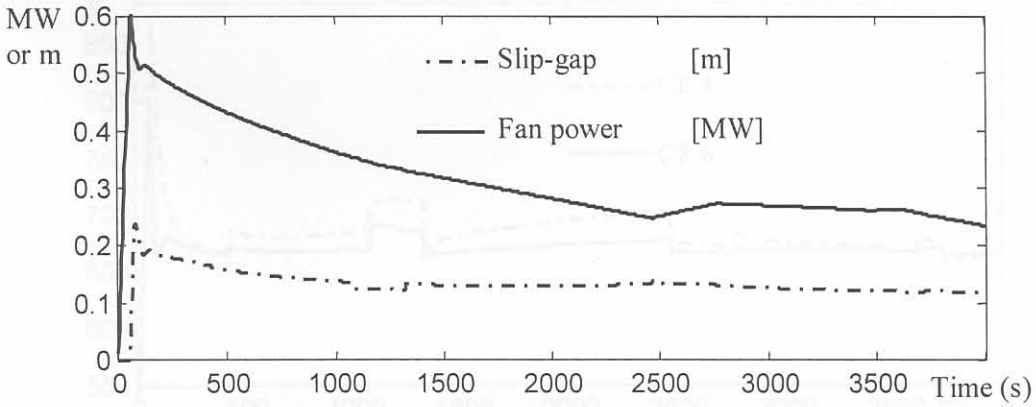


Figure 8.18 Control signals: Table 8.7: C8.5

The emphasis shift from relative pressure regulation to off-gas temperature regulation is undesirable. The off-gas temperature is not supposed to be regulated, only limited while the relative pressure is supposed to be regulated. The off-gas temperature also does not come close to its limit, and there is room for it to increase. When the output variables corresponding to C8.4, and C8.5 are compared, it is seen that a compromise between the two sets of controller performances will be more desirable. By reducing the factor applied in the last two cost weight adjustments, a suitable compromise can be reached. Experiments show that this compromise does indeed reverse the emphasis such that more emphasis is again placed on relative pressure regulation. At the same time, the off-gas %CO is still significantly lower compared to that produced by the controller settings in Table 8.6, while the off-gas temperature is no longer as strictly regulated. Table 8.8 gives the final controller settings.

Table 8.8: Final controller settings C8.6

| Y(1) | Y(2) | Y(3) | U(1) | U(2) | M | P |
|---|---|---|---|---|---|---|
| 4.5 | **1.6** | **0.6** | 400 | 400 | 2 | 6 |

Fig.8.19 compares the relative pressure regulation between C8.4 and C8.6.

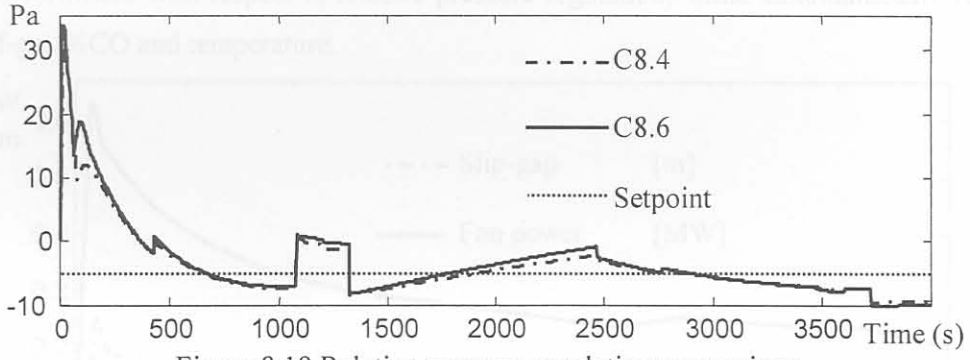


Figure 8.19 Relative pressure regulation comparison

Fig.8.20 compares the off-gas temperature produced by C8.4 and C8.6.

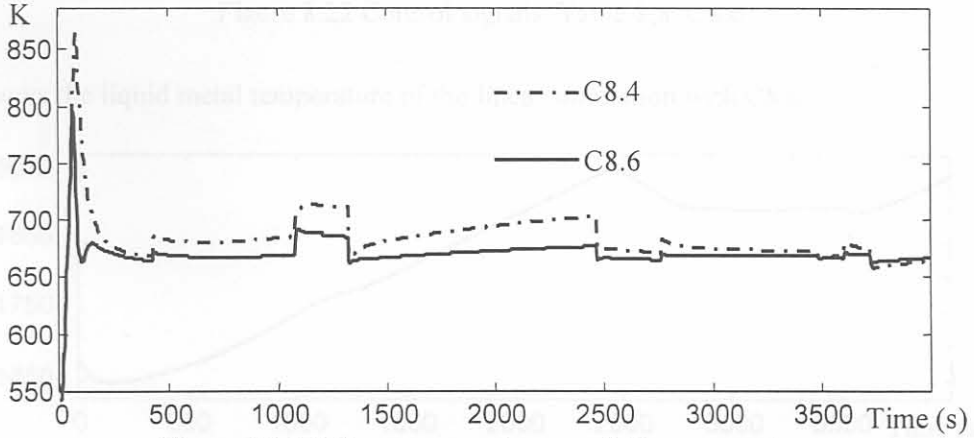


Figure 8.20 Off-gas temperature regulation comparison

Fig.8.21 compares the off-gas %CO produced by C8.4 and C8.6.

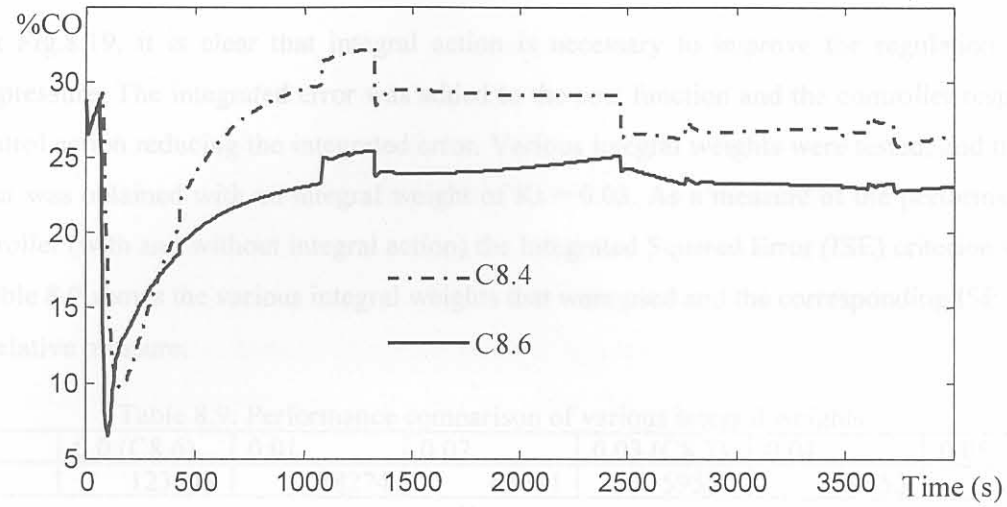


Figure 8.21 Off-gas %CO comparison

Fig.8.22 shows the control signals of the final controller. It is evident that the compromise results in smoother control actions and at the same time strengthening them against the effects of unmeasured disturbances. The final controller settings enable the controller to maintain practically the same performance with respect to relative pressure regulation, while simultanuously reducing both the off-gas %CO and temperature.

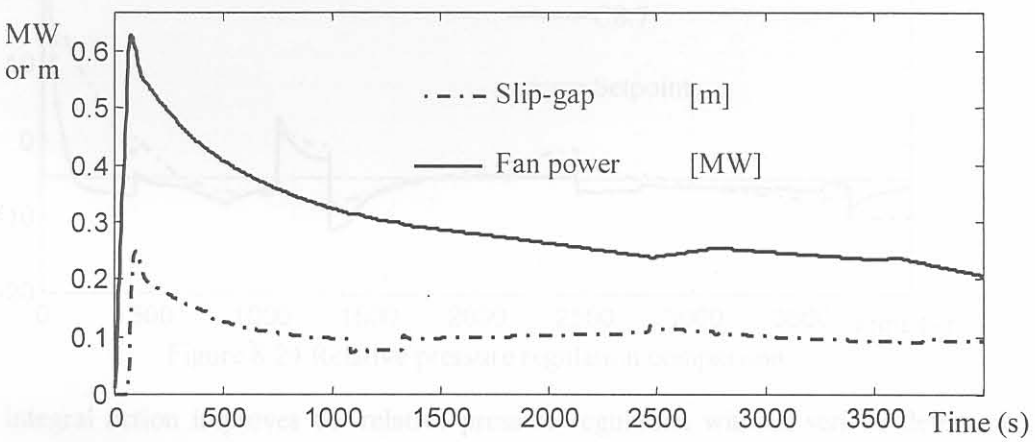


Figure 8.22 Control signals: Table 8.8: C8.6

Fig.8.23 shows the liquid metal temperature of the linear simulation with C8.6.

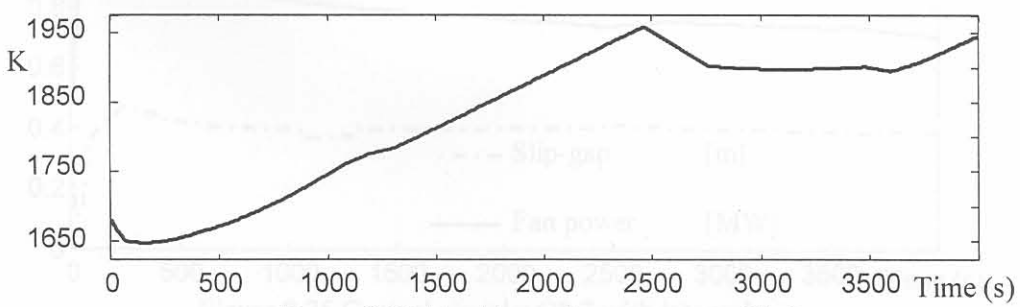


Figure 8.23 Liquid metal temperature: C8.6

## 8.4 INTEGRAL ACTION

From Fig.8.19, it is clear that integral action is necessary to improve the regulation of the relative pressure. The integrated error was added to the cost function and the controller responded with control action reducing the integrated error. Various integral weights were tested, and the best controller was obtained with an integral weight of Ki = 0.03. As a measure of the performance of the controller (with and without integral action) the Integrated Squared Error (ISE) criterion will be used. Table 8.9 shows the various integral weights that were used and the corresponding ISE values for the relative pressure.

Table 8.9: Performance comparison of various integral weights

| Weight | 0.0 (C8.6) | 0.01 | 0.02 | 0.03 (C8.7) | 0.04 | 0.05 |
|---|---|---|---|---|---|---|
| ISE | 123449 | 78274 | 63611 | 59557 | 59753 | 60301 |

In Fig.8.24 the performance of the controller with integral action (C8.7) on relative pressure is compared to that of the controller without integral action (C8.6):

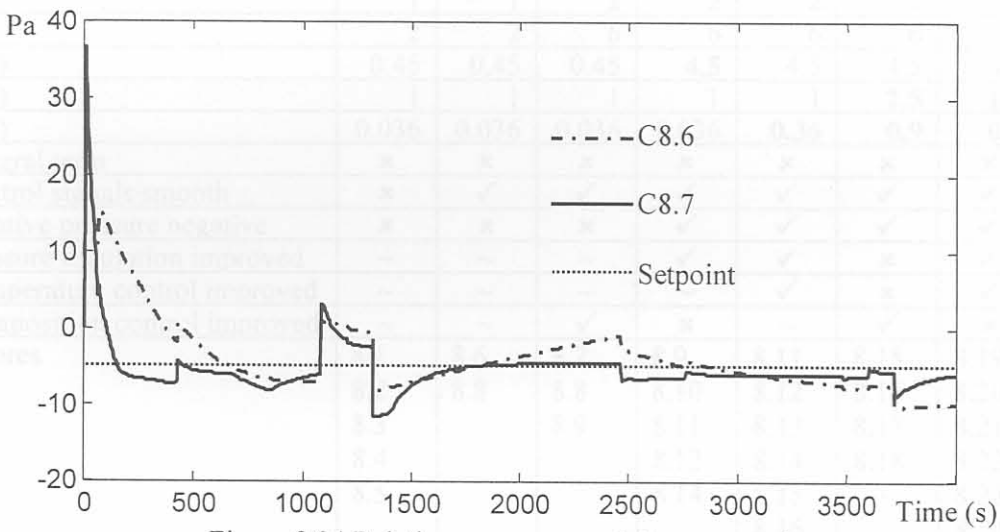


Figure 8.24 Relative pressure regulation comparison

The integral action improves the relative pressure regulation without serious deterioration of either of the other two outputs. Fig.8.25 shows the control signals corresponding to C8.7:

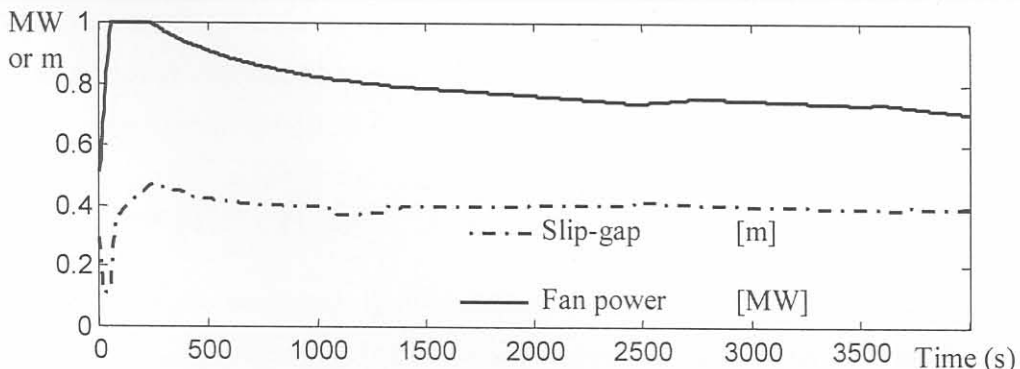


Figure 8.25 Control signals: C8.7 with integral

## 8.5 CONCLUSION

The controller was designed by selecting the various parameters that are available for design. By increasing the input cost function weights, the control signal noise was reduced. By increasing the manipulation horizon (M) and the prediction horizon (P), the range over which optimisation is done is increased, thus improving the controller's ability to select the optimal MVs. Selecting the output cost function weights achieves the necessary emphasis shifts. The use of an integral term in the cost function enables the controller to eliminate unwanted offsets, and therefore improves the setpoint tracking and regulation. Table 8.10 gives a summary of the various controllers in this chapter, indicating characteristics and the figures where the corresponding inputs or outputs are shown:

Table 8.10 Summary of control characteristics

| | C8.0 | C8.1 | C8.2 | C8.3 | C8.4 | C8.5 | C8.6 | C8.7 |
|---|---|---|---|---|---|---|---|---|
| U(1)&U(2) | 1 | **400** | 400 | 400 | 400 | 400 | 400 | 400 |
| M | 1 | 1 | **2** | 2 | 2 | 2 | 2 | 2 |
| P | 2 | 2 | **6** | 6 | 6 | 6 | 6 | 6 |
| Y(1) | 0.45 | 0.45 | 0.45 | **4.5** | 4.5 | 4.5 | 4.5 | 4.5 |
| Y(2) | 1 | 1 | 1 | 1 | 1 | **2.5** | **1.6** | 1.6 |
| Y(3) | 0.036 | 0.036 | 0.036 | 0.036 | **0.36** | **0.9** | **0.6** | 0.6 |
| Integral term | × | × | × | × | × | × | × | ✓ |
| Control signals smooth | × | ✓ | ✓ | ✓ | ✓ | ✓ | ✓ | ✓ |
| Relative pressure negative | × | × | × | ✓ | ✓ | ✓ | ✓ | ✓ |
| Pressure regulation improved | ~ | ~ | ~ | ✓ | ✓ | × | ✓ | ✓ |
| Temperature control improved | ~ | ~ | ~ | ~ | ✓ | × | ✓ | ~ |
| Composition control improved | ~ | ~ | ✓ | × | ~ | ✓ | × | ~ |
| Figures | 8.1<br>8.2<br>8.3<br>8.4<br>8.5 | 8.6<br>8.8 | 8.7<br>8.8<br>8.9 | 8.9<br>8.10<br>8.11<br>8.12<br>8.14 | 8.11<br>8.12<br>8.13<br>8.14<br>8.15<br>8.16<br>8.17<br>8.19<br>8.20<br>8.21 | 8.15<br>8.16<br>8.17<br>8.18 | 8.19<br>8.20<br>8.21<br>8.22<br>8.23<br>8.24 | 8.24<br>8.25 |

# CHAPTER 9: CONTROL IMPLEMENTATION

## 9.1 INTRODUCTION

The aim of this chapter is to illustrate how the controller is implemented on the full non-linear plant model, with the use of custom written software. In the implementation it will be necessary to perform a final fine-tuning of the controller. A brief explanation of the implementation software structure is also necessary. The final controller is evaluated against manual control, as shown in the simulation in Chapter 5.

During the controller design phase, the objective was to obtain a controller with acceptable performance. Once this objective is reached, the next step is to test the controller on the "plant" for which it was designed and to fine-tune it. Fine-tuning or "on-line tuning" is essentially done using trial-and-error. To make it effective however, a strategy is devised to determine how tuning parameters should be utilised in the process. The strategy is based on findings from the previous chapter. There are three rules that will be applied:

- If a limited output does not come close to its limit, decrease its cost function weight;
- If a limited output exceeds its limit, increase its cost function weight and/or take its setpoint further away from (further lower than) the limit, so as to regulate it better;
- If the relative pressure can be regulated better, increase its cost function weight, unless it causes undesirable oscillatory or unstable behaviour.

In order to do meaningful tests, a fundamental understanding of the simulation system is necessary. To illustrate the chronological order of the program implementation, a program flowchart [50] is used. Program flowcharts are also used to facilitate the discussions of the MPC and the quadratic programming (QP) algorithms.

In Section 9.2 the structure of the non-linear closed loop simulation is explained. Section 9.3 gives the structure of the MPC algorithm. Section 9.4 gives the structure of the QP optimisation algorithm. Section 9.5 gives the structure of the plant simulation. In Section 9.6 the fine-tuning of the controller is discussed and illustrated. The evaluation of each successive improvement is done and the results are shown. In Section 9.7 the achievement of the control objectives are discussed.

## 9.2 SIMULATION STRUCTURE

The structure of the simulation is illustrated in the program flowchart in Fig.9.1, where the blocks with bold edges indicate algorithms that are discussed in more detail. The disturbance inputs and initial conditions are the same as those discussed in Chapter 5. The internal model prediction

matrices are calculated in advance, since the assumption of superposition is used with the internal model predictions. This assumption is valid for the internal model, since it is a linear system. For matrix manipulations such as matrix inversion see [51,52] and (programmed in C) [53].

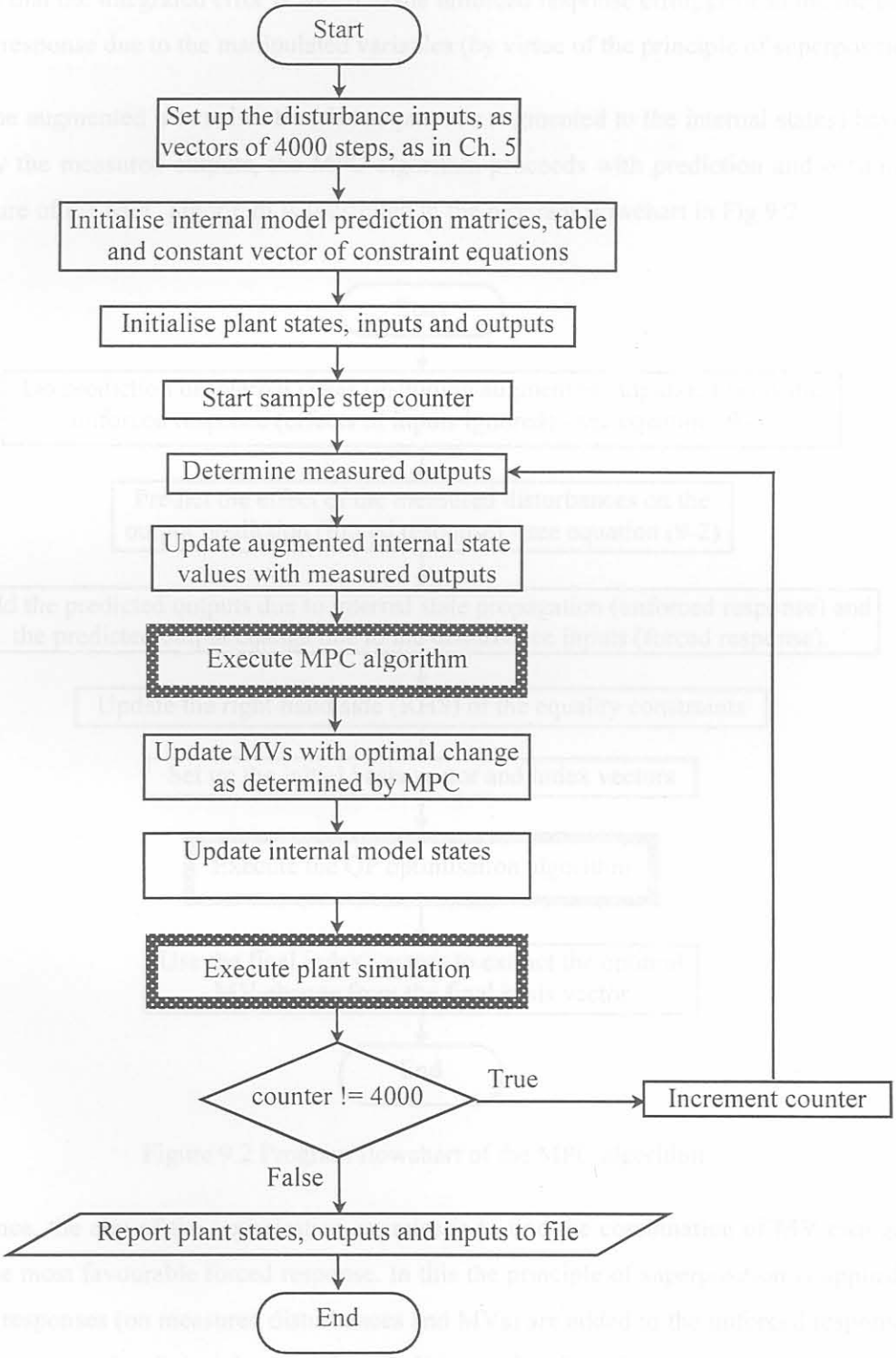


Figure 9.1 Program flowchart of non-linear simulation structure

## 9.3 MPC ALGORITHM

For the basic MPC algorithm there is no integrated error term and since it was added only later (Section 8.4) to improve the regulation capability of the controller, it is not shown here. It suffices to mention that the integrated error is added to the unforced response error, prior to the inclusion of the forced response due to the manipulated variables (by virtue of the principle of superposition).

After the augmented internal states (the outputs are augmented to the internal states) have been updated by the measured outputs, the MPC algorithm proceeds with prediction and optimisation. The structure of the MPC algorithm is illustrated in the program flowchart in Fig.9.2.

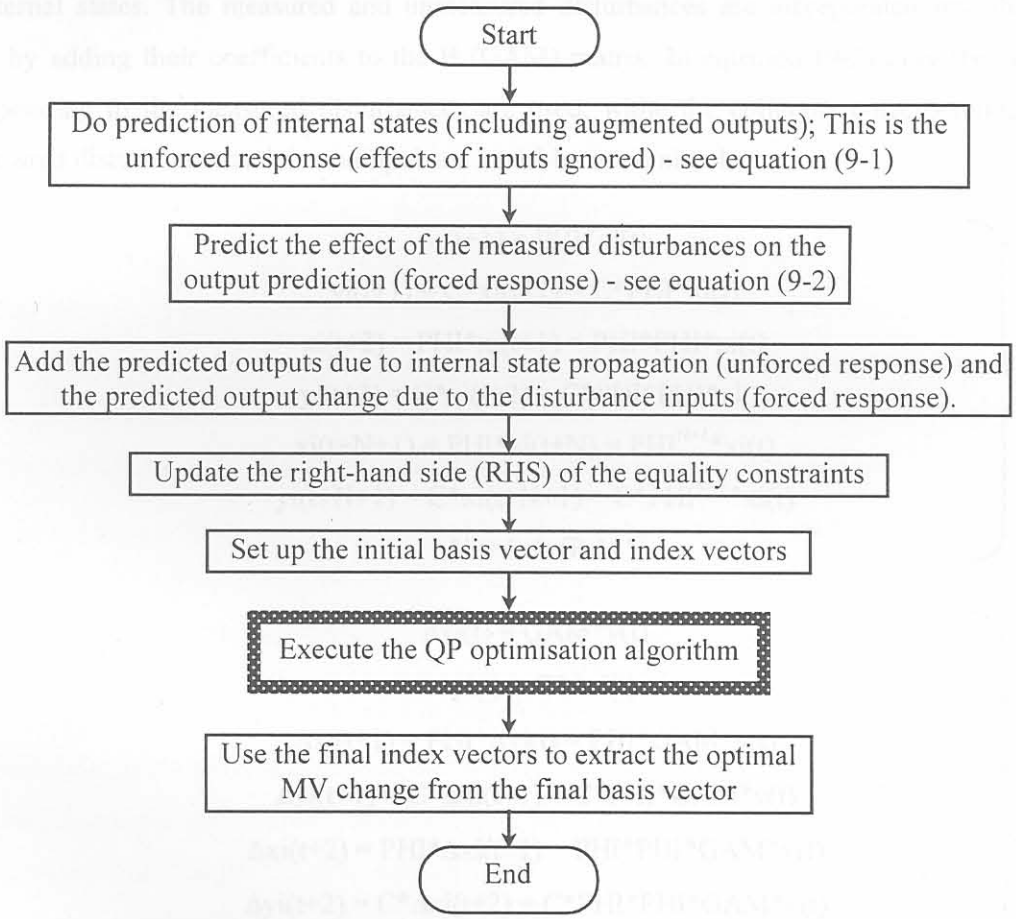


Figure 9.2 Program flowchart of the MPC algorithm

In essence, the aim of the optimisation exercise is to find the combination of MV changes that produce the most favourable forced response. In this the principle of superposition is applied since the forced responses (on measured disturbances and MVs) are added to the unforced response. The unforced response is shown in equation (9-1) and the forced response (on the measured disturbances) is shown in equation (9-2).

The following parameters appear in equations (9-1) and (9-2):

xi – internal model states, augmented with the outputs;

yi – internal model outputs;

v – measured disturbances.

$\Delta$xi and $\Delta$yi are the forced responses due to the measured disturbances, and are added to xi and yi respectively, by virtue of the priciple of superposition.

The PHI and GAM matrices are the discrete time versions of the A and B matrices of a continous time-invariant linear system model. The PHI matrix has a dimension equal to the sum of the number of states and the number of outputs. This is due to the augmentation of the outputs to the internal states. The measured and unmeasured disturbances are incorporated into the linear model by adding their coefficients to the B (GAM) matrix. In equation (9-2) only the collumns corresponding to the measured disturbances are used, while the collumns corresponding to the unmeasured disturbances and the manipulated variables are omitted.

$$
\begin{aligned}
xi(t+1) &= PHI*xi(t) \\
yi(t+1) &= C*xi(t+1) = C*PHI*xi(t) \\
xi(t+2) &= PHI*xi(t+1) = PHI*PHI*xi(t) \\
yi(t+2) &= C*xi(t+2) = C*PHI*PHI*xi(t) \\
xi(t+N+1) &= PHI*xi(t+N) = PHI^{N+1}*xi(t) \\
yi(t+N+1) &= C*xi(t+N+1) = C*PHI^{N+1}*xi(t) \\
N &= 1 \rightarrow (P-1)
\end{aligned}
\qquad (9\text{-}1)
$$

$$
\begin{aligned}
\Delta xi(t) &= GAM*v(t) \\
\Delta yi(t) &= C*\Delta xi(t) \\
\Delta xi(t+1) &= PHI*\Delta xi(t) = PHI*GAM*v(t) \\
\Delta yi(t+1) &= C*\Delta xi(t+1) = C*PHI*GAM*v(t) \\
\Delta xi(t+2) &= PHI*\Delta xi(t+1) = PHI*PHI*GAM*v(t) \\
\Delta yi(t+2) &= C*\Delta xi(t+2) = C*PHI*PHI*GAM*v(t) \\
\Delta xi(t+N+1) &= PHI*\Delta xi(t+N) = PHI^{N+1}*GAM*v(t) \\
\Delta yi(t+N+1) &= C*\Delta xi(t+N+1) = C*PHI^{N+1}*GAM*v(t) \\
N &= 1 \rightarrow (P-1)
\end{aligned}
\qquad (9\text{-}2)
$$

## 9.4 QUADRATIC PROGRAMMING ALGORITHM

George B. Dantzig originally formulated the QP algorithm used by Morari and Ricker [12] in the MPC toolbox for Matlab®. Boot [47], Dano [54] and Peressini *et al* [55] discuss this algorithm, and [56,57,58] discuss related theory in optimisation and optimality in mathematical programming.

A brief summary of the algorithm will suffice. The algorithm is also known as the "Simplex" method or the "Dantzig-van de Panne" method, and is preferred to the other methods (Wolfe's method and Beale's method) as it has proven to be far more efficient [54].

The simplex method is intended for linear systems with a quadratic cost (performance-) function and linear inequality constraints. The QP algorithm is guaranteed (for a linear system) to progress monotonically [47] towards an optimal solution. To apply the QP algorithm, a linear system model is necessary, so that the principle of superposition may be used. This implies that if there is a feasible optimal solution, then the algorithm will find it in a finite number of iterations.

If there is no feasible solution (due to severe constraints that cannot possibly be satisfied), then the algorithm returns without a solution. Therefore, if there is a (any) feasible solution, the algorithm will return with an optimal feasible solution. The objective with the simplex method is to obtain a table in standard form, while the solution has all the basis (containing the primal variables) elements non-negative. To do this, a set of rules is followed, which is explained in [47,54,55] and briefly described in Fig.9.3 that summarises the main procedures of the algorithm.

The following variables are mentioned in Fig.9.3: The dual variables are Lagrangian multipliers for the inequality constraint equations, while the primal variables are the actual input or output variables that feature in the constraint equations.

The common simplex method is used in linear programming as well as quadratic programming. In the common simplex method a variable is selected for replacement as follows:

- From the column (q) of the variable that is to be introduced to the basis, form the quotients of the basis element $B_i$ and the table element $TAB_{iq}$ for all i, (the available rows);
- Test which quotient is the smallest non-negative, let
  $Q_{min} = B_p/TAB_{pq} <= B_i/TAB_{iq}$ for all i, **and** $Q_{min} >= 0$;
- Then the variable in row (p) of the basis is the one to be replaced;
- In other words, $TAB_{pq}$ is to be the pivot element (pivoting exactly as in Gaussian elimination).

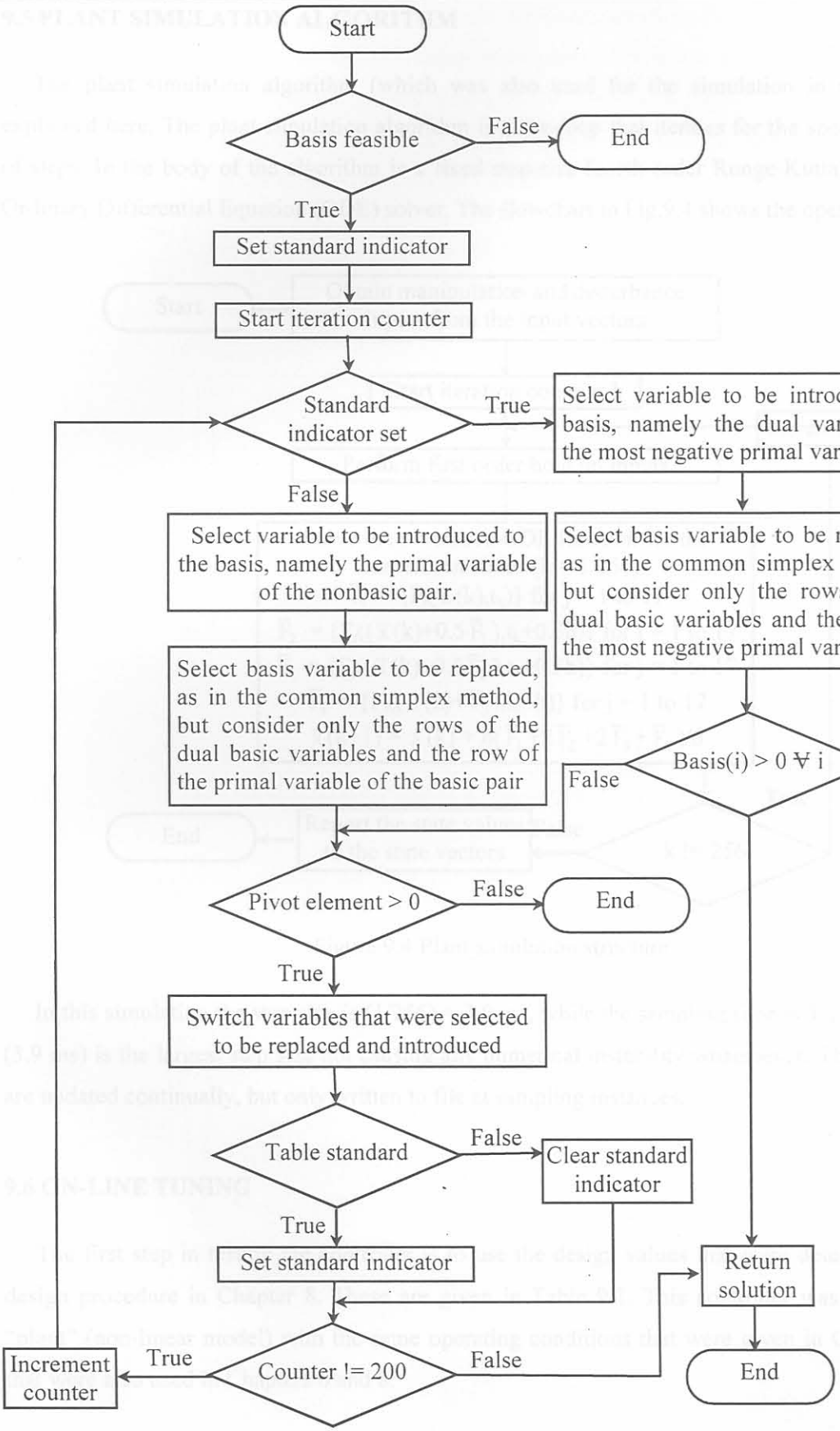


Figure 9.3 Quadratic programming algorithm

## 9.5 PLANT SIMULATION ALGORITHM

The plant simulation algorithm (which was also used for the simulation in Chapter 5) is explained here. The plant simulation algorithm is a **for**-loop that iterates for the specified number of steps. In the body of the algorithm is a fixed step-size fourth-order Runge-Kutta multivariable Ordinary Differential Equation (ODE) solver. The flowchart in Fig.9.4 shows the operation:

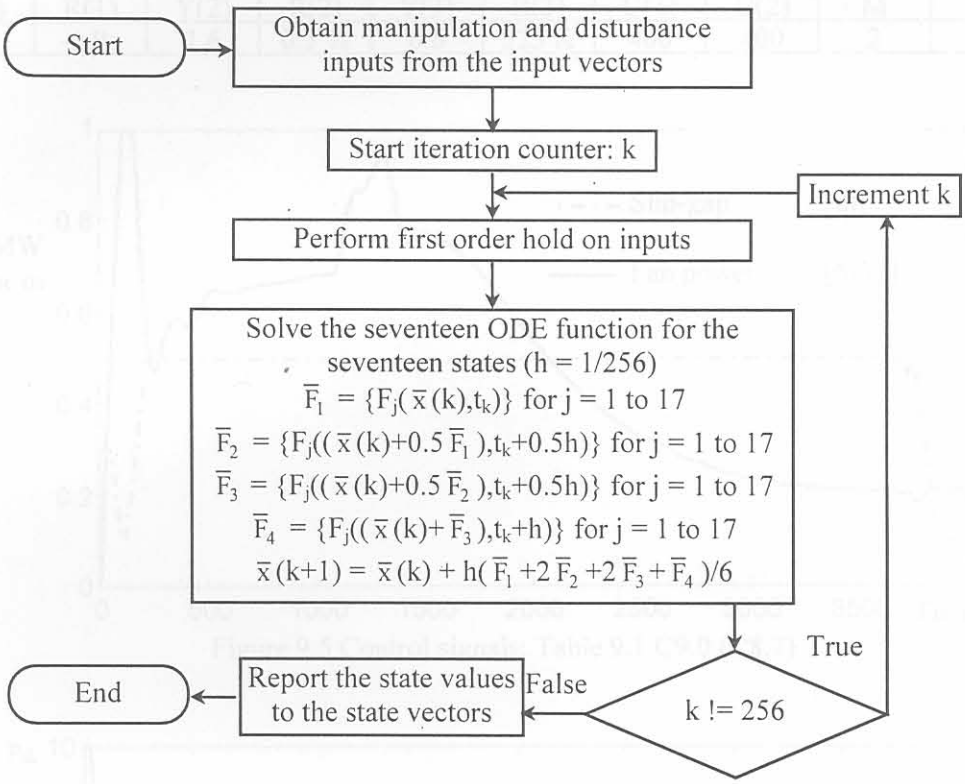


Figure 9.4 Plant simulation structure

In this simulation the step size is (1/256) = 3.9 ms, while the sampling time is 1 s. The step size (3.9 ms) is the largest step size not causing any numerical instability whatsoever. The state values are updated continually, but only written to file at sampling instances.

## 9.6 ON-LINE TUNING

The first step in testing the controller is to use the design values that were determined by the design procedure in Chapter 8. These are given in Table 9.1. This controller was tested on the "plant" (non-linear model) with the same operating conditions that were given in Chapter 5, and that were also used in Chapters 6 and 8.

The control signals are shown in Fig.9.5, and the three outputs in Fig.9.6, Fig.9.7 and Fig.9.8. After several experiments with the non-linear closed-loop simulation it was determined that the setpoint for the off-gas temperature needs to be made at least 100 K below the off-gas temperature limit, otherwise an infeasible QP problem results. To remedy this the setpoint for the off-gas temperature was set at 523 K. The other settings are also shown in Table 9.1.

Table 9.1: Controller settings from linear design (C9.0 = = C8.7)

| Y(1) | R(1) | Y(2) | R(2) | Y(3) | R(3) | U(1) | U(2) | M | P |
|---|---|---|---|---|---|---|---|---|---|
| 4.5 | -5 Pa | 1.6 | 0.5 % | 0.6 | 523 K | 400 | 400 | 2 | 6 |

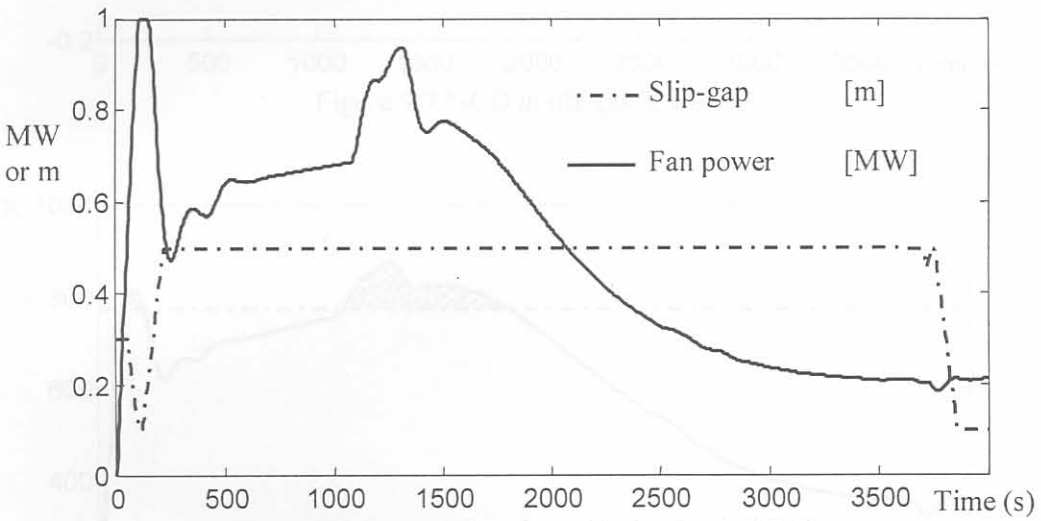


Figure 9.5 Control signals: Table 9.1 C9.0 (C8.7)

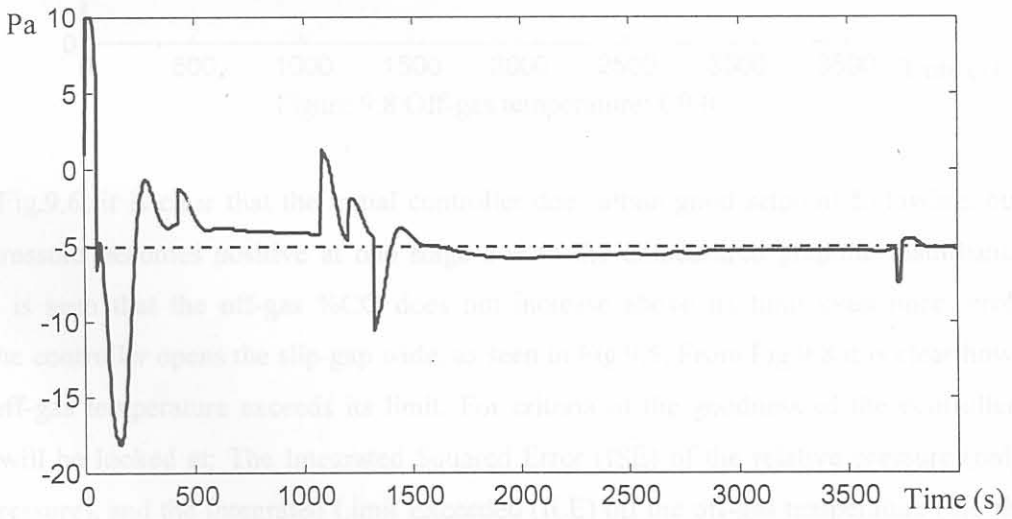


Figure 9.6 Relative pressure: C9.0

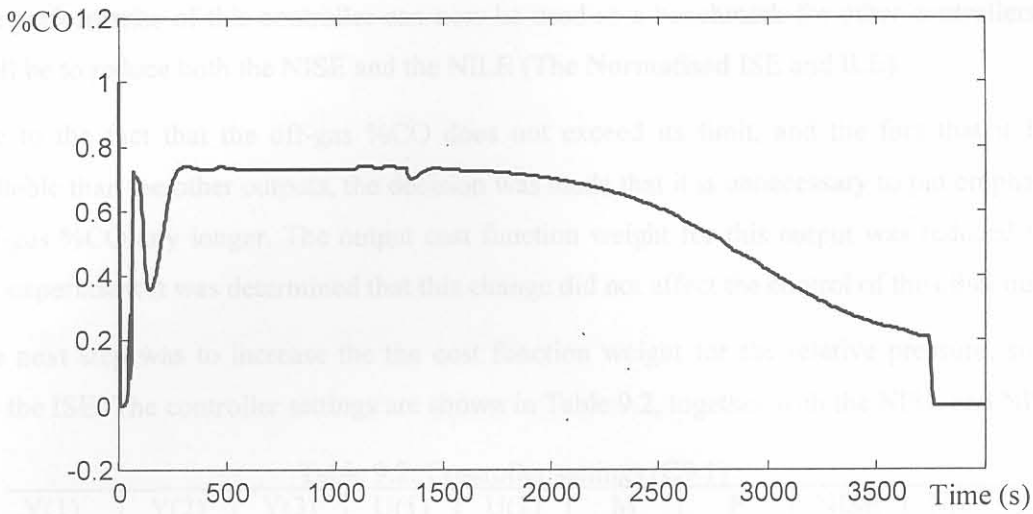


Figure 9.7 %CO in off-gas: C9.0

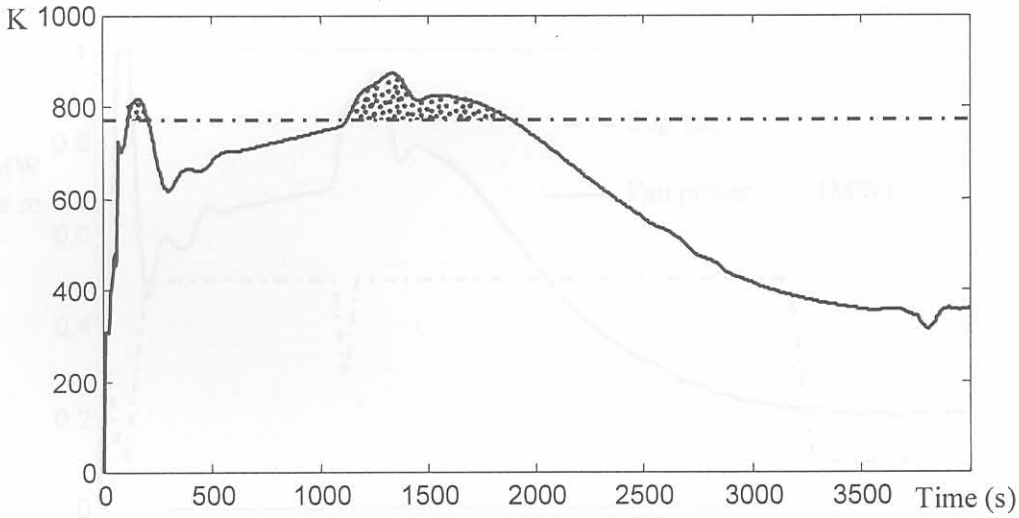


Figure 9.8 Off-gas temperature: C9.0

From Fig.9.6, it is clear that the initial controller does attain good setpoint following, but the relative pressure becomes positive at one stage due to the unmeasured graphite disturbance. In Fig.9.7 it is seen that the off-gas %CO does not increase above its limit even once, probably because the controller opens the slip-gap wide, as seen in Fig.9.5. From Fig.9.8 it is clear however, that the off-gas temperature exceeds its limit. For criteria of the goodness of the controller two numbers will be looked at: The Integrated Squared Error (ISE) of the relative pressure (only the relative pressure), and the Integrated Limit Exceeded (ILE) off the off-gas temperature (the shaded part in Fig.9.8). For the initial controller the values were as follows:

ISE(C9.0) = 32593 if normalised it is NISE = 1;

ILE(C9.0) = 41724 if normalised it is NILE = 1.

The performance of this controller can now be used as a benchmark for other controllers. The aim will be to reduce both the NISE and the NILE (The **Normalised** ISE and ILE).

Due to the fact that the off-gas %CO does not exceed its limit, and the fact that it is less controllable than the other outputs, the decision was made that it is unnecessary to put emphasis on the off-gas %CO any longer. The output cost function weight for this output was reduced to 1.0, and by experiment it was determined that this change did not affect the control of the other outputs.

The next step was to increase the the cost function weight for the relative pressure, so as to reduce the ISE. The controller settings are shown in Table 9.2, together with the NISE and NILE:

Table 9.2: Controller settings (C9.1)

| Y(1) | Y(2) | Y(3) | U(1) | U(2) | M | P | NISE | NILE |
|---|---|---|---|---|---|---|---|---|
| **5.5** | 1.0 | 0.6 | 400 | 400 | 2 | 6 | 0.9198 | 1.0574 |

The control signals of C9.1 are shown in Fig.9.9 and the relative pressure in Fig.9.10.

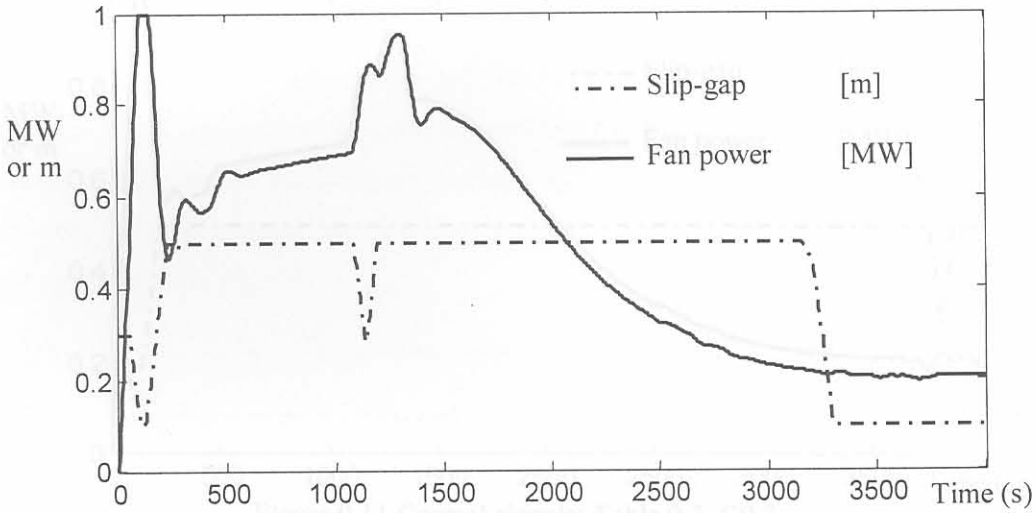


Figure 9.9 Control signals: Table 9.2: C9.1

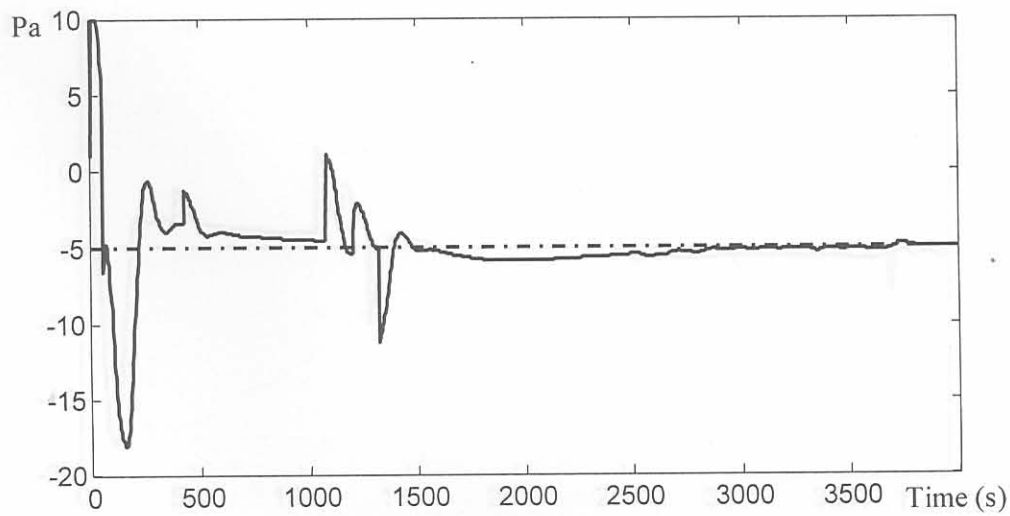


Figure 9.10 Relative pressure: C9.1

The performance of C9.1 relative to C9.0 is obtained by normalising the ISE and the ILE of C9.1 with respect to that of C9.0. The normalised ISE (NISE) and the normalised ILE (NILE) will be used as performance criteria from now on. For C9.1 these are:

NISE = 0.9198

NILE = 1.0574

The next step is to increase the cost function weight for the off-gas temperature so as to decrease the ILE. The controller settings are shown in Table 9.3, together with the NISE and NILE:

Table 9.3: Controller settings (C9.2)

| Y(1) | Y(2) | Y(3) | U(1) | U(2) | M | P | NISE | NILE |
|---|---|---|---|---|---|---|---|---|
| 5.5 | 1.0 | **0.8** | 400 | 400 | 2 | 6 | 0.9531 | 0.9413 |

The control signals of C9.2 are shown in Fig.9.11 and the relative pressure in Fig.9.12. The increased effort to reduce the off-gas temperature compromised the relative pressure regulation.

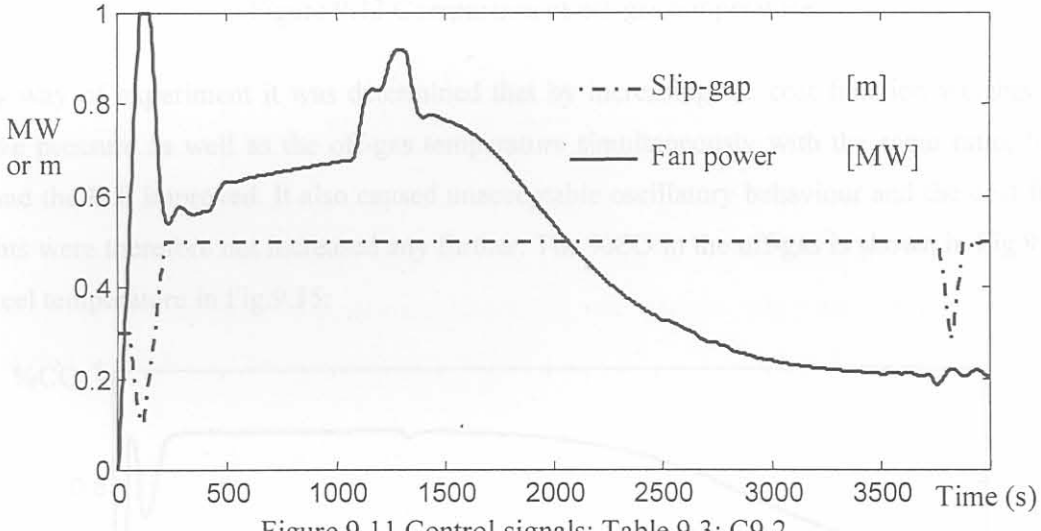


Figure 9.11 Control signals: Table 9.3: C9.2

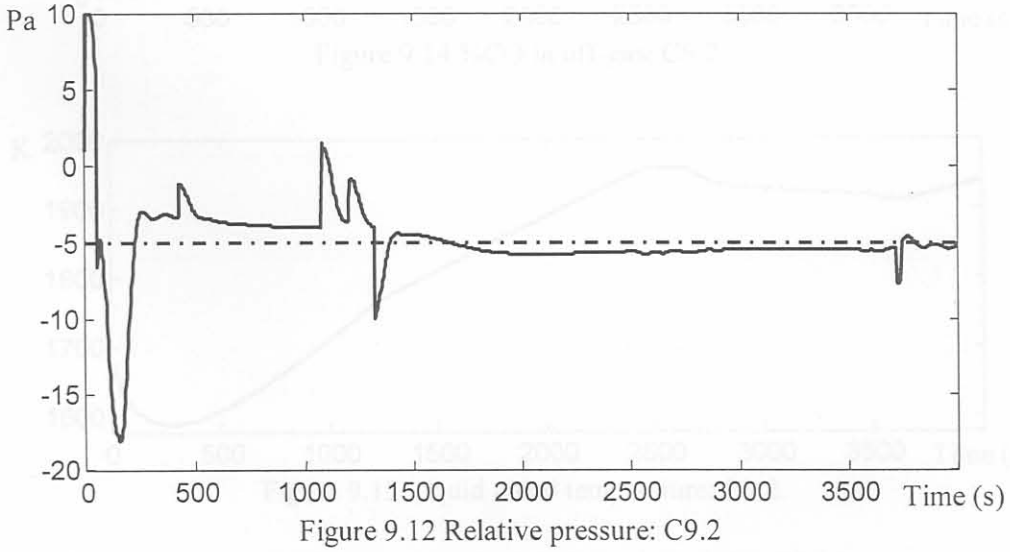


Figure 9.12 Relative pressure: C9.2

At the same time, the off-gas temperature was brought slightly out of the exceed limit area so as to reduce the NILE, as is shown in Fig.9.13:

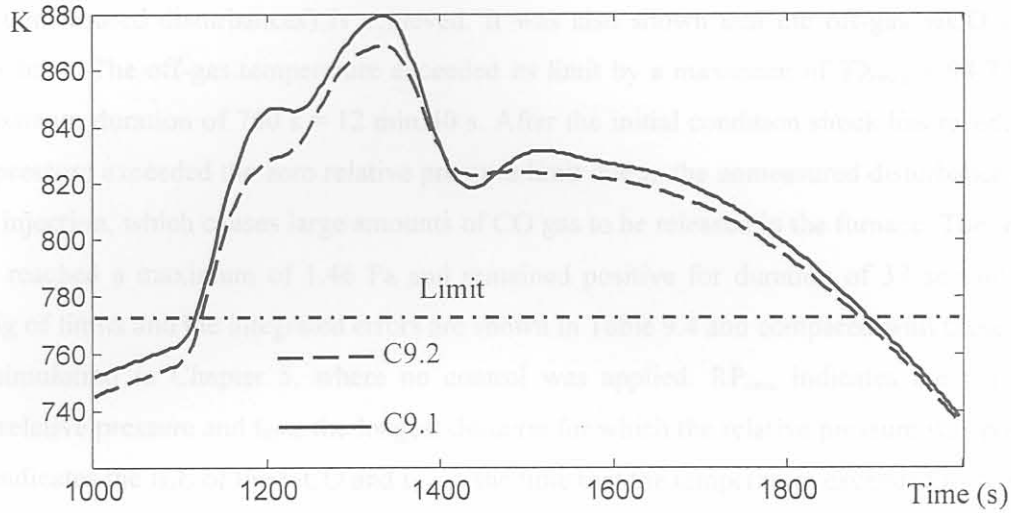


Figure 9.13 Comparison of off-gas temperature

By way of experiment it was determined that by increasing the cost function weights for the relative pressure as well as the off-gas temperature simultaneously with the same ratio, both the ISE and the ILE improved. It also caused unacceptable oscillatory behaviour and the cost function weights were therefore not increased any further. The %CO in the off-gas is shown in Fig.9.14 and the steel temperature in Fig.9.15:

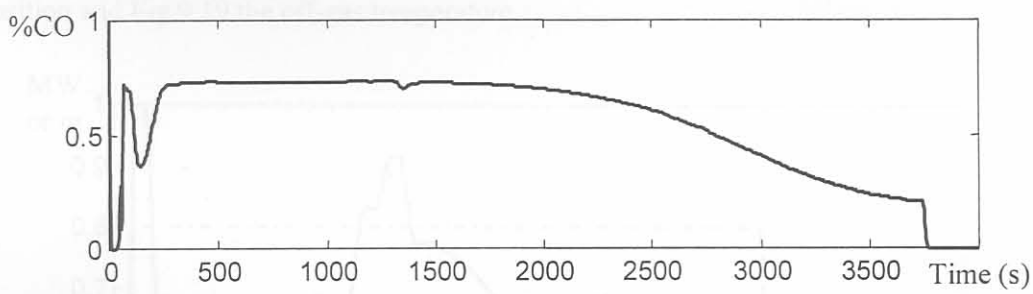


Figure 9.14 %CO in off-gas: C9.2

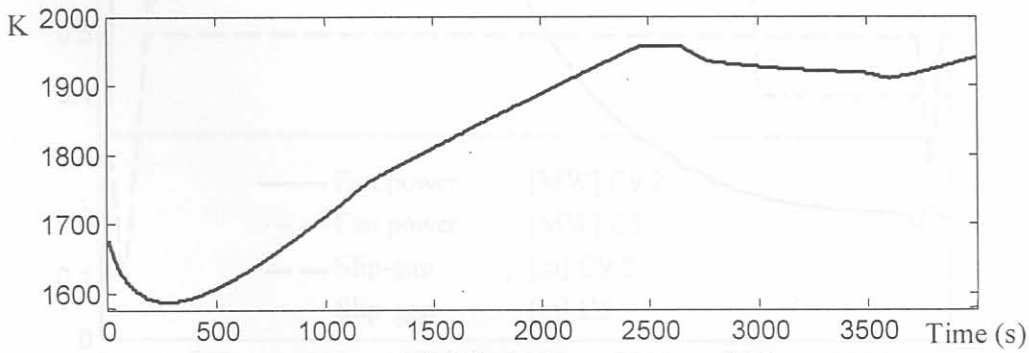


Figure 9.15 Liquid metal temperature: C9.2

## 9.7 CONTROL EVALUATION

It was illustrated in the previous section that acceptable regulation of the relative pressure (despite unmeasured disturbances) is achieved. It was also shown that the off-gas %CO is kept below its limit. The off-gas temperature exceeded its limit by a maximum of $TX_{max}$ = 94.7 K and for a maximum duration of 760 s = 12 min:40 s. After the initial condition shock has receded, the relative pressure exceeded the zero relative pressure limit due to the unmeasured disturbance of the graphite injection, which causes large amounts of CO gas to be released in the furnace. The relative pressure reached a maximum of 1.46 Pa and remained positive for duration of 37 seconds. The exceeding of limits and the integrated errors are shown in Table 9.4 and compared with those of the similar simulation in Chapter 5, where no control was applied. $RP_{max}$ indicates the maximum positive relative pressure and $t_{RP>0}$ the longest duration for which the relative pressure was positive. $ILE_{\%CO}$ indicates the ILE of the %CO and $t_{T>limit}$ the time that the temperature exceeded its limit.

Table 9.4: Controller evaluation (C9.2) against manual control (Chapter 5)

| Controller | NISE | $RP_{max}$ | $t_{RP>0}$ | $\%CO_{max}$ | $ILE_{\%CO}$ | NILE | $TX_{max}$ | $t_{T>limit}$ |
|---|---|---|---|---|---|---|---|---|
| None | 3.2461 | 4.10 Pa | 263 s | 3.54 % | 1894 | 1.5682 | 92.4 K | 1140 s |
| C9.2 | 0.9531 | 1.46 Pa | 37 s | 0.74 % | 0 | 0.9413 | 94.7 K | 760 s |

To visualise the comparison in Table 9.4 the following four figures for comparison are included: Fig.9.16 compares the manipulated variables for C9.2 against the manual control of Chapter 5. Fig.9.17 compares the relative pressure between the two options, Fig.9.18 compares the off-gas composition and Fig.9.19 the off-gas temperature.

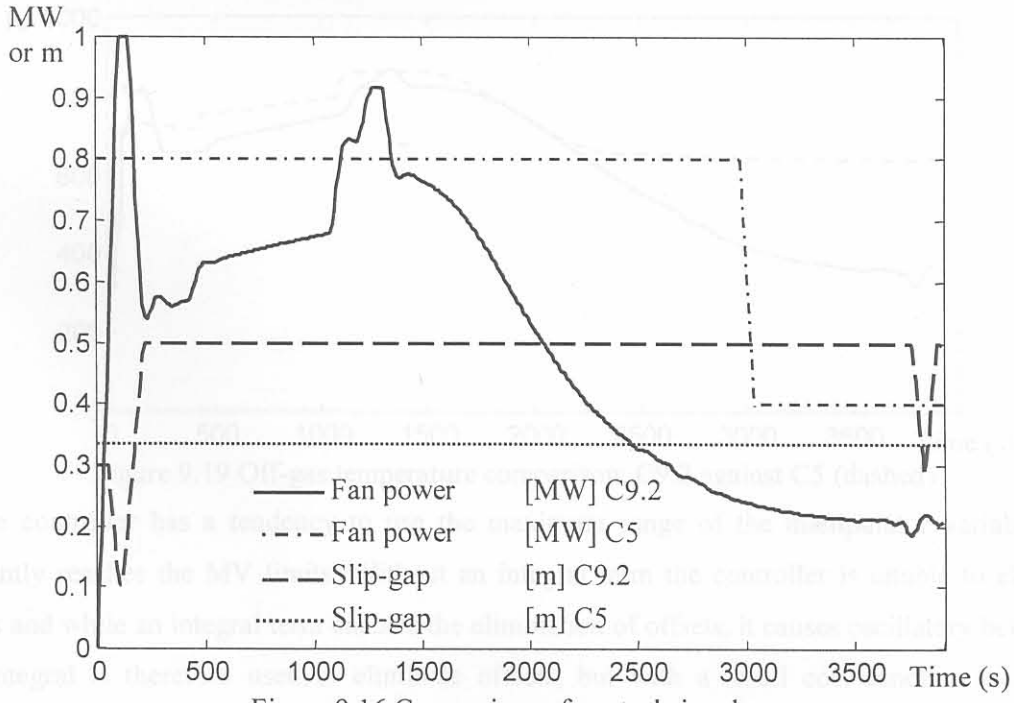


Figure 9.16 Comparison of control signals

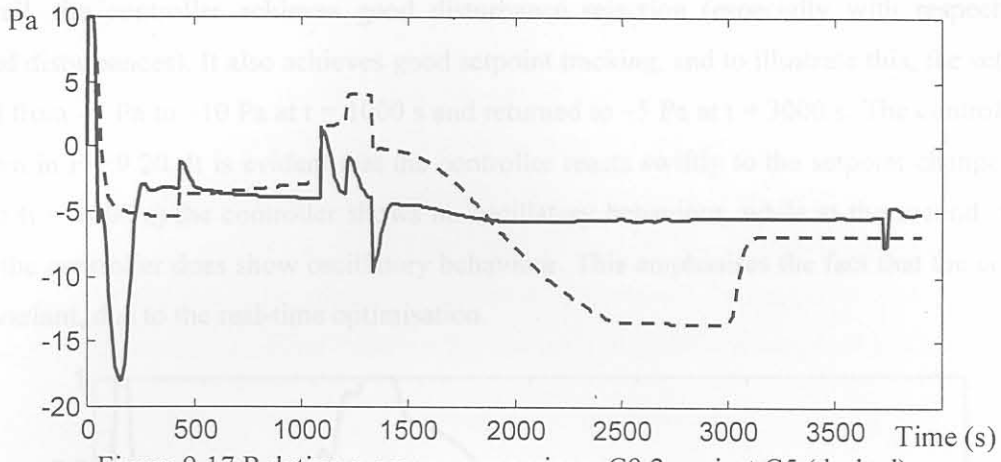


Figure 9.17 Relative pressure comparison: C9.2 against C5 (dashed)

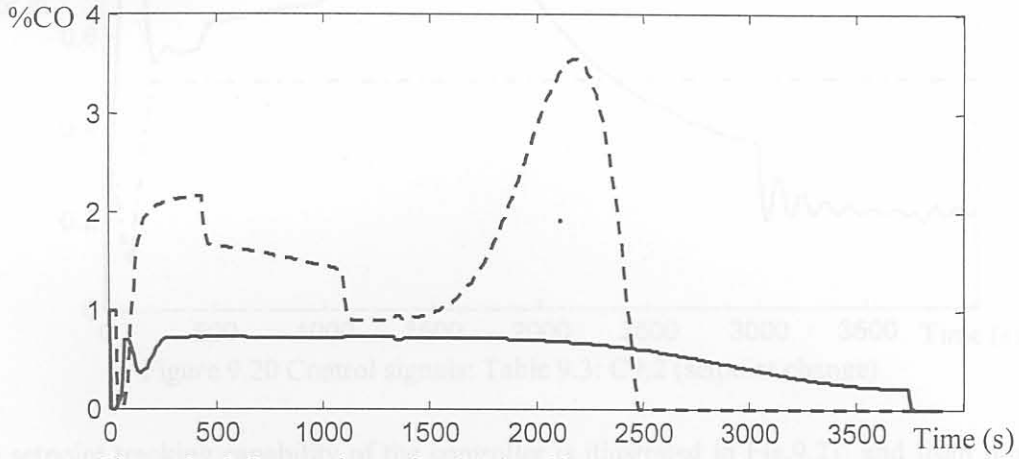


Figure 9.18 Comparison of %CO in off-gas: C9.2 against C5 (dashed)

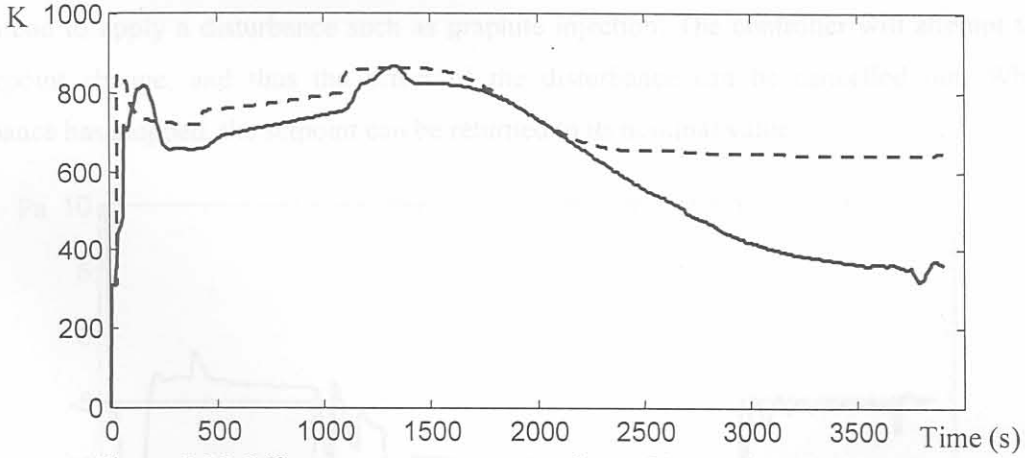


Figure 9.19 Off-gas temperature comparison: C9.2 against C5 (dashed)

The controller has a tendency to use the maximum range of the manipulator variables and frequently reaches the MV limits. Without an integral term the controller is unable to eliminate offsets and while an integral term enables the elimination of offsets, it causes oscillatory behaviour. The integral is therefore used to eliminate offsets, but with a small cost function weight, as determined in Chapter 8.

Overall, the controller achieves good disturbance rejection (especially with respect to the measured disturbances). It also achieves good setpoint tracking, and to illustrate this, the setpoint is changed from –5 Pa to –10 Pa at t = 1000 s and returned to –5 Pa at t = 3000 s. The control signals are shown in Fig.9.20. It is evident that the controller reacts swiftly to the setpoint change. At the first step (t = 1000 s) the controller shows no oscillatory behaviour, while at the second step (t = 3000 s) the controller does show oscillatory behaviour. This emphasises the fact that the controller is time-variant, due to the real-time optimisation.

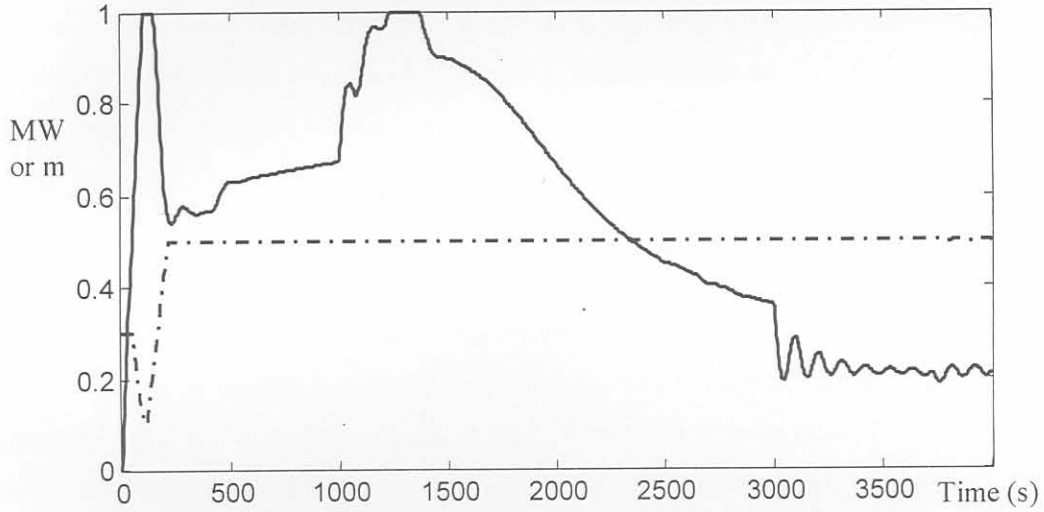


Figure 9.20 Control signals: Table 9.3: C9.2 (setpoint change)

The setpoint tracking capability of the controller is illustrated in Fig.9.21, and from this graph the deduction can be made that operators may temporarily make the setpoint more negative when they intend to apply a disturbance such as graphite injection. The controller will attempt to track the setpoint change, and thus the effect of the disturbance can be cancelled out. When the disturbance has stopped, the setpoint can be returned to its nominal value.

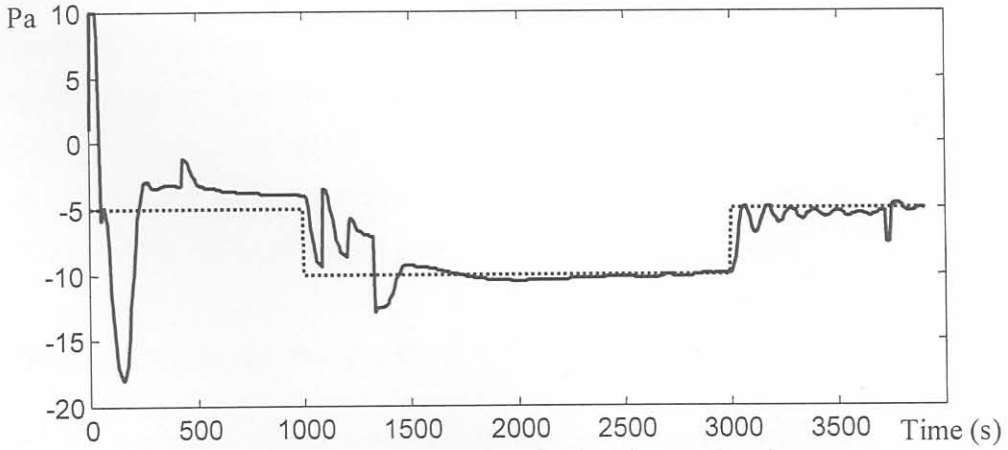


Figure 9.21 Relative pressure: C9.2 with setpoint changes

## 9.8 CONCLUSION

In Section 9.2 the structure of the non-linear closed loop simulation was discussed. Section 9.3 explained the structure of the MPC algorithm. In Section 9.4 the structure of the QP optimisation algorithm was explained. Section 9.5 discussed the structure of the plant simulation. In Section 9.6 the fine-tuning of the controller was discussed and illustrated. The evaluation of each successive improvement is performed as the results were shown. In Section 9.7 the achievement of the control objectives were discussed. The final conclusions and recommendations are given in Chapter 10.

# CHAPTER 10: CONCLUSION AND RECOMENDATIONS

## 10.1 SUMMARY OF APPROACH

The subject treated in this dissertation was motivated from industrial practice, and a solution was obtained that could be applied in the actual plant control system. Since no plant model was available, an extensive modelling effort was conducted. The model derived in this dissertation was intended for the testing of control strategies using off-gas variables in the control of an EAF. Derivation of a multivariable non-linear state-space model for the process was treated. The assumptions that were made and the state space representation provided a comprehensive framework for the development of an EAF process model. First principles of thermodynamics were then used to derive the model, ensuring behaviour consistent with physical observations. Typical operating conditions for a furnace were discussed, and a simulation was conducted with these operating conditions. In order to apply the model to represent a specific industrial furnace, the adjustable parameters in the model were selected such that the model responses concur with those of the actual furnace. After verification this plant model was then regarded as the process for which a controller had to be designed. A linear model approximated the plant model to give a simplified mathematical abstraction of the process. It was accepted as a reasonable approximation of the process, and an analysis of the linear system showed that it is stable. The analysis also showed that the linear system is output controllable, although the internal state vector is not completely observable. Qualitative control objectives were translated to quantitative control specifications.

Controller design for the linear system was performed in the Matlab environment. Model Predictive Control was the preferred control design method, due to the use of an internal model and the use of optimisation. Experiments with the controller parameters were done to obtain the best nominal controller. These include the cost function multipliers for the controlled and manipulated variables, as well as the control and prediction horizons. The effect of various inputs and disturbances was determined. The emphasis was divided between improving EAF efficiency and ensuring environmental protection and the nominal controller was obtained. Integral action was required to eliminate offsets, and it was added to the unforced response. The controller was then applied to the plant model, and tested on the process it was intended for. The controller was evaluated against the option of manual control, and achieved much improved performance.

## 10.2 CONTRIBUTION OF THIS WORK

The main contribution of this dissertation is to demonstrate the feasibility of using the off-gas variables for EAF process control. Since many unsteady-state models are proprietary, they are not published in the literature. There are a few exceptions [7,13], which give partial model derivations

for EAF processes. The model derived in this dissertation, and the publication of it, is therefore seen as an important contribution to the literature. With the GCP [14] as guideline, MPC was applied to the process [11] and evaluated, and this is also seen as a relevant contribution. One publication in an international journal [7] on the subject of the metallurgical modelling of the EAF process, and two conference articles (IFAC MMM) [8,11] have been published on the work done in this dissertation.

In order to assert the value of this dissertation to the engineering community, it is necessary to review its purpose. In the particular industrial process treated in this dissertation, automatic control systems have not yet been used to improve the process efficiency by regulating the off-gas process. This dissertation shows that it will be possible to do just that, and it also elaborates on the method to be used. When the knowledge gained through this dissertation is applied on an industrial EAF, it will result in an improved regulation of the EAF relative pressure, which will in turn result in less energy waste and higher process efficiency. In the competing environment of the global economy the application of such a new automatic control system to an existing production facility, should prove beneficial, even if only small efficiency improvements are reached.

Another result of this dissertation is the example of the method to practically apply MPC to an industrial process. There are several practical points that have to be considered when MPC is applied, such as the interface between the absolute variables of the "outside world" and the deviation variables of the internal model of the controller. Problems such as these and others have been treated in this dissertation, and therefore present an example of MPC application to an industrial process.

## 10.3 RECOMMENDATIONS

The recommendations given here are for future work that can be undertaken in undergraduate projects or in postgraduate dissertations, depending on the level of complexity.

The following recommendations for further work are concerned with modelling:

1. The gas phase system, including the furnace freeboard and the water-cooled duct, should be modelled by Computational Fluid Dynamic (CFD) modelling, supported by combustion modelling. This problem will probably have to be made two-dimensional, if not three-dimensional, to obtain sufficient accuracy. An attempt to achieve this by means of a one-dimensional CFD model was done for this dissertation, but failed to achieve the necessary accuracy. The derivation is shown in [59], and can be taken as a guideline for initial work in such a project. It must be emphasised here that a dynamic model is required, in contrast with steady state CFD simulations, examples of which are also shown in [59]. Such a dynamic

model will significantly enhance the accuracy of the off-gas model, and it will improve further understanding of the process.

2. The exact relationship between electrode position, transformer tap positions and power transfer to the liquid metal pool should be modelled and incorporated into the model. The effect of the slag-depth will also have to considered. The motivation for this additional modelling is that it will enable the control engineer to include the transformer tap position and electrode position as manipulated variables in the control design.
3. The phosphorus content in the liquid metal pool should be taken into account. This implies that the chemistry (e.g. basicity of the slag, FeO and MgO content of the slag, amount of CaO dissolved in the liquid phase) and temperature of the slag should also be considered.
4. The cooling water measurements of the furnace and duct walls must be taken into account.

The following recommendations for further work are concerned with control applications:

1. With the electrical model available, and added to the existing model, the control engineer can use the electrode position, the transformer tap position and also the DRI feed rate as manipulated variables in the controller design to control the liquid metal pool temperature and the tap-to-tap time
2. With the slag-basicity and phosphorus relationship modelled and added to the existing model, the control engineer can use the slag-addition inputs as manipulated variables to control the slag-basicity and the dephosphorisation rate.
3. The entire process (with all models included) should be implemented on an industrial furnace. All the available MVs should be used to control the entire operation. This should be integrated with existing control systems to yield a complete Computer Integrated Manufacturing (CIM) system [60].

## REFERENCES

1. International Iron and Steel Institute, "Statistics", *Iron & Steelmaker*, Vol. 25, no. 5, pp. 18, May 1998.
2. L. Fourie, "Iron and Steelmaking – A Perspective on the Past, Present and Future", *SAIMM Colloquium on Pyrometallurgy*, Mintek, Randburg, May 1997.
3. D. Crosthwaite, "Pyrometallurgy and the Environment", *SAIMM Colloquium on Pyrometallurgy*, Mintek, Randburg, May 1997.
4. J.A.T. Jones, "Interactions between electric arc furnace operations and environmental concerns", *Iron and Steel Engineer,* Vol. 72, no. 12, pp. 37-46, December 1995.
5. W.T. Lankford (editor) *et al.*, *The making, shaping and treating of steel* 10th edition, Association of Iron and Steel Engineers, Pittsburgh 1985.
6. C. Petersohn, E. Burstrom and P. Hahlin, "Mefarc – a dynamic process control system for electric arc furnaces", *4th European Electric Steel Congress*, Madrid, November 1992.
7. J.G. Bekker, I.K. Craig, and P.C. Pistorius, "Modelling and Simulation of an Electric Arc Furnace Process", *ISIJ Int.*, Vol.39, no.1, pp. 23-32, January 1999.
8. J.G. Bekker, I.K. Craig and P.C. Pistorius, "Modelling and Specification for Control of an EAF Off-Gas Process", *9th IFAC MMM Conf.*, Cologne, Germany, September 1998.
9. M.A. Reuter, M. Oosthuizen, I.J. Barker, M.S. Rennie and A. De Waal, "The dynamic response of submerged-arc furnaces to electrode movement", 8th IFAC MMM Conf., Sun City, South Africa, pp. 97-102 August 1995.
10. P.E. King and M.D. Nyman, "Modeling and control of an electric arc furnace using a feedforward artificial neural network", *Journal of Applied Physics*, Vol. 80, no. 3, pp. 1872-1877, August 1996.
11. J.G. Bekker, I.K. Craig and P.C. Pistorius, "Model Predictive Control of an EAF Off-gas Process", *Accepted for publication*, IFAC World Congress, Beijing, July 1999.
12. M. Morari and N.L. Ricker, *Model Predictive Control Toolbox User's Guide*, The Mathworks, Inc., Natick, pp. 71-74, 1995.
13. R.D. Morales, H. Rodriguez-Hernandez, P. Garnica-Conzalez and J.A. Romero-Serrano, "A Mathematical Model for the Reduction Kinetics of Iron Oxide in Electric Furnace Slags by Graphite Injection", *ISIJ Int.*, Vol. 37, no. 11, pp. 1072-1080, November 1997.
14. I.K. Craig, "On the role of the general control problem in control engineering education", *IFAC: 4th Symposium on Advances in Control Education*, Istanbul,Turkey, Jul. 1997.

15. R. Plessing, "The Electric Arc Furnace Process", *Practice of Steelmaking 2*, Edited by H. Trenkler and W. Krieger, Volume 8, Metallurgy of Iron, A Supplement to Gmelin Handbook of Inorganic Chemistry, Gmelin-Durrer, Springer-Verlag, pp.72-167, 1985.

16. D.G. Fink(ed) and H.W. Beaty(ed), *Standard Handbook for Electrical Engineers*, Twelfth Edition, McGraw-Hill, New York, pp. 10_56-10_57, 1987.

17. E.H. McIntyre, "Electrical Input Into EAFs, Part VII", *Iron & Steelmaker*, Vol. 18, no. 9, pp. 54-55, September 1991.

18. W. Masclanka, "The use of Sponge iron in the electric arc furnace", *International Symposium on Modern Developments in Steelmaking*, Jamshedpur, India, February 1981.

19. E.H. McIntyre and E.R. Landry, "EAF Steelmaking – Process and Practice Update", *Iron & Steelmaker*, Vol. 20, no. 5, pp. 61-66, May 1993.

20. D.E. Seborg, T.F. Edgar and D.A. Mellichamp, *Process Dynamics and Control*, John Wiley & Sons, New York, pp. 16-25, 1989.

21. G. Stephanopoulos, *Chemical Process Control – An Introduction to Theory and Practice,* Prentice Hall, New Jersey, 1984, pp. 43; 215-216; 424.

22. S. Köhle, "Effects on the electric energy and electrode consumption of arc furnaces", *Stahl und Eisen*, Vol. 112, no. 11, pp. 59-67, November 1992.

23. P.R. Austin, H. Nogami and J. Yagi, "A Mathematical Model of Four Phase Motion and Heat Transfer in the Blast Furnace", *ISIJ Int.*, Vol. 37, no. 5, pp. 458-467, May 1997.

24. E. Sridhar and A.K. Lahiri, "Steady state model for current and temperature distributions in an electric smelting furnace", *Steel Research*, Vol. 65, no. 10, pp. 433-437, October 1994.

25. P. Gardin, C. Soide, A. Dez and I. Guillaume, "Use of physical and numerical simulation methods to characterise gas flow in tri-electrode electric arc furnace", *Ironmaking and Steelmaking*, Vol. 19, no. 4, pp. 306-309, April 1992.

26. O.A. Zhulkovsky, A.G. Chernyatevich and A.V. Gress, "Numerical simulation of in-vessel off-gas post-combustion", *Steel in translation*, Vol. 23, no. 1, pp. 73-77, January 1993.

27. R.J. Fruehan, "Potential Benefits of Gas Stirring in an Electric Arc Furnace", *ISS trans.*, Vol. 12, no. 1, pp. 33-40, January 1991.

28. B. Sarma, A.W. Cramb and R.J. Fruehan, "Reduction of FeO in Smelting Slags by Solid Carbon: Experimental results", *Met. Trans. B*, Vol. 27B, no. 11, pp. 717-730, November 1996.

29. E. Plöckinger and O. Etterich, *Elektrostahlerzeugung*, 3rd edition, Verlag Stahleisen m.b.H., Dusseldorf, pp. 88-89, 1979.

30. J.M.A. Geldenhuis, "Fundamentals of Steelmaking", *SAIMM Colloquium on Pyrometallurgy*, Mintek, Randburg, May 1997.

31. E.T. Turkdogan, *Fundamentals of Steelmaking*, Institute of Materials, London, pp. 183 & 209-244, 1996.

32. O. Kubaschewski, C.B. Alcock and P.J. Spencer, *Materials Thermochemistry*, 6th edition, Revised of Kubaschewski and Alcock's Metallurgical Thermochemistry, Pergamon Press, Oxford, 1993.

33. E.T. Turkdogan, *Physicochemical properties of molten slags and glasses*, The Metals Society, London, 1983.

34. A. Rist and J. Chipman, "L'activité du carbone dissous dans le fer liquide", *Revue de Métallurgie*, Vol. 53, pp. 796-807, 1958.

35. G.K. Sigworth and J.F. Elliott, "The thermodynamics of liquid dilute iron alloys", *Metal Science*, Vol. 8, pp. 298-310, 1974.

36. M.A. Saad, *Compressible Fluid Flow*, Prentice Hall, Englewood Cliffs, 1985.

37. K. Furuta, A. Sano and D. Atherton, *State Variable Methods in Automatic Control,* John Wiley & Sons, New York, pp. 31-33; 78-82; 176-207, 1988.

38. J.G. Reid, *Linear System Fundamentals – Continuous and Discrete, Classic and Modern*, Mcgraw-Hill, New York, pp. 210-218, 1983.

39. C.O. Bennet and J.E. Myers, *Momentum, Heat and Mass Transfer*, Third Edition, McGraw-Hill, New York, 1982.

40. International Iron and Steel Institute, "EAF Roundup", *Iron & Steelmaker*, Vol. 25, no. 5, pp. 21-50, May 1998.

41. J.P. Bentley, *Principles of Measurement Systems*, Third Edition, Longman Scientific & Technical, Singapore, pp. 275-303, 1995.

42. S. Skogestad and I. Postlethwaite, *Multivariable Feedback Control - Analysis and Design*, John Wiley & Sons, New York, pp. 122-139, 1996.

43. W.J. Grantham and T.L. Vincent, *Modern Control Systems Analysis and Design*, John Wiley Sons, New York, pp. 46-65, 1993.

44. J. Douglas and M. Athans, "Multivariable Poles, Zeros, and Pole-zero Cancellations", *The Control Handbook*, Edited by W.S. Levine, CRC Press, Florida, pp. 445-450, 1996.

45. D.W. Clarke and R. Scattolini, "Constrained Receding-Horizon Predictive Control", *Proc. IEE*, Vol. 138D, no. 4, pp. 347-354, July 1991.

46. D.W. Clarke, C. Mohtadi and P.S. Tuffs, "Generalized Predictive Control - Part I. The Basic Algorithm", *Automatica*, Vol. 23, no. 2, pp. 137-148, February 1987.

47. J.C.G. Boot, *Quadratic Programming: Algorithms – Anomalies – Applications*, Volume 2 of Studies in Mathematical and Managerial Economics, North Holland Publishing Company, Amsterdam, pp. 186-196, 1964.

48. C. Bordons and E.F. Camacho, "A Generalized Predictive Controller for a Wide Class of Industrial Processes", *IEEE Trans. Contr. Syst. Technol.*, Vol.6, no.3, pp. 372-387, May 1998.

49. T.J.J. van den Boom, *Model Based Predictive Control*, LernModul Nr. 6, Swiss Society for Automatic Control, Zurich, pp. 14-16, 1996.

50. H.M. Deitel and P.J. Deitel, *C how to program*, Prentice Hall Int., London, pp. 62-63, 1992.

51. P.V. O'Neil, *Advanced Engineering Mathematics*, Third Edition, P.W.S. Publishing Company, Boston, pp. 573-832, 1993.

52. J.H. Mathews, *Numerical Methods for Mathematics, Science, and Engineering*, Second Edition, Prentice Hall, New Jersey, pp. 122-188; 423-461; 400-420, 1992.

53. W.H. Press, S.A. Teutolsky, W.T. Vetterling and B.P. Flannery, *Numerical Recipes in C – The Art of Scientific Computing*, Second Edition, Cambridge University Press, Cambridge, 1994.

54. S. Dano, *Nonlinear and Dynamic Programming*, Springer-Verlag, Wien, pp. 33-59, 1975.

55. A.L. Peressini, F.E. Sullivan and J.J. Uhl Jr., *The Mathematics of Nonlinear Programming*, Springer-Verlag, New York, pp. 258-266, 1988.

56. A.O. Converse, *Optimization*, Holt, Rinehart and Winston, New York, pp. 3-22 243-258, 1970.

57. A. Ben-Israel, A. Ben-Tal and S. Zlobec, *Optimality in Nonlinear Programming*, John Wiley & Sons, New York, 1981.

58. B.D. Craven, *Mathematical Programming and Control Theory*, Chapman and Hall, London, 1978.

59. J.G. Bekker, *Technical Report, EAF off-gas CFD model derivation and program code*, University of Pretoria, 1998. (In the interim available from Prof. I.K. Craig)

60. M.P. Groover, *Automation, Production Systems, and Computer Integrated Manufacturing*, Prentice Hall, New Jersey, 1987.

## APPENDIX A : LIST OF SYMBOLS

$x_1$ = m($Fe_{(S)}$), mass of solid iron [kg]
$x_2$ = m($Fe_{(L)}$), mass of liquid steel [kg]
$x_3$ = m(C), carbon in solution in steel [kg]
$x_4$ = m(Si), silicon in solution in steel [kg]
$x_5$ = m($Slag_{(S)}$), solid slag mass [kg]
$x_6$ = m($Slag_{(L)}$), liquid slag mass [kg]
$x_7$ = m(FeO), FeO in slag [kg]
$x_8$ = m($SiO_2$), $SiO_2$ in slag [kg]
$x_9$ = m(CO), carbon-monoxide [kg]
$x_{10}$ = m($CO_2$), carbon-dioxide [kg]
$x_{11}$ = m($N_2$), nitrogen in gas-phase [kg]
$x_{12}$ = T(fluid group), temperature [K]
$x_{13}$ = T(solid group), temperature [K]
$x_{14}$ = P(furnace) relative pressure [Pa]
$x_{15}$, $x_{16}$, $x_{17}$ comprise the off-gas flow
$y_1$ = relative pressure measurement [Pa]
$y_2$ = liquid steel temperature [K]
$y_3$ = off-gas %CO [%]
$y_4$ = off-gas temperature [K]
$u_1$ = ṁ(turb), Off-gas turbine flow [kg/s]
$u_2$ = w(slipgap), Slip gap width [m]
$v_1$ = ṁ (Oxy), oxygen fuel flow [kg/s]
$v_2$ = p(Arc), Electric arc power [kW]
$v_3$ = ṁ (DRI), DRI addition flow [kg/s]
$w_1$ = ṁ (slag), Slag addition [kg/s]
$w_2$ = ṁ (graphite), Graphite injected [kg/s]

Table A.1 gives the values of dimensionless constants. Table A.2 gives the air and area constants. Table A.3 gives the rate and thermal constants. Four constant temperatures were assumed to be at 300 K: $T_{DRI}$, $T_{slag}$, $T_{O2}$, $T_{AIR}$. Thermodynamic data such as latent heat, specific heat or enthalpy of formation were obtained from Kubaschewski *et al* [32] except were a reference in the chapters would indicate a different source.

Table A.1 Dimensionless Constants

| $K_{gr}$ | $k_U$ | $k_{XC}$ | $k_{XSi}$ | $k_{PR}$ |
|---|---|---|---|---|
| 15.0 | 8.44 | $491*10^{-6}$ | $8.08*10^{-8}$ | 0.2 |

Table A.2 Air and Area Constants

| Air [$mol.kg^{-1}$] | | Area [$m^2.kg^{-1}$] | |
|---|---|---|---|
| $k_{AIR1}$ | $k_{AIR2i}$ | $k_{area1}$ | $k_{area2}$ |
| 7.3 | 27.4 | 0.005 | 0.12 |

Table A.3 Rate and Thermal Constants

| Rate [$kg.s^{-1}$] | | Thermal [$kW.K^{-1}.m^{-2}$] | |
|---|---|---|---|
| $k_{dC}$ | $k_{dSi}$ | $k_{ther1}$ | $k_{ther5}$ |
| 12 | 144 | 0.4 | 0.2 |

M = manipulation horizon

P = prediction horizon

**U** = input cost function weight matrix (diagonal)

**Y** = output cost function weight matrix (diagonal)

$K_I$ = integral cost function weight

$\gamma_C$ = activity coefficient of carbon in liquid steel

$\gamma_{FeO}$ = activity coefficient of FeO in slag

$\bar{\gamma}$ = error vector used in cost function of MPC

$\bar{r}$ = output setpoint vector

$\bar{y}$ = output vector

$\psi$ = cost function

## Appendix B: Plant Data

| Minutes | Time | Electricity | Oxygen | | | DRI | Antra | Dolo | Lime | Foam | T(Celcius) | %C |
|---|---|---|---|---|---|---|---|---|---|---|---|---|
| | | Kwh | Nm3 | Nm3 | Nm3 | Kg | | | | | | |
| 1 | **11:54** | 680 | 0 | 0 | 0 | 0 | 0 | 0 | 0 | 0 | | |
| 2 | **11:55** | 1360 | 0 | 0 | 0 | 0 | 0 | 0 | 0 | 0 | | |
| 3 | **11:56** | 2310 | 0 | 0 | 0 | 0 | 0 | 0 | 0 | 0 | | |
| 4 | **11:57** | 3260 | 0 | 0 | 0 | 0 | 0 | 0 | 0 | 0 | | |
| 5 | **11:58** | 3260 | 0 | 0 | 0 | 0 | 0 | 0 | 0 | 0 | | |
| 6 | **11:59** | 3260 | 0 | 0 | 0 | 0 | 0 | 0 | 0 | 0 | | |
| 7 | **12:00** | 3260 | 0 | 0 | 0 | 0 | 0 | 0 | 0 | 0 | | |
| 8 | **12:01** | 3260 | 0 | 0 | 0 | 0 | 0 | 0 | 0 | 0 | | |
| 9 | **12:02** | 3260 | 0 | 0 | 0 | 0 | 0 | 0 | 0 | 0 | | |
| 10 | **12:03** | 3260 | 0 | 0 | 0 | 0 | 0 | 0 | 0 | 0 | | |
| 11 | **12:04** | 3260 | 0 | 0 | 0 | 0 | 0 | 0 | 0 | 0 | | |
| 12 | **12:05** | 3260 | 0 | 0 | 0 | 0 | 0 | 0 | 0 | 0 | | |
| 13 | **12:06** | 3260 | 0 | 0 | 0 | 0 | 0 | 0 | 0 | 0 | | |
| 14 | **12:07** | 3260 | 0 | 0 | 0 | 0 | 0 | 0 | 0 | 0 | | |
| 15 | **12:08** | 3260 | 0 | 0 | 0 | 0 | 0 | 0 | 0 | 0 | | |
| 16 | **12:09** | 3260 | 27 | 32 | 58 | 0 | 0 | 0 | 0 | 0 | | |
| 17 | **12:10** | 3593 | 54 | 100 | 155 | 0 | 0 | 0 | 0 | 0 | | |
| 18 | **12:11** | 3594 | 82 | 169 | 251 | 0 | 0 | 0 | 0 | 0 | | |
| 19 | **12:12** | 4641 | 110 | 237 | 347 | 0 | 0 | 0 | 0 | 0 | | |
| 20 | **12:13** | 5688 | 138 | 306 | 444 | 0 | 0 | 0 | 0 | 0 | | |
| 21 | **12:14** | 6735 | 166 | 374 | 540 | 0 | 0 | 0 | 0 | 0 | | |
| 22 | **12:15** | 8120 | 199 | 448 | 647 | 0 | 0 | 0 | 0 | 0 | | |
| 23 | **12:16** | 8829 | 232 | 522 | 754 | 0 | 0 | 0 | 50 | 0 | | |
| 24 | **12:17** | 9876 | 266 | 595 | 861 | 0 | 0 | 0 | 100 | 0 | | |
| 25 | **12:18** | 10923 | 299 | 669 | 968 | 0 | 0 | 0 | 150 | 0 | | |
| 26 | **12:19** | 11970 | 332 | 743 | 1075 | 0 | 0 | 0 | 200 | 0 | | |
| 27 | **12:20** | 13017 | 366 | 816 | 1182 | 0 | 0 | 0 | 250 | 0 | | |
| 28 | **12:21** | 14064 | 399 | 890 | 1289 | 0 | 0 | 0 | 300 | 0 | | |
| 29 | **12:22** | 15111 | 432 | 964 | 1396 | 0 | 0 | 0 | 350 | 0 | | |
| 30 | **12:23** | 16158 | 466 | 1037 | 1503 | 0 | 0 | 0 | 400 | 0 | | |
| 31 | **12:24** | 17205 | 499 | 1111 | 1610 | 0 | 0 | 0 | 450 | 0 | | |
| 32 | **12:25** | 18252 | 532 | 1185 | 1717 | 0 | 0 | 0 | 500 | 0 | | |
| 33 | **12:26** | 19299 | 566 | 1258 | 1824 | 0 | 0 | 0 | 550 | 0 | | |
| 34 | **12:27** | 20346 | 599 | 1332 | 1931 | 0 | 0 | 0 | 600 | 25 | | |
| 35 | **12:28** | 21393 | 632 | 1406 | 2038 | 0 | 0 | 0 | 650 | 50 | | |
| 36 | **12:29** | 22440 | 666 | 1479 | 2145 | 500 | 0 | 0 | 700 | 75 | | |
| 37 | **12:30** | 23487 | 699 | 1553 | 2252 | 1000 | 0 | 0 | 750 | 100 | | |
| 38 | **12:31** | 24534 | 733 | 1627 | 2359 | 1500 | 0 | 0 | 800 | 100 | | |
| 39 | **12:32** | 25582 | 767 | 1700 | 2467 | 2000 | 0 | 0 | 850 | 100 | | |
| 40 | **12:33** | 26629 | 800 | 1774 | 2574 | 2500 | 0 | 0 | 900 | 100 | | |
| 41 | **12:34** | 27676 | 834 | 1848 | 2682 | 3000 | 0 | 0 | 950 | 100 | | |
| 42 | **12:35** | 28723 | 868 | 1921 | 2789 | 3500 | 0 | 0 | 1000 | 100 | | |
| 43 | **12:36** | 29770 | 902 | 1995 | 2897 | 4000 | 0 | 0 | 1050 | 100 | | |
| 44 | **12:37** | 30817 | 936 | 2069 | 3004 | 4500 | 0 | 0 | 1100 | 100 | 1551 | |
| 45 | **12:38** | 31864 | 969 | 2108 | 3077 | 5000 | 0 | 0 | 1150 | 100 | 1551 | 0.056 |
| 46 | **12:39** | 32911 | 1002 | 2148 | 3150 | 5500 | 117 | 50 | 1200 | 100 | 1551 | 0.056 |
| 47 | **12:40** | 33958 | 1036 | 2222 | 3258 | 6000 | 233 | 100 | 1250 | 100 | 1551 | 0.056 |
| 48 | **12:41** | 35005 | 1070 | 2296 | 3366 | 6500 | 350 | 150 | 1300 | 100 | 1551 | 0.056 |
| 49 | **12:42** | 36052 | 1104 | 2370 | 3474 | 7000 | 467 | 200 | 1350 | 100 | 1551 | 0.056 |
| 50 | **12:43** | 37099 | 1138 | 2410 | 3548 | 7500 | 467 | 250 | 1400 | 100 | 1551 | 0.056 |
| 51 | **12:44** | 38146 | 1172 | 2450 | 3622 | 8000 | 467 | 300 | 1450 | 100 | 1551 | 0.056 |
| 52 | **12:45** | 39193 | 1206 | 2489 | 3696 | 8500 | 467 | 350 | 1500 | 100 | 1605 | 0.056 |
| 53 | **12:46** | 40240 | 1241 | 2529 | 3770 | 9000 | 467 | 400 | 1550 | 100 | 1605 | 0.048 |
| 54 | **12:47** | 41287 | 1275 | 2569 | 3845 | 9500 | 467 | 450 | 1600 | 100 | 1605 | 0.048 |

| | | | | | | | | | | | | |
|---|---|---|---|---|---|---|---|---|---|---|---|---|
| 55 | **12:48** | 42334 | 1310 | 2610 | 3919 | 10000 | 467 | 500 | 1650 | 100 | 1605 | 0.048 |
| 56 | **12:49** | 43381 | 1344 | 2650 | 3994 | 10500 | 467 | 550 | 1700 | 100 | 1605 | 0.048 |
| 57 | **12:50** | 44428 | 1379 | 2690 | 4069 | 12333 | 467 | 600 | 1750 | 100 | 1605 | 0.048 |
| 58 | **12:51** | 45475 | 1413 | 2731 | 4144 | 14167 | 467 | 650 | 1800 | 100 | 1630 | 0.048 |
| 59 | **12:52** | 46522 | 1448 | 2771 | 4219 | 16000 | 467 | 700 | 1850 | 100 | 1630 | 0.035 |
| 60 | **12:53** | 47569 | 1448 | 2771 | 4219 | 17833 | 467 | 750 | 1900 | 100 | 1630 | 0.035 |
| 61 | **12:54** | 48616 | 1448 | 2771 | 4219 | 19667 | 467 | 800 | 1950 | 100 | 1630 | 0.035 |
| 62 | **12:55** | 49664 | 1448 | 2771 | 4219 | 20667 | 467 | 850 | 2000 | 100 | 1630 | 0.035 |
| 63 | **12:56** | 50711 | 1448 | 2771 | 4219 | 21667 | 467 | 900 | 2050 | 100 | 1602 | 0.035 |
| 64 | **12:57** | 51758 | 1448 | 2771 | 4219 | 22667 | 467 | 950 | 2100 | 100 | 1602 | 0.03 |
| 65 | **12:58** | 52805 | 1448 | 2771 | 4219 | 23667 | 467 | 1000 | 2150 | 100 | 1602 | 0.03 |
| 66 | **12:59** | 53852 | 1448 | 2771 | 4219 | 24667 | 467 | 1050 | 2200 | 100 | 1602 | 0.03 |
| 67 | **13:00** | 54899 | 1448 | 2771 | 4219 | 25667 | 467 | 1100 | 2250 | 100 | 1602 | 0.03 |
| 68 | **13:01** | 55946 | 1448 | 2771 | 4219 | 26667 | 467 | 1150 | 2300 | 100 | 1602 | 0.03 |
| 69 | **13:02** | 56993 | 1448 | 2771 | 4219 | 27667 | 467 | 1200 | 2350 | 100 | 1609 | 0.03 |
| 70 | **13:03** | 58040 | 1448 | 2771 | 4219 | 28667 | 467 | 1250 | 2400 | 100 | 1609 | 0.03 |
| 71 | **13:04** | 59087 | 1448 | 2771 | 4219 | 29667 | 467 | 1300 | 2450 | 100 | 1609 | 0.03 |
| 72 | **13:05** | 60134 | 1448 | 2771 | 4219 | 30667 | 467 | 1350 | 2500 | 100 | 1609 | 0.03 |
| 73 | **13:06** | 61181 | 1448 | 2771 | 4219 | 31667 | 467 | 1400 | 2550 | 100 | 1609 | 0.03 |
| 74 | **13:07** | 62228 | 1448 | 2771 | 4219 | 33433 | 467 | 1450 | 2600 | 100 | 1609 | 0.03 |
| 75 | **13:08** | 63275 | 1448 | 2771 | 4219 | 35200 | 467 | 1500 | 2650 | 100 | 1625 | 0.03 |
| 76 | **13:09** | 64322 | 1448 | 2771 | 4219 | 35200 | 467 | 1500 | 2700 | 100 | 1625 | 0.03 |
| 77 | **13:10** | 65369 | 1448 | 2771 | 4219 | 35200 | 467 | 1500 | 2750 | 100 | 1625 | 0.03 |
| 78 | **13:11** | 66416 | 1448 | 2771 | 4219 | 35200 | 467 | 1500 | 2750 | 100 | 1625 | 0.03 |
| 79 | **13:12** | 67463 | 1448 | 2771 | 4219 | 35200 | 467 | 1500 | 2750 | 100 | 1625 | 0.025 |
| 80 | **13:13** | 68510 | 1448 | 2771 | 4219 | 35200 | 467 | 1500 | 2750 | 100 | 1625 | 0.025 |
| 81 | **13:14** | 69557 | 1448 | 2771 | 4219 | 35200 | 467 | 1500 | 2767 | 100 | 1625 | 0.025 |
| 82 | **13:15** | 70605 | 1448 | 2771 | 4219 | 35200 | 467 | 1500 | 2767 | 100 | 1627 | 0.025 |

# Appendix C: Linear system

A

| | | | | | | | | | | | | | | | | |
|---|---|---|---|---|---|---|---|---|---|---|---|---|---|---|---|---|
| -8E-04 | 0 | 0 | 0 | 0 | 0 | 0 | 0 | 0 | 0 | 0 | -8E-04 | -5E-04 | 0 | 0 | 0 | 0 |
| 0.0008 | -1E-05 | 0.0058 | 0.0086 | 0 | -7E-05 | 0.0008 | -7E-05 | 0 | 0 | 0 | 0.0008 | 0.0005 | 0 | 0 | 0 | 0 |
| 0 | 3E-06 | -0.002 | 6E-06 | 0 | 1E-05 | -8E-05 | 1E-05 | 0 | 0 | 0 | 0 | 0 | 0 | 0 | 0 | 0 |
| 0 | 1E-07 | 7E-07 | -0.002 | 0 | 1E-07 | -7E-07 | 1E-07 | 0 | 0 | 0 | 0 | 0 | 0 | 0 | 0 | 0 |
| 0 | 0 | 0 | 0 | -1E-03 | 0 | 0 | 0 | 0 | 0 | 0 | -6E-05 | -3E-04 | 0 | 0 | 0 | 0 |
| 0 | 0 | 0 | 0 | 0.001 | 0 | 0 | 0 | 0 | 0 | 0 | 6E-05 | 0.0003 | 0 | 0 | 0 | 0 |
| 0 | 1E-05 | -0.006 | -0.009 | 0 | 7E-05 | -8E-04 | 7E-05 | 0 | 0 | 0 | 0 | 0 | 0 | 0 | 0 | 0 |
| 0 | -3E-07 | -1E-06 | 0.0046 | 0 | -2E-07 | 1E-06 | -2E-07 | 0 | 0 | 0 | 0 | 0 | 0 | 0 | 0 | 0 |
| 5E-08 | -2E-07 | 5E-05 | -4E-07 | 0 | -9E-07 | 5E-06 | -9E-07 | -0.001 | 0.0013 | 0.0013 | -5E-06 | -1E-05 | 0.0012 | -0.006 | 0.0055 | 0 |
| 0 | 0 | 0 | 0 | 0 | 0 | 0 | 0 | 0.0006 | -0.002 | 0.0006 | -1E-06 | 3E-06 | -0.002 | -0.003 | 0.0026 | 0 |
| 0 | 0 | 0 | 0 | 0 | 0 | 0 | 0 | 0.0007 | 0.0007 | -0.002 | -1E-06 | 3E-06 | -0.002 | -0.003 | 0.0031 | 0 |
| -8E-06 | -6E-07 | -2E-04 | 0.0006 | -1E-05 | 2E-06 | -2E-05 | 1E-06 | 0 | 0 | 0 | -1E-04 | 1E-04 | 0.0016 | 0 | 0 | 0 |
| 4E-07 | 0 | 0 | 0 | -1E-06 | 0 | 0 | 0 | 0 | 0 | 0 | 0.0006 | -8E-04 | 0 | 0 | 0 | 0 |
| -4E-04 | -6E-04 | 0.1379 | 0.0308 | -5E-04 | -0.003 | 0.0139 | -0.003 | 9E-16 | 6E-16 | 1E-15 | -0.006 | 0.0054 | -8.599 | -31.67 | 31.672 | 0 |
| 0 | 0 | 0 | 0 | 0 | 0 | 0 | 0 | 0 | 0 | 0 | 0 | 0 | 0 | 0 | 1 | 0 |
| 0 | 0 | 0 | 0 | 0 | 0 | 0 | 0 | 0 | 0 | 0 | 0 | 0 | 0 | 0 | 0 | 1 |
| 0 | 0 | 0 | 0 | 0 | 0 | 0 | 0 | 0 | 0 | 0 | 0 | 0 | 0 | -0.093 | -1.287 | -2.194 |

C

| | | | | | | | | | | | | | | | | |
|---|---|---|---|---|---|---|---|---|---|---|---|---|---|---|---|---|
| 0 | 0 | 0 | 0 | 0 | 0 | 0 | 0 | 0 | 0 | 0 | 0 | 0 | 1 | 0 | 0 | 0 |
| 0 | 0 | 0 | 0 | 0 | 0 | 0 | 0 | 0 | 0 | 0 | 1 | 0 | 0 | 0 | 0 | 0 |
| 0 | 0 | 0 | 0 | 0 | 0 | 0 | 0 | 0 | 0 | 0 | 0 | 0 | 0 | 0.4981 | -0.498 | 0 |
| 0 | 0 | 0 | 0 | 0 | 0 | 0 | 0 | 0 | 0 | 0 | 0 | 0 | 0 | 0.7361 | -0.736 | 0 |
| 0 | 0 | 0 | 0 | 0 | 0 | 0 | 0 | 0.0011 | -2E-04 | -1E-04 | 0.0002 | 0 | -6E-04 | 0.0005 | -5E-04 | 0 |
| 0 | 0 | 0 | 0 | 0 | 0 | 0 | 0 | 0 | 0 | 0 | 0.3229 | 0 | 0 | 55.591 | -55.59 | 0 |

B

| | | | | | | |
|---|---|---|---|---|---|---|
| 0 | 0 | 0 | 0 | 0 | 0 | 0 |
| 0 | 0 | -3.5 | 0 | 0.825 | 0 | 10.392 |
| 0 | 0 | 0 | 0 | 0 | 0 | 0 |
| 0 | 0 | 0 | 0 | 0 | 0 | 0 |
| 0 | 0 | 0 | 0 | 0 | 1 | 0 |
| 0 | 0 | 0 | 0 | 0 | 0 | 0 |
| 0 | 0 | 3.5 | 0 | 0.13 | 0 | -13.36 |
| 0 | 0 | 0 | 0 | 0.045 | 0 | 0 |
| 0 | 0.0775 | 0.0187 | 0 | 0 | 0 | 0.07 |
| 0 | 0.0361 | -0.005 | 0 | 0 | 0 | 0 |
| 0 | 0.0431 | -0.005 | 0 | 0 | 0 | 0 |
| 0 | 0 | 0.0945 | 1E-05 | -0.007 | -0.006 | -0.203 |
| 0 | 0 | 0 | 0 | 0 | 0 | 0 |
| 0 | 442.75 | 5.2881 | 0.0006 | -0.368 | -0.359 | 186.41 |
| 0 | 0 | 0 | 0 | 0 | 0 | 0 |
| 0 | 0 | 0 | 0 | 0 | 0 | 0 |
| 1 | 0 | 0 | 0 | 0 | 0 | 0 |

D

| | | | | | | |
|---|---|---|---|---|---|---|
| 0 | 0 | 0 | 0 | 0 | 0 | 0 |
| 0 | 0 | 0 | 0 | 0 | 0 | 0 |
| 0 | -5.224 | 0 | 0 | 0 | 0 | 0 |
| 0 | -7.72 | 0 | 0 | 0 | 0 | 0 |
| 0 | -0.904 | 0 | 0 | 0 | 0 | 0 |
| 0 | -934.2 | 0 | 0 | 0 | 0 | 0 |